INVESTIGATIONS OF A POTENTIAL HIGH-EFFICIENCY THERMOELECTRIC GENERATOR

by

Douglas Martin MacBride

B.S., Mechanical Engineering
Massachusetts Institute of Technology, 1994

Submitted to the Department of Mechanical Engineering
in Partial Fulfillment of the Requirements for the Degree of

MASTER OF SCIENCE IN MECHANICAL ENGINEERING

at the

MASSACHUSETTS INSTITUTE OF TECHNOLOGY

September 1996

Signature of Author_____
Department of Mechanical Engineering
September, 1996

Certified by_____
Professor John G. Brisson
Department of Mechanical Engineering
Thesis Supervisor

Accepted by_____
Professor Ain A. Sonin
Department of Mechanical Engineering
Chairman, Graduate Committee

INVESTIGATIONS OF A POTENTIAL HIGH-EFFICIENCY THERMOELECTRIC GENERATOR

by

Douglas Martin MacBride

Submitted to the Department of Mechanical Engineering
on September 1, 1996 in partial fulfillment of the requirements for the
degree of Master of Science in Mechanical Engineering

ABSTRACT

James Scott Strachan and Harold Aspden of the University of Edinburgh, Scotland and the University of Southampton, England, respectively, have reported a solid-state device that allows for high efficiency energy conversion.[3-9] The device comprises several hundred layers of bimetallic coated polyvinylidene-fluoride (PVDF) film connected in a series-parallel capacitor arrangement. Strachan and Aspden report reversible energy conversion with efficiencies up to 70% that of Carnot.[9]

In the present study, the construction details of the Strachan-Aspden device and the dielectric, pyroelectric, and piezoelectric properties of PVDF are reviewed. Possible energy conversion modes in a single layer of PVDF are investigated. A strain gauge bonding technique for PVDF is developed to construct PVDF stacks similar to those described by Strachan. A replica of one of the working thermoelectric generator device designs produced by Strachan and Aspden is constructed and evaluated.

No anomalous electrical effects or energy conversion effects are observed in either the single PVDF layer experiment or in the Strachan-Aspden replica device experiment. None of Strachan's reported results are confirmed. Possible explanations for the operation of the Strachan-Aspden devices are reviewed, but no satisfactory explanation has yet come to light.

Thesis Supervisor: John G. Brisson

Title: Assistant Professor of Mechanical Engineering

ACKNOWLEDGEMENTS

I am indebted to my thesis supervisor, Professor John Brisson, for his encouragement and guidance during the entire course of this research project. I am also grateful to Professor Joseph Smith for his supervision of this research and his helpful advice. I would also like to thank Doris Elsemiller, Robert Gertsen, Brian Bowers, Ashok Patel, Paul Huang, and Greg Nellis at the MIT Cryogenic Engineering Laboratory for their assistance. Joe Gerstmann and John Cox of Advanced Mechanical Technology (AMTI), Inc., Watertown, MA, provided guidance, support, and a stimulating environment in which to carry out this research. I would also like to thank the entire staff at AMTI for their helpful advice and assistance.

TABLE OF CONTENTS

NOMENCLATURE

A	= cross-sectional area, capacitive area, face area, m^2
B	= magnetic field, gauss
c	= velocity of sound, m/s
c_{jj}	= elastic constant, Pa
C	= capacitance, stack secondary capacitance, Farad
C_a	= acrylic layer capacitance, Farad
C_m	= mylar layer capacitance, Farad
C_s	= oscilloscope input capacitance, Farad
C_0	= stack primary capacitance, Farad
COP	= coefficient of performance
COP_{mac}	= maximum coefficient of performance for a thermoelectric heat pump
COP_{rev}	= coefficient of performance for a reversible cycle
d	= film thickness, stack thickness, m
d_{ij}	= piezoelectric strain constant, m/V
E	= electric field, N/C
E_{steel}	= Young's modulus of steel, Pa
f_m	= spring-mass resonant frequency, Hz
f_0	= half-wave resonant frequency, Hz
f_{PVDF}	= half-wave resonant frequency of the PVDF "listener" stack, Hz
f_{stack}	= half-wave resonant frequency of the PVDF-acrylic composite stack, Hz
F_{eff}	= effective force, N
g_{ij}	= piezoelectric stress constant, Vm/N
i	= current, A
i_0	= oscillating current amplitude, A
I	= current, A
j	= $(-1)^{1/2}$
k	= thermal conductivity, W/mK
k_{ij}	= electromechanical coupling constant
k_{33PVDF}	= electromechanical coupling constant of PVDF - 3,3 direction
K	= stiffness, N/m
K_{comp}	= composite stiffness of the steel conical sections and stack assembly, N/m
K_{cone}	= stiffness of the steel conical sections of the inertial clamp halves, N/m
K_{Cu}	= stiffness of the copper layer, N/m
K_d	= "driver" element stiffness, N/m

K_l = "listener" element stiffness, N/m

K_{Mylar} = stiffness of the mylar layer, N/m

K_{PZT} = stiffness of the PZT driver, N/m

K_{PVDF} = stiffness of the PVDF layer, N/m

K_{Pyrex} = stiffness of the Pyrex layer, N/m

K_{stack} = stiffness of the PVDF-PZT composite stack assembly, N/m

l = length, thickness, m

L = length, m, effective stack inductance, H

M = mass, kg

p = pyroelectric constant, C/m^2K

P = electric polarization, C/m^2, power consumption of the PVDF layer, W

ΔPZT = free deflection of the PZT driver, m

q = free charge, C

q_0 = oscillating amplitude of free charge, C

Q = heat input, W, quality factor

r_1 = larger radius of the steel conical section, m

R = effective stack resistance, oscilloscope input resistance, Ω

R_p = parallel combination resistance, Ω

R_{tot} = total resistance of the thermoelectric circuit, Ω

S = absolute thermopower, V/K

t = thickness, m, time, s

$tan\delta$ = mechanical loss tangent

T = acoustic transmission coefficient

T_{ave} = mean absolute temperature of a thermoelectric heat pump, K

T_C = cold-side temperature, K

T_H = hot-side temperature, K

ΔT = temperature difference, K

ΔT_{max} = maximum temperature difference supportable by a thermoelectric heat pump, K

V = voltage, V

V_{drive} = drive voltage, V

V_{in} = drive voltage, V

V_{meas} = measured voltage, V

V_{open} = open circuit voltage, V

V_{out} = output voltage of a piezoelectric sensor, V

x = spatial variable

Z = acoustic impedance, kg/m^{2}s, figure of merit for a thermoelectric device, 1/K, electrical impedance, Ω

Z_{PVDF} = acoustic impedance of PVDF, kg/m^{2}s

Z_{PZT} = acoustic impedance of PZT, kg/m^{2}s

Z_{water} = acoustic impedance of water, kg/m^{2}s

α = phase difference, °

α_D = phase difference between the PZT and PVDF drive voltages, °

$\alpha_{P\text{-}P}$ = phase difference between the PZT drive and PVDF load resistor voltages, phase difference between the PVDF drive and PZT sensor voltages, °

$\alpha_{V\text{-}I}$ = phase differencebetween the PZT and PVDF drive voltages and currents,°

ε = electromotive force, V, relative dielectric constant

ε_0 = relative dielectric constant = 8.854 x 10^{-12} Farad/m

μ = magnetic permeablity, Tm/A

μ_0 = magnetic permeability of free space = 1.26 x 10^{-6} Tm/A

η_C = Carnot efficiency

ρ = material density, kg/m^3

ω = angular drive frequency, rad/s

Subscripts

a = property of acrylic

Al = property of aluminum

i, j = electromechanical axes

Ni = property of nickel

p = property of PVDF

LIST OF FIGURES

LIST OF TABLES

1. INTRODUCTION

The Peltier, Seebeck, and Thomson thermoelectric effects in metals and semiconductors are known to allow solid-state conversion of thermal to electrical energy, and vice-versa. However, large scale devices utilizing this effect are not feasible, as heat conduction along the current flow path strongly limits the efficiency of operation and achievable power to weight ratios are quite low. The highest efficiency realizable for a large scale semiconductor thermoelectric generator is approximately 12% of the Carnot efficiency limit.[1,2]

James Scott Strachan and Harold Aspden of the University of Edinburgh, Scotland and the University of Southampton, England, respectively, have reported a solid-state device that allows for high efficiency energy conversion.[3-9] The device comprises several hundred layers of bimetallic coated polyvinylidene-fluoride (PVDF) film connected in a series-parallel capacitor arrangement. They report reversible energy conversion with efficiencies up to 70% that of Carnot.[9] Strachan and Aspden claim that a combination of Peltier and Seebeck thermoelectric effects in the bimetallic coatings of the individual PVDF layers allows for high efficiency thermoelectric energy conversion when operating the device as a high-frequency resonator.[3-6]

The operation of an AC bimetallic "thermopile" in this fashion has not been observed before. In addition, PVDF exhibits both pyroelectric and piezoelectric properties, which may be involved in the operation of the device as a thermoelectric

converter. Although Strachan and Aspden have fabricated three working versions of this design, their results have not been repeated by any other researchers.

The present study's purpose is to determine the construction details of the Strachan-Aspden device and reproduce their results. Experiments will be performed to study the properties of PVDF film and to investigate possible modes of operation of the Strachan-Aspden AC thermoelectric generator device. A replica of one of the working thermoelectric generator device designs produced by Strachan and Aspden will be constructed and evaluated.

The scope of this thesis is to present the results of experiments performed to test various possible mechanisms for energy conversion in the PVDF material and experiments performed with a replica of one of the Strachan-Aspden prototype designs. An overview of the previous work performed by Strachan and Aspden is given in Chapter Two. Material aspects of PVDF, including piezoelectric and pyroelectric properties, are given in Chapter Three. An experiment performed to test for energy conversion in a single layer of PVDF film is described in Chapter Four. The development of a bonding procedure for PVDF is described in Chapter Five. Experiments performed using a replica of one of the Strachan-Aspden prototype designs are described in Chapter Six. Conclusions and recommendations for future work are given in Chapter Seven.

This research is performed in collaboration with Advanced Mechanical Technology, Inc., Watertown, MA, and is funded by U.S. DoD under contract MDA904-95-C-2236.

2. THE STRACHAN PVDF THERMOELECTRIC DEVICE

2.1 Background

Scott Strachan originally conceived the PVDF stack as a method to produce a sonic "laser" - a device to progressively amplify a travelling wavefront that would allow for the creation of a high-intensity ultrasonic pulse from a low acoustic impedance device. This sonic "laser" could be used as a lithotriptor - a device to shatter kidney stones in the human body.[10,11]

The acoustic impedance Z of a material is given by[12]

$$Z = \rho c \tag{2-1}$$

where ρ is the material density and c is the velocity of sound in the material. The acoustic transmission coefficient T, defined as the ratio of the transmitted stress amplitude to the incident stress amplitude of an acoustic wave normally traversing a boundary between two dissimilar media, is given by[13]

$$T = \frac{2Z_2}{Z_1 + Z_2} \tag{2-2}$$

where Z_1 is the acoustic impedance of the medium of incidence and Z_2 is the acoustic impedance of the medium of transmission.

The acoustic impedance of human tissue is closely approximated by that of water (Z_{water} = 1.5 x 10^6 kg/m^{2}s), and is more closely matched by the acoustic impedance of the polymer piezoelectric PVDF (Z_{PVDF} = 3.9 x 10^6 kg/m^{2}s) than the hard ceramic piezoelectric lead zirconate titanate (also known as PZT, Z_{PZT} = 3.0 x 10^8 kg/m^{2}s). The transmission coefficient for PVDF to water is calculated to be 0.56, as opposed to 0.01 for PZT to water. Therefore, a sonic "laser" constructed of PVDF would allow for more effective transmission of a sonic pulse to human tissue than a similar device constructed from PZT.[12]

Strachan constructed such a travelling wave amplifier device utilizing several hundred layers of PVDF film. He then discovered that the device would produce a periodic voltage spike when driven with a high-voltage AC drive circuit when a temperature gradient was imposed across the PVDF stack. The energy of the voltage spike was proportional to the temperature gradient across the stack.[10] This led him to suspect that a thermoelectric effect was causing the observed voltage spikes and prompted further research into the energy conversion aspects of the device. Much of the experimental work performed by Strachan that is reported in this chapter was described in private communications to Charles Bullock at Carrier Corporation[10] and Professor Joseph L. Smith at MIT.[11] It should be noted that much of the information Strachan provided about his experiments was incomplete and/or inconsistent. The author's best understanding of Strachan's experiments and results will be presented here.

2.2 The First Prototype Device

The original PVDF device constructed as a sonic "laser" by Strachan contained approximately 400 layers of 28 μm thick PVDF film, coated on one side with a 2200 angstrom thick nickel layer and a 800 angstrom thick aluminum layer. A schematic of the stack layout is shown in Figures 2-1, 2-2, and 2-3. The PVDF layers were interleaved with BASF mylar recording tape, with the iron oxide-coated side of the recording tape bonded to the bare side of the PVDF film. The magnetic recording tape was inserted between the PVDF layers as part of a triggering mechanism devised by Strachan. This triggering system could supposedly allow the stack to be electrically pulsed in phase by a special triggering circuit so as to provide amplification of the travelling acoustic wave.[10]

The PVDF stack was constructed using ethyl cyanoacrylate adhesive to bond all surfaces. The recording tape and PVDF surfaces were treated with a 2% solution of tetrabutyltitanate (also known as tetrabutylorthotitanate) in petroleum ether in an arid

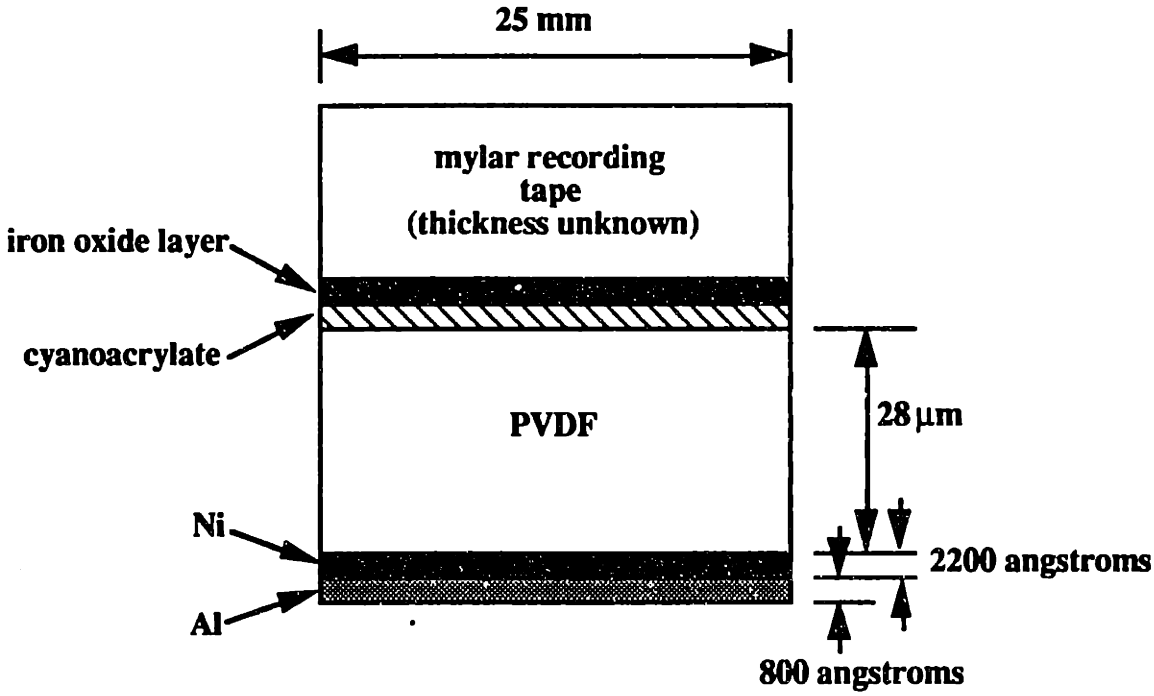

Figure 2-1. Schematic of the unit cell used for PVDF stack element construction. Adapted from Aspden and Strachan[11]. The depth dimension is 2.5 mm into the page.

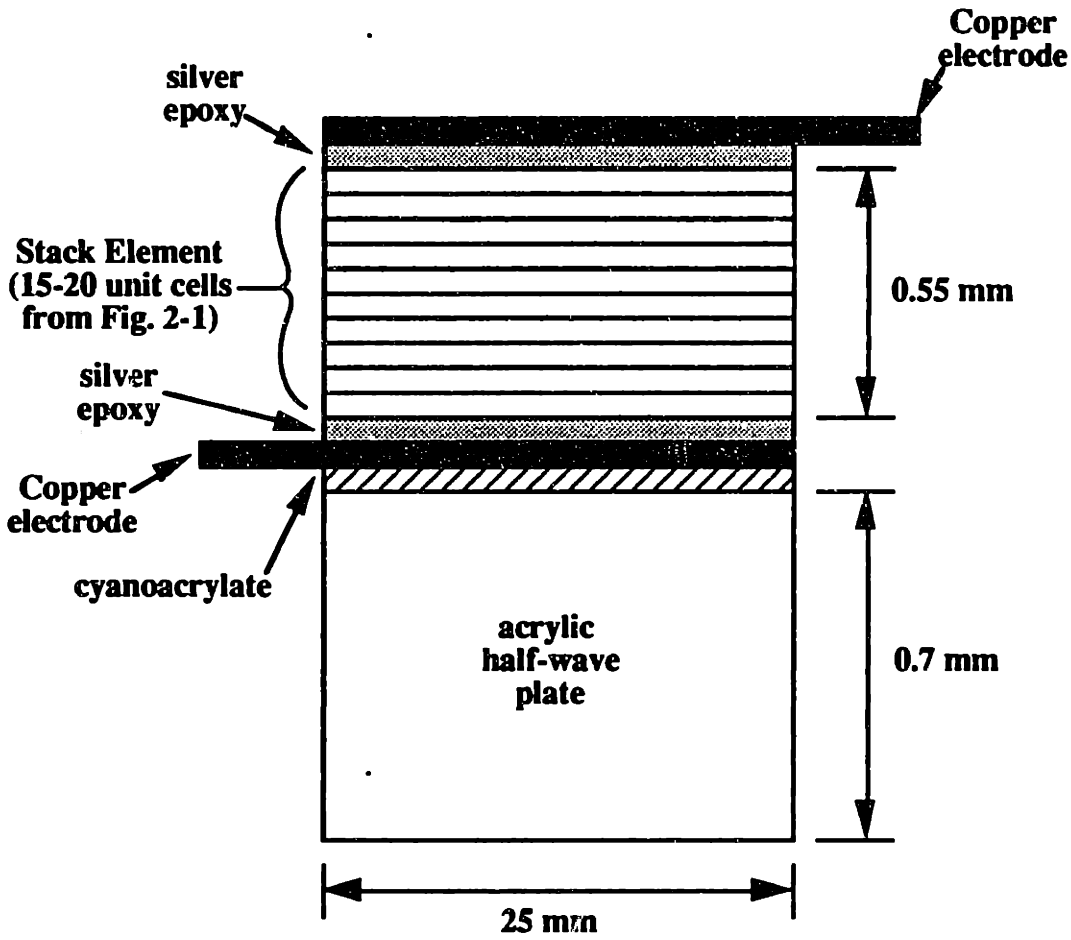

Figure 2-2. Schematic of a stack element, showing the copper electrodes and acrylic half-wave plate. Adapted from Aspden and Strachan [11]. The depth dimension is 2.5 mm into the page.

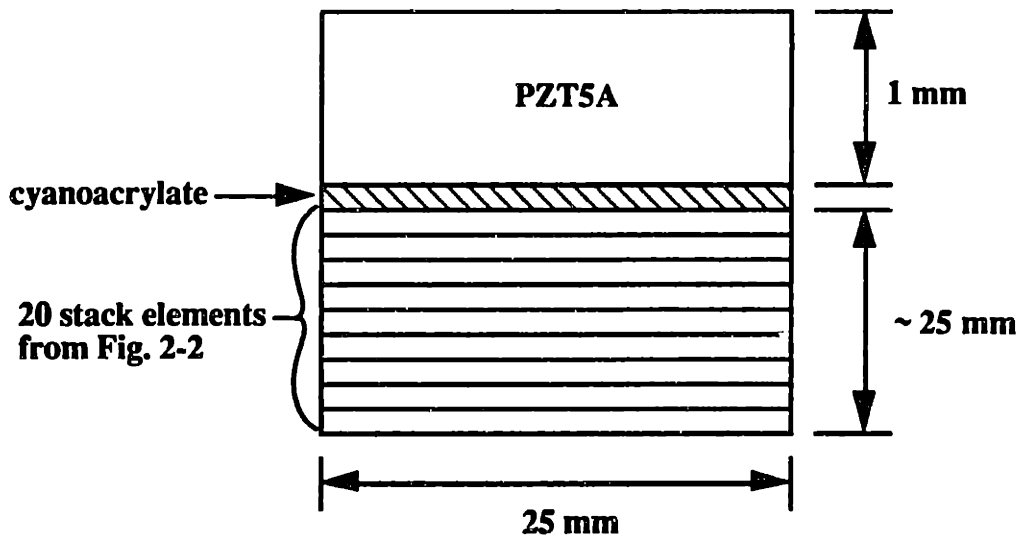

Figure 2-3. Schematic of the first prototype device stack layout, showing the PZT 5A driver. Adapted from Strachan [11]. The depth dimension is 2.5 mm into the page.

atmosphere. After the petroleum ether was allowed to evaporate completely, the surfaces were exposed to a 100% humidity atmosphere at 40 °C. The surfaces were then washed with petroleum ether. The titanate layer on the surfaces maintains a pH above 7 on the surface, allowing the ethyl cyanoacrylate adhesive to cure more easily. A teflon coated lamination jig was used in the construction of the stack. As each layer was added, a press was applied to the jig with a force of 1-6 metric tons (9800-58800 N).[10] This corresponds to a pressure of approximately 150-950 MPa in the stack, which is 2.5-16 times greater than the compressive yield stress of PVDF (~60 MPa).

The layers had a face dimension of 25 mm x 2.5 mm. The PVDF and recording tape were built up to a stack thickness of 0.55 mm. The 0.55 mm stack is half-wave resonant at 2 MHz, which matches the half-wave resonant frequency of the 1 mm thick PZT driver element. This would provide for maximum acoustic power transmission through the device at 2 MHz.[13] Several elements of this type were produced. Each element was subjected to a test voltage of 5000 V to detect errors in fabrication (electrical shorting between layers, improper bonding, etc.).[10]

Each element was then bonded to copper leads using Emerson and Cumming silver-loaded epoxy. A stack of 20 elements was assembled, with 2 MHz half-wave resonant plates of acrylic bonded between each element in the stack. A PZT type 5A element with silver electrodes of 2 MHz half-wave resonant frequency was bonded to the stack to provide acoustical drive. Each element was then connected to a triggered drive circuit. The PZT driver was pulsed with a conventional high voltage AC electrical drive. The device worked insofar as the sequential triggering of the PVDF layers was achieved using the motion of the recording tape as a trigger. This produced an amplified acoustic wave and, in effect, acted as a sonic "laser". However, the device would burn out the drive electronics when a temperature gradient was applied across the 2.5 mm dimension of the stack.[10]

Using an oscilloscope, Strachan observed the output voltage of one of the PVDF elements which was not connected to the drive circuit as the device was operated. Strachan's observation of the element output voltage versus time is shown in Figure 2-4. Strachan observed a voltage spike of several thousand volts magnitude superimposed on the PVDF element output voltage when a temperature gradient was applied across the stack. The spikes would shift phase with respect to the oscillating element output voltage by 180° when the direction of the temperature gradient was reversed. Strachan suspected that an energy conversion mechanism, possibly related to thermoelectric effects within the bimetallic coating of the PVDF film, was causing the observed voltage spike in response to an applied temperature gradient.[10]

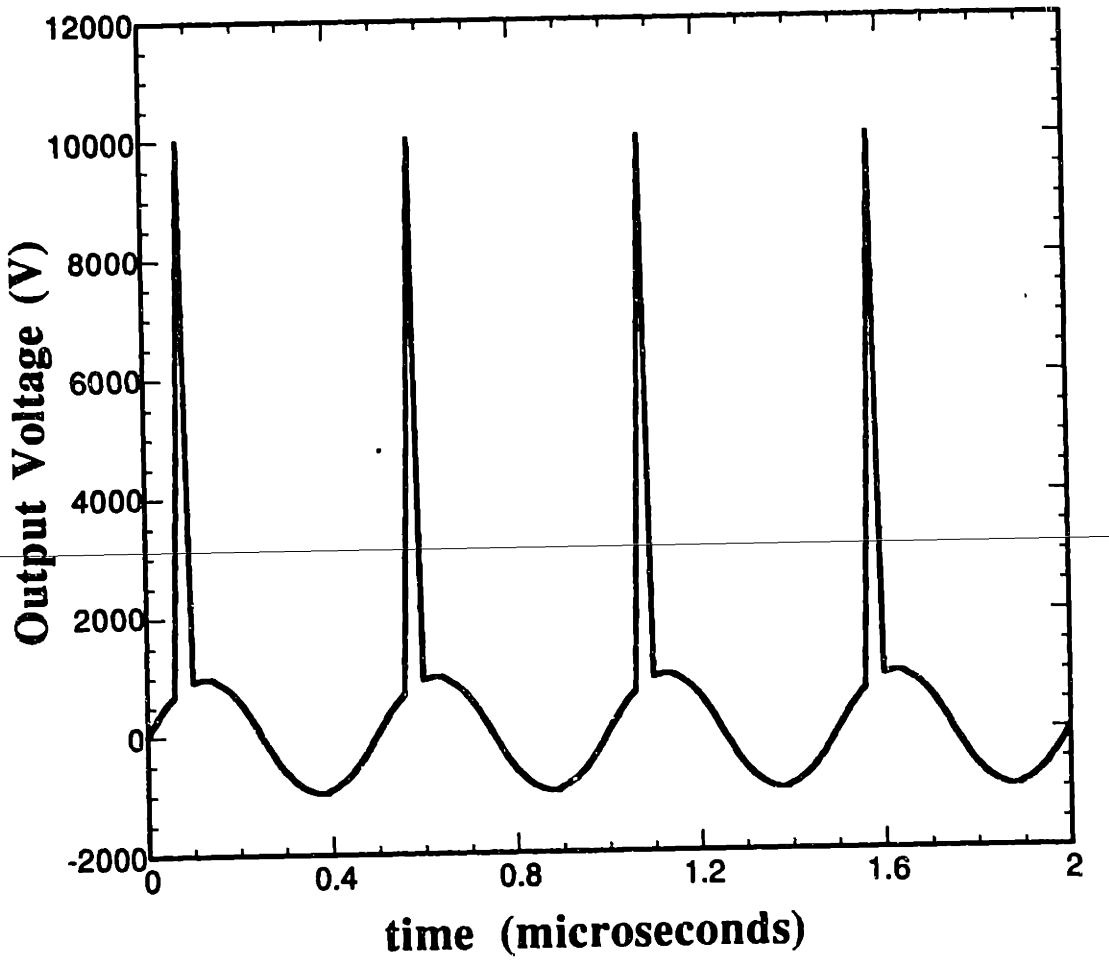

Figure 2-4. Strachan's observation of the voltage spiking from the first prototype device. The plot is constructed using simulated data. Adapted from Strachan [10].

Strachan attempted to investigate the energy conversion aspects of the device. By connecting a low impedance to the PVDF stack, Strachan found that the voltage spike was as high as 10000 volts and lasted approximately 20 nanoseconds. The voltage spike was only observed when a temperature gradient was applied across the stack. The energy of the voltage spike was proportional to the temperature gradient across the stack. The maximum energy measured in the voltage spike was 5 x 10^{-5} joules, corresponding to a temperature differential of 70 °C across the stack.[10]

The device was then connected to a power generation circuit, shown in Figure 2-5. The PZT driver and PVDF stack were connected through a transformer to a germanium diode rectifier and a DC load. The transformer served to couple the high output voltages of the PZT-PVDF stack to the low voltage rectifier circuit. A VMOS switch (GE - F15N05L) was incorporated in the PZT-PVDF circuit, and was triggered by Strachan's triggering circuit. The stack was thermally bonded to a heat sink on the lower face and an aluminum tray on the upper face to provide a temperature gradient across the stack (see Figure 2-6). When a piece of ice was applied to the upper face of the stack, the stack would self oscillate, triggering the VMOS switch at 500 kHz. A small electric motor could be operated using the DC power generated through the rectifier circuit.[10]

The circuit used to operate the device as a heat pump is shown in Figure 2-7. The PZT driver and PVDF stack were connected through a transformer to the battery circuit, containing the VMOS switch triggered by the PVDF stack and a 7.2 V battery. This circuit would also self-oscillate at 500 kHz, and would freeze liquid water into ice on the top surface. No performance or efficiency data is available for the first prototype.[11]

2.3 The Second Prototype Device

The construction of the second prototype device was similar to the first device, except the BASF mylar recording tape was not included in the PVDF stack elements and no PZT driver was incorporated into the stack. The PVDF film was coated on one side with a 400 angstrom thick Nickel layer and a 200 angstrom thick Aluminum layer. The layers had a face dimension of 30 mm x 2.5 mm. The copper electrodes were made narrower than the width of the stack (2.5 mm dimension) to decrease the heat conduction leak across the stack. The PVDF stack elements contained 15 layers of PVDF. There were 20 such elements, connected in parallel to the test circuit.[9]

A schematic of the test setup is shown in Figure 2-8. The stack was thermally bonded to a heat sink on the lower face and a aluminum plate on the upper face. A small can of water containing four 10 ohm resistance heaters was placed on the upper face of the device. The temperatures of the upper and lower face were measured using platinum

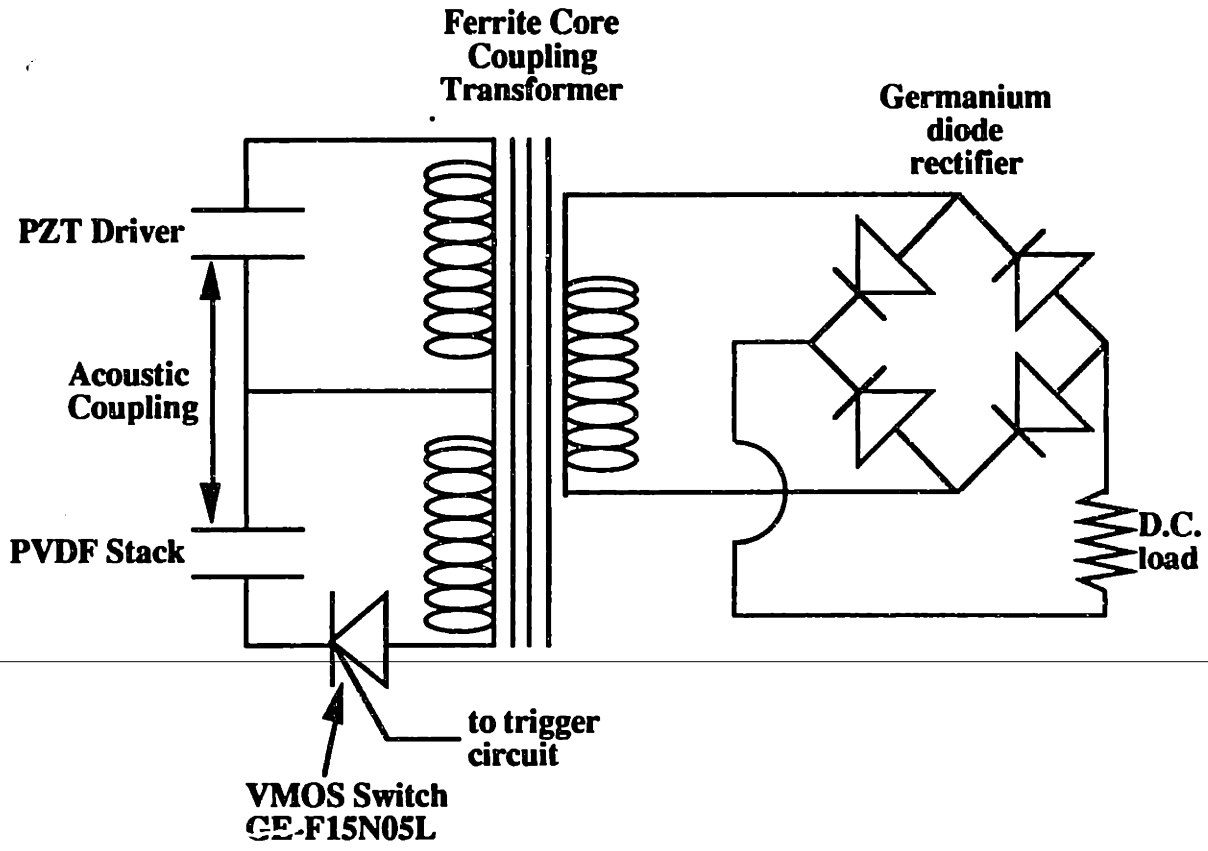

Figure 2-5. Circuit for power generation operation of the first prototype device. Adapted from Aspden and Strachan [11].

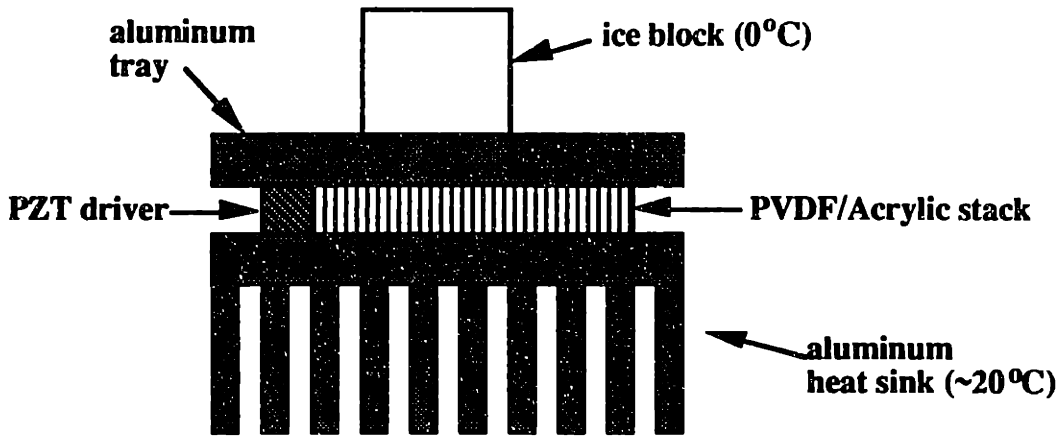

Figure 2-6. Schematic of the temperature gradient setup for the first prototype device.

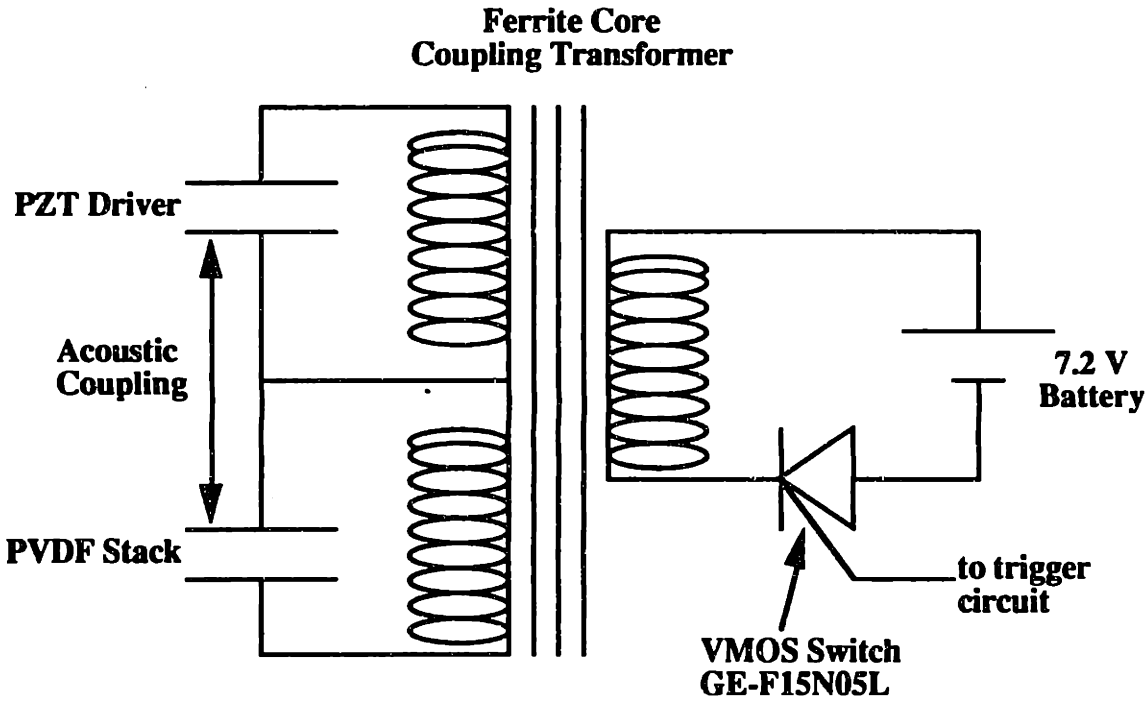

Figure 2-7. Circuit for heat pump operation of the first prototype device. Adapted from Aspden and Strachan [11].

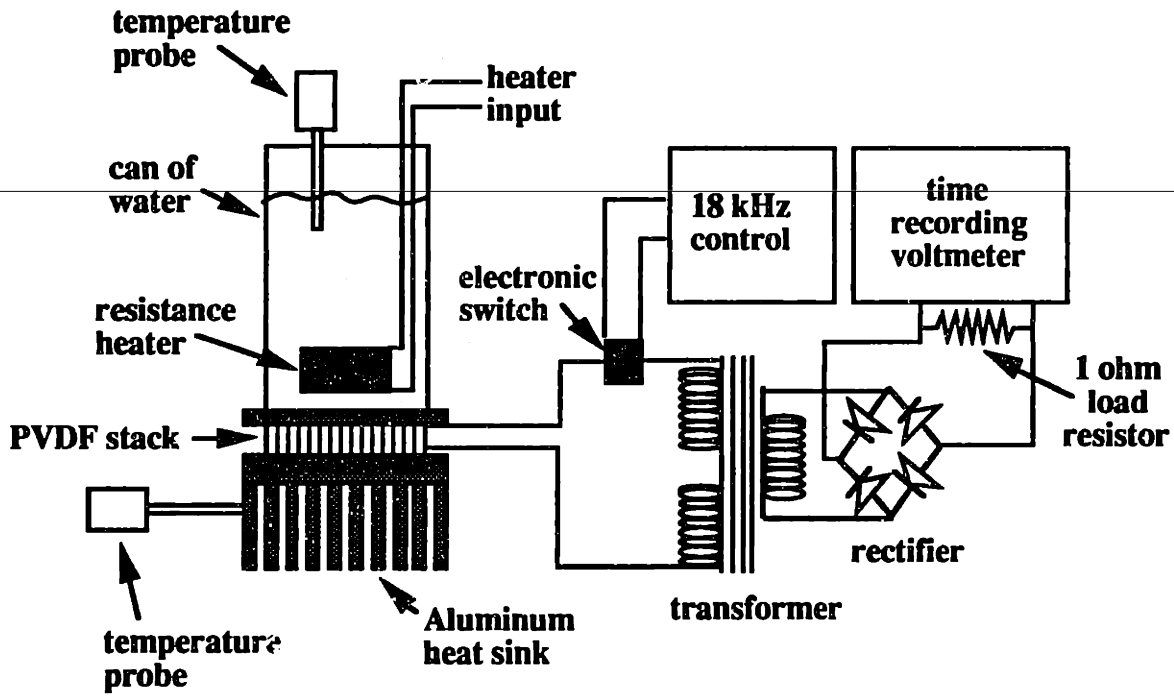

Figure 2-8. Schematic of the experimental setup for the second prototype device. Adapted from Aspden [9].

resistance probes. The PVDF stack was connected through a transformer to a rectifier circuit and a 1 ohm load resistor. The voltage across the load resistor was measured using a time recording voltmeter. The circuit was switched by a function generator operating at 18 kHz. The second prototype would not self oscillate, owing to the presence of the external frequency control. Thus, it could only be operated in the power generation mode.[9]

Tests of energy conversion efficiency were conducted using the second prototype device. The efficiency for an energy conversion device operating between two temperature reservoirs is defined as the ratio of net positive work transfer to net heat transfer from the hot-side temperature reservoir. The Carnot efficiency limit is the efficiency for a reversible cycle as limited by the Second Law of Thermodynamics, and is taken as the maximum attainable efficiency. The Carnot efficiency η_c is given by:[14]

$$\eta_c = 1 - \frac{T_C}{T_H} \tag{2-3}$$

where T_H is the temperature of the hot-side reservoir and T_C is the temperature of the cold-side reservoir.

Operating at a hot side temperature of 47.5 °C and a cold side temperature of 20.8 °C, the net heat input for the second prototype was 3.34 watts and the net power output into the 1 ohm load was 0.202 watts. This corresponds to an efficiency of 6.0%. The Carnot efficiency limit η_c for the hot- and cold-side temperatures is calculated to be 8.3%. Therefore, the efficiency of the second prototype device was 73% of the Carnot efficiency limit. This measure of device efficiency did not include the power required for the electronic switch, which was controlled by, and drew a negligible amount of power from, an external function generator.[9]

2.4 The Third Prototype Device

The third prototype device was constructed using stack elements that had been originally been assembled for use in the first prototype device. The PVDF material was therefore the same as that used in the first prototype device and the PVDF stack included interleaved layers of mylar recording tape. A PZT driver was also incorporated into the PVDF stack. The device circuitry and heat sink setup were similar to those of the first prototype, shown in Figures 2-5 through 2-7. The third prototype could operate in both the power generation and heat pump modes, and tests were performed to characterize the device performance for each mode of operation.[11]

In the power generation mode, a frozen block of 6 mL of water (T_C = 0 °C) was melted on the upper surface of the device, while the lower surface was held at room temperature (T_H = 26.5 °C) through contact with a heat sink. Melting of the ice required 9 minutes. The heat throughput of the device was calculated to be 3.7 watts, and the electrical power generated was measured to be 0.15 watts. This corresponds to 47% of the Carnot efficiency limit.[6]

For a device operating as a heat pump, a measure of device efficiency is given by the *coefficient of performance*, or COP, which is defined as the ratio of net heat transfer from the cold-side temperature reservoir to net work input. The second law limit on the COP for a reversible cycle, COP_{rev}, is given by:[14]

$$COP_{rev} = \frac{1}{T_H/T_C - 1} \tag{2-4}$$

When operated in the heat pump mode, the device was used to freeze 3 mL of water in 73 seconds. The cooling power was calculated to be 13.7 watts, and the electrical power input was measured to be 6.3 watts. The temperature difference was measured to be 26 °C, ignoring any temperature gradient in the frozen water layer. This corresponds to a COP of 2.17, or 21% of the reversible limit.[6]

The operation of the third prototype was demonstrated in a video produced by Aspden and Strachan.[15] In the demonstration, the device was used to run a DC motor using a small block of ice. The device was also operated in the power generation mode using warm water (T = 63 °C). A 7.2 V battery was then attached to the device and liquid water was frozen on the upper surface of the device. Switching between the power generation and heat pump modes and vice versa was achieved by exchanging the rectifier circuit leads between the DC motor and the battery.

2.5 Aspden and Strachan's Explanation for Device Operation

Both Strachan and Aspden suspected that a thermoelectric effect in the bimetallic coatings of the PVDF layers was involved in the energy conversion operation of the device. Aspden proposed several mechanisms related to thermoelectric effects within the metallic coatings to explain the energy conversion effect. No satisfactory explanation has yet come to light. Strachan performed some simple experiments to test some of these proposed mechanisms. An overview of these explanations and experiments is given here for completeness. An analysis of DC thermoelectricity and magnetic field effects in the Ni-Al bimetallic coating of the PVDF film is also presented.

2.5.1 Thermoelectric Effects

The three thermoelectric effects: the Seebeck effect, the Peltier effect, and the Thomson effect, are well known to allow reversible conversion of electrical energy into thermal energy.

The Seebeck effect results from maintaining two junctions between two dissimilar conductors at different temperatures. A voltage across a break in one of the two conductors is observed which is proportional to the temperature difference. The voltage produced is dependent upon the two conductors used.[16]

The Peltier effect is observed as the liberation or absorption of thermal energy at the junction of two dissimilar conductors when an electrical current is passed through the junction. Conversely, by liberating or absorbing heat at a junction of two dissimilar conductors, an electrical current is induced through the junction. The relationship between the direction of current flow and the direction of thermal energy flow at the junction is dependent upon the two conductors used.[16]

The Thomson effect is observed as volumetric heat absorption or liberation in a conductor through which an electrical current flows along a temperature gradient. The heat absorption or liberation is independent of the irreversible Joule heating. The relationship between the direction of current flow, the direction of positive temperature gradient, and the sign of the heat generation is related to the specific conductor used.[16]

2.5.2 Aspden's Explanation of the Thermoelectric Effects in the PVDF Stack

Aspden's hypothesis for the operation of the prototype devices is described in several publications, with several notable discrepancies between each version of the hypothesis.[3-6] The author's best understanding of Aspden's hypothesis is presented here.

The PVDF stacks used in all three of the prototype devices contain several hundred bimetallic coatings of aluminum and nickel, all oriented perpendicular to the AC excitation and parallel to the direction of the temperature gradient. These bimetallic layers, along with the PVDF dielectric material, form approximately 15-20 capacitors connected in series in each stack element. The stack elements are then connected in parallel to the drive circuit.

When a temperature gradient is established across the bimetallic layers, the Seebeck effect promotes transverse current flow in one direction in the aluminum layer, and in the opposite direction in the nickel layer. A circulating DC thermoelectric current is established in the bimetallic layers in this way (see Figure 2-9). Peltier cooling and heating at either side of the stack results from the current flow through the aluminum-nickel junction.

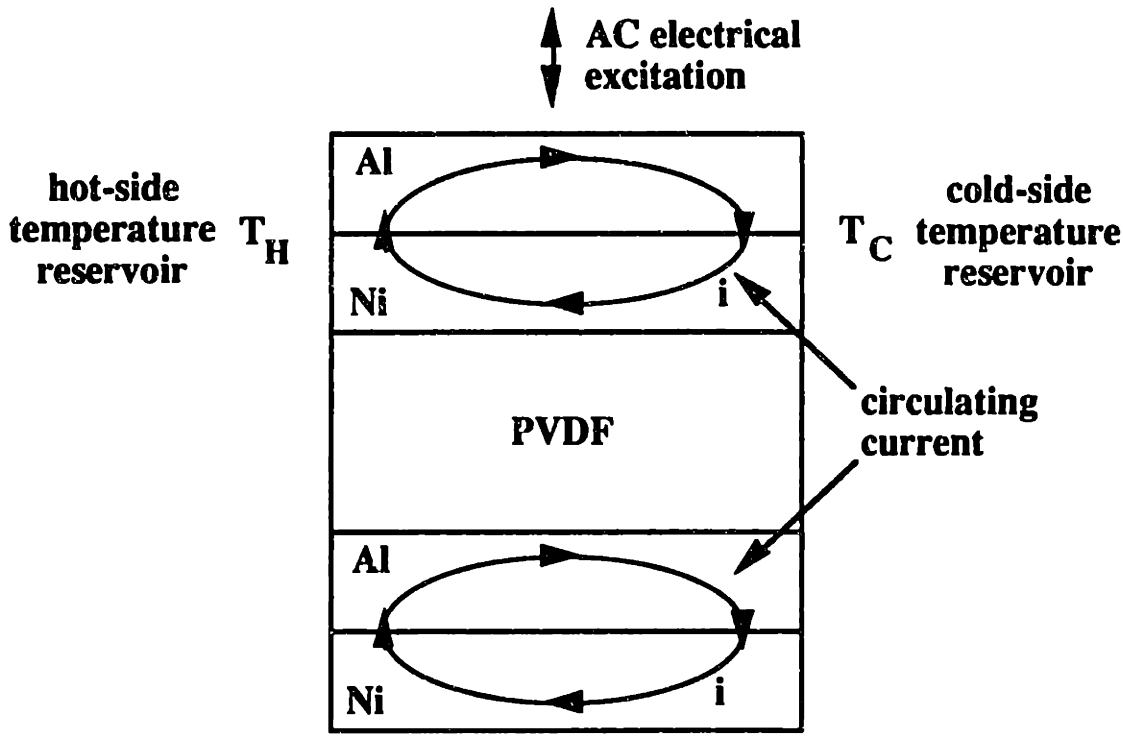

Figure 2-9. Schematic of circulating current flow in the bimetallic layer, with AC current superimposed, as described by Aspden. Adapted from Aspden [3].

When an AC current perpendicular to the bimetallic layer is superimposed on this circulating current, the junction currents are now pulsed at the frequency of the AC excitation. Aspden feels that over a full AC cycle, a positive net electrical power is produced by the AC charging and discharging of the capacitor formed by the bimetallic layers and the PVDF dielectric material. This may be due to the AC behavior of the junction current locations, the effect of temperature on the thermoelectric coefficients of aluminum and nickel, and/or the Nernst effect (relating a temperature gradient to both electric and magnetic fields in a conductor). It is unclear from Aspden's explanation exactly how energy conversion is realized in the prototype devices.[3-6]

2.5.3 Experiments Performed by Strachan to Test the Aspden Hypothesis

In order to test some of the assertions made by Aspden regarding the operation principle of the prototype devices, Strachan performed a series of simple experiments to observe the circulating current postulated by Aspden. By placing a Hall Effect sensor very close to a single PVDF film, across which a temperature gradient could be applied, Strachan hoped to measure the magnetic field produced by the circulating currents in the bimetallic layer related to the presence of a temperature gradient and periodic mechanical excitation.[11]

A schematic of the experimental setup is shown in Figure 2-10. A single film of 110 μm thick PVDF, coated with aluminum and/or nickel layers of various thicknesses, was used. The PVDF film was clamped in a vise with a PZT driver and an acrylic layer. A very small Hall Effect sensor was placed against the stack at the location of the metal layer(s) to measure the magnetic field generated by circulating thermoelectric currents within the metallic layer(s), as proposed by Aspden. A temperature gradient was applied in the direction parallel to the side on which the Hall effect sensor was placed.[11]

The tests were run by applying a 21 kHz AC voltage to the PZT driver and measuring the output of the Hall sensor as a function of distance from the stack and PZT driver voltage. With the film isothermal (no temperature gradient applied), no magnetic field was detected for any of the metallic layer combinations used. Using a bimetallic coating of 12.5 μm nickel and 3 μm aluminum, with a temperature gradient applied to the stack, a periodic magnetic field of approximately 0.75-1.0 gauss was observed. The field strength varied at the same frequency as the PZT drive, but lagged the drive voltage by 90°. The field increased with PZT driver voltage, and decreased rapidly with increased distance from the stack. Using a 25 μm thick coating of nickel, the same effect was observed with a temperature gradient applied, but the measured magnetic field was significantly lower. No magnetic field was observed when aluminum-coated PVDF was

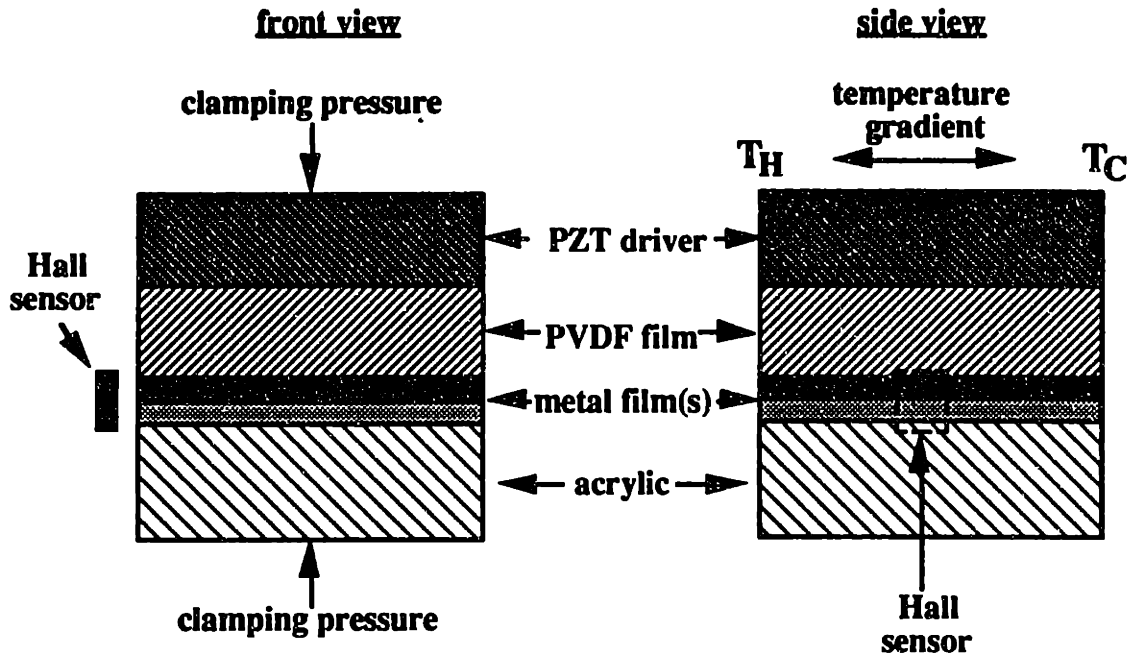

Figure 2-10. Schematic of Strachan's magnetic field measurement test setup. Adapted from Aspden and Strachan [11].

used. When the bimetallic-coated PVDF was compressed in the temperature gradient, with no PZT drive, a DC magnetic field was detected.[11]

The observation of a DC magnetic field associated with an applied temperature gradient across the Ni-Al bimetallic coating is consistent with well known thermoelectric effects. An analysis of the circulating DC thermoelectric currents and magnetic field effects in the Ni-Al bimetallic coating is given in section 2.5.5. The observation of an AC magnetic field associated with an AC stress condition and a DC temperature gradient is anomalous in that it cannot be explained by conventional thermoelectricity. The results of these experiments, although somewhat sketchy, do provide some support for Aspden's claims of AC circulating thermoelectric currents in the bimetallic films. However, the test procedures are not rigorous enough to provide any conclusive results as to the operation of the prototype devices.

2.5.4 Analysis of a DC Ni-Al Thermoelectric Converter

For a Ni-Al thermocouple operating as a heat pump (refrigerator), the maximum temperature difference that can be supported, ΔT_{max}, is given by[17]

$$\Delta T_{\max} = 2T_{ave}\frac{\sqrt{1+ZT_{ave}}-1}{\sqrt{1+ZT_{ave}}+1} \tag{2-5}$$

where T_{ave} is the mean absolute temperature and Z is the figure of merit for the thermoelectric device, given by[17]

$$Z = \frac{(S_{Ni}-S_{Al})^2}{\left[(k_{Ni}\rho_{Ni})^{1/2}+(k_{Al}\rho_{Al})^{1/2}\right]^2} \tag{2-6}$$

where S_{Ni}, S_{Al}, k_{Ni}, k_{Al}, ρ_{Ni}, and ρ_{Al} are the absolute thermopowers, thermal conductivities, and bulk resistivities of Ni and Al, respectively.

The maximum achievable COP for a thermoelectric heat pump operating at a temperature difference ΔT, COP_{max}, is given by[17]

$$COP_{\max} = \frac{T_{ave}\left(\sqrt{1+ZT_{ave}}-1\right)}{\Delta T\left(\sqrt{1+ZT_{ave}}+1\right)} - 1/2 \tag{2-7}$$

Using S_{Ni} and S_{Al} values of -19.5 and 1.66 μV/K, respectively,[2] k_{Ni} and k_{Al} values of 91 and 237 W/mK, respectively,[18] and ρ_{Ni} and ρ_{Al} values of 0.068 and 0.028 μΩm, respectively,[19] and a T_{ave} value of 283 K (10 °C), ΔT_{max} is calculated to be 0.48 K. The COP_{max} that corresponds to this ΔT_{max} is calculated to be 0.007.

Strachan reported a COP of 2.17 at a ΔT of 26 K in the third prototype device.[6] These calculations clearly show that DC thermoelectric effects cannot explain the operation of the prototype devices.

2.5.5 Analysis of the Circulating DC Thermoelectric Currents and Magnetic Field Effects in the Bimetallic Layers

The model of the Ni-Al bimetallic PVDF coating for the analysis of the DC thermoelectric currents is shown in Figure 2-11. The dimensions are the same as those used in the construction of the first prototype device. It is assumed that no shorting between the layers occurs - i.e. the Ni-Al junctions are located at either end of the conduction path. The electromotive force ε is given by[2]

$$\varepsilon = (S_{Ni} - S_{Al})\Delta T \tag{2-8}$$

where ΔT is the temperature difference across the two junctions. The closed circuit current i is given by

$$i = \frac{\varepsilon}{R_{tot}} \tag{2-9}$$

where R_{tot} is the total resistance around the circuit, given by

$$R_{tot} = \frac{\rho_{Ni} l}{A_{Ni}} + \frac{\rho_{Al} l}{A_{Al}} \tag{2-10}$$

where A_{Ni} and A_{Al} are the cross-sectional areas of the nickel and aluminum layers, respectively, and l is the length of the conduction path (2.5 mm). Using a ΔT of 70 K, i is the calculated to be 18 mA.

The magnetic field inside the nickel layer, B, assuming planar current flows located at the center of the nickel and aluminum layers, is given approximately by[19]

$$B \cong \frac{\mu_{Ni}\mu_0 i}{a} \qquad (2\text{-}11)$$

where μ_{Ni} is the relative permeability of nickel, μ_0 is the permeability of free space (μ_0 = 1.26 x 10^{-6} Tm/A), and a is the width of the conduction path (25.4 mm). Using a μ_{Ni} value of 300 for magnetic field strengths of less than ~10 gauss,[20] B is calculated to be approximately 2.6 gauss. This shows order of magnitude agreement with the magnetic field measurements performed by Strachan, although it should be noted that his measurements were performed outside the Nickel layer, he used thicker metal films, and the magnitude of the temperature gradient he used is not known. Also, the thermoelectric currents and observed magnetic field are DC effects (associated with a DC temperature gradient). These effects cannot explain the AC magnetic field (supposedly associated with an AC thermoelectric current) observed by Strachan.

2.6 Other Possible Explanations for the Prototype Device Operation

It has been postulated by Y. Kucherov [21] that some of the temperature gradient effects on the bimetallic coated PVDF film, resulting in AC and DC electrical effects, may be due to a chemical reaction occurring between uncompensated radicals in the PVDF and the metallic films. These reactions could be initiated and/or enhanced by the presence of the temperature gradient and/or electrical excitation of the PVDF film. Also, considering the complex surface treatment and cyanoacrylate adhesive used by Strachan in constructing the stack, an electrochemical reaction related to some or all of the substances used could result in some of the observed behavior.[10]

PVDF is pyroelectric - the electric polarization of the film is dependent on the temperature of the film. PVDF film is also piezoelectric - the strain condition in the film affects the electric polarization of the film, and vice versa. When the stack is excited by a PZT mechanical driver, in the presence of a temperature gradient, and is connected as an electrically capacitive layer, a combination of these pyroelectric and piezoelectric effects could possibly result in a "thermo-mechano-electric" effect, which could act in an energy conversion mode. The piezoelectric, pyroelectric, and dielectric properties of PVDF will be explored in greater detail in the following chapter.

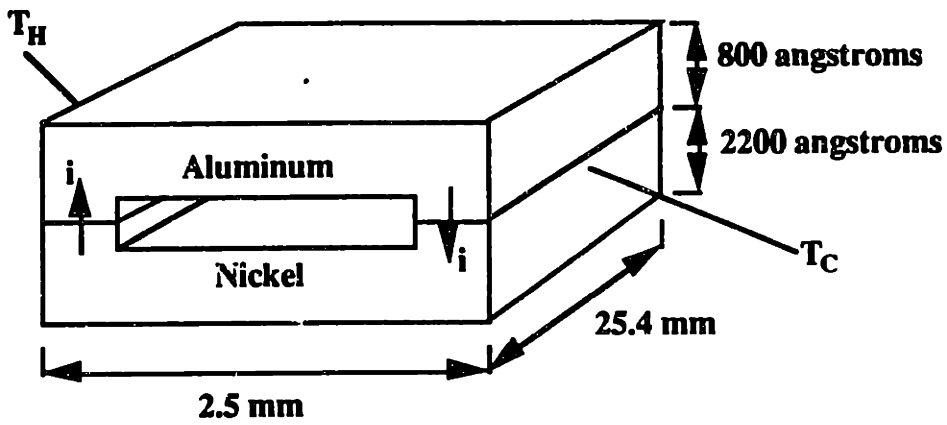

Figure 2-11. Model of the Al-Ni bimetallic PVDF coating for the analysis of the circulating DC thermoelectric currents.

3. PVDF - MATERIAL ASPECTS

3.1 Introduction

Although Aspden and Strachan's explanations for the energy conversion operation of the three prototype devices considers only thermoelectric effects in the bimetallic coatings of the PVDF layers in the stack, PVDF itself exhibits many interesting properties that may or may not be significant in the energy conversion operation of the prototype devices. Specifically, it is both pyroelectric and piezoelectric. The details of these properties, as well as some other material aspects of PVDF film, will be described in this chapter.

3.2 General Properties of PVDF

Polyvinylidene fluoride is a long chain semicrystalline polymer of the repeat unit (CH_2-CF_2). It has similar mechanical properties to other rigid engineering plastics, with good chemical resistance and excellent electrical properties. PVDF is tough, lightweight, transparent, and flexible. It is readily manufactured in sheet form and can be fabricated in complex shapes for specific applications.[22,23]

PVDF exhibits a very high net dipole moment. There are three distinct crystalline forms of the polymer, the relative prevalence of which is dependent on processing. The most desirable, in terms of exploiting the piezoelectric and pyroelectric nature of the material, is the polar "beta" phase. The beta phase is produced by stretching the film at

temperatures below 80 °C. The beta phase polymer must be "poled," a process that consists of exposing the polymer to an electric field of 5-10 x 10^7 V/m at elevated temperatures (80-110 °C) for an extended period of time (~1-2 hours).[24-26]

The effect of temperature on the decay of pyroelectric and piezoelectric activity of PVDF has been extensively studied. No significant decay is observed for operating at temperatures up to 70 °C for short periods of time.[22] An operating temperature of 100 °C is considered the upper limit for most PVDF applications.[24]

A summary of many of the mechanical and electrical properties of PVDF is given in Table 3-1. These data are adapted from several sources,[22-25,27] and either a representative value or a range is given for each property.

3.3 Pyroelectric Properties of PVDF

The pyroelectric coefficient relates the change in polarization of a material to a change in temperature.[28] For PVDF, the pyroelectric coefficient has been measured to be 5-25 x 10^{-6} C/m^{2}K at 20 °C.[22,24,25] The pyroelectric coefficient is temperature dependent. Data from a study performed by Burkard and Pfister [29] of the temperature dependence of the pyroelectric coefficient of PVDF is shown in Figure 3-1.

Pyroelectricity in PVDF is due to two mechanisms. The first, known as primary pyroelectricity, is a change in a polarization due to a change in temperature with constant sample dimensions. The second, known as secondary pyroelectricity, is a change in polarization due to variation of sample dimension with changing temperature, related to the thermal expansion of the film. Secondary pyroelectricity has been found to contribute up to 50% of the total pyroelectric coefficient.[25,28] The pyroelectric effect is reversible, in that the capacitive charge corresponding to a given temperature is independent of the rate of heating or cooling.[28]

PVDF is often used as a substrate for infrared detectors. Pyroelectric infrared detectors made using PVDF consist of an electroded PVDF film coated on one side with an absorbing layer of graphite or gold-black. A change in temperature due to absorption of incident radiant energy is detected as an electrical output at the device electrodes.[24]

3.4 Piezoelectric Properties of PVDF

PVDF is anisotropic - the stretching and poling operations produce three distinct axes. Therefore, a coordinate system is required in specifying the piezoelectric constants, which relate electrical polarization to mechanical stress. The coordinate system used is shown in Figure 3-2. The stretch direction is denoted by the (1) axis, the transverse direction by the (2) axis, and the polarization direction by the (3) axis.

Density	1760 kg/m^3
Thermal Conductivity	0.1-0.25 W/mK
Thermal Expansion Coefficient	80-140 x 10^{-6} /K
Specific Heat	1.3 kJ/kgK
Young's Modulus	1-3 x 10^9 Pa
Poisson's Ratio	0.31
Tensile Strength	160-300 x 10^6 Pa (stretch direction) 30-55 x 10^6 Pa (transverse direction)
Compressive Strength	55-70 x 10^6 Pa
Dielectric Constant (@ 1 MHz)	12
Dielectric Strength	100 kV/mm
Dissipation Factor (@ 1 MHz)	0.018
Velocity of Sound	2200 m/s

Table 3-1. General properties of PVDF film. From *KYNAR Piezo Film Technical Manual* [22] Inderherbergh [23], Davis [24], Kepler and Anderson [25], and Park and Yoshino [27].

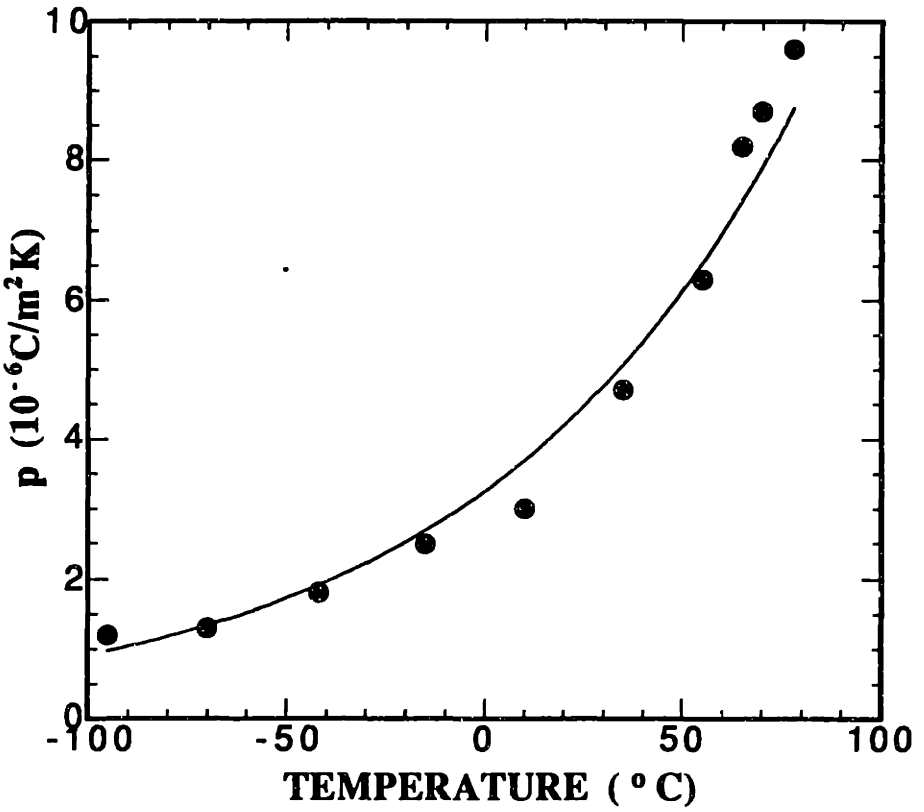

Figure 3-1. Pyroelectric coefficient *p* of PVDF versus temperature. Adapted from Burkard and Pfister [29].

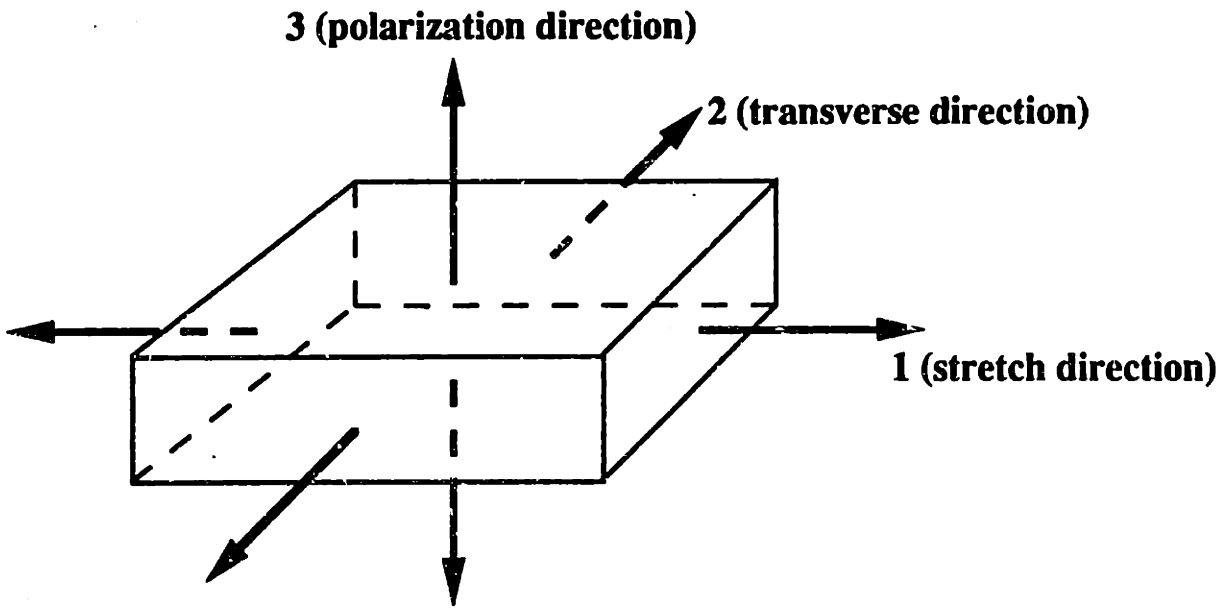

Figure 3-2. Coordinate system used for identifying the piezoelectric constants of PVDF.

Numbered subscripts identify the vector and tensor directions. The first numerical subscript identifies the axis of polarization or applied electric field. The second numerical subscript identifies the axis of mechanical stress or strain. Positive electrical action results in an increase in polarization. Positive mechanical action is tensile. The "d" and "g" constants are defined as follows:

d_{31} - is the ratio of the mechanical strain in the (1) direction to the applied electric field in the (3) direction when the film is unconstrained in the (2) and (3) directions.

d_{32} - is the ratio of the mechanical strain in the (2) direction to the applied electric field in the (3) direction when the film is unconstrained in the (2) and (3) directions.

d_{33} - is the ratio of the mechanical strain in the (3) direction to the applied electric field in the (3) direction when the film is unconstrained in the (1) and (2) directions.

g_{31} - is the ratio of the electric field developed in the (3) direction to the applied mechanical stress applied in the (1) direction.

g_{32} - is the ratio of the electric field developed in the (3) direction to the applied mechanical stress applied in the (2) direction.

g_{33} - is the ratio of the electric field developed in the (3) direction to the applied mechanical stress applied in the (3) direction.

The "d" constants are in units of strain per electric field strength, [m/m/V/m], or [m/V]. The "g" constants are in units of electric field strength per mechanical stress, [V/m/N/m^2], or [Vm/N].

The electromechanical coupling constants, or "k" constants, give a measure of the energy conversion efficiency for a piezoelectric material. The square of the coupling constant, k_{ij}^2, is defined as the transformed energy divided by the total energy input between the (i) electrical axis and the (j) mechanical axis.

The piezoelectric constants are related by the following approximation (which is only an order of magnitude estimate):[22]

$$k_{ij}^2 \cong d_{ij} g_{ij} c_{jj} \tag{3-1}$$

where c_{jj} is the elastic constant of PVDF along the mechanical axis j. The piezoelectric constants for PVDF are given in Table 3-2. Equation (3-1) applies only to the tensile piezoelectric and coupling constants. Piezoelectric shear constants (d_{15}, d_{24}, k_{15}, k_{24}) for PVDF are also known.[25]

The piezoelectric constants of PVDF are frequency dependent. Measurements performed by Schewe [30] show that d_{31} for PVDF decreases from 28 x 10^{-12} V/m at 10 Hz to 17.5 x 10^{-12} V/m at 25 kHz. The piezoelectric constants are also temperature dependent. Representative data from a study performed by Ohigashi [31] is shown in Figure 3-3.

3.5 Measurement of the Dielectric Constant and Dissipation Factor of PVDF versus Frequency

Aspden's hypothesis for the operation of the prototype devices involves an AC effect superimposed on the circulating DC thermoelectric currents in the bimetallic coatings of the PVDF layers. Aspden predicts the presence of a transverse AC magnetic field due to this circulating current, which Strachan has supposedly confirmed by experiment (see section 2.5).[11]

Although Aspden's hypothesis predicts that the transverse magnetic field is only an artifact of the thermoelectric effects in the bimetallic coatings, the magnetic field itself may provide the necessary "symmetry breaking" condition to establish the direction of heat pumping or electrical power generation relative to the direction of electrical excitation in the prototype devices. That is, the magnetic field is the only electrical phenomenon oriented in the transverse direction of the PVDF layers. Therefore, it may contribute to the establishment of the direction of entropy flow in the thermoelectric device.

The purpose of this experiment is to determine if the presence of a transverse magnetic field affects the dielectric constant or dissipation factor of PVDF. If an effect exists, it could possible be involved in the energy conversion aspects of the Strachan prototype devices. Measurements of the relative dielectric constant and dissipation factor of PVDF are performed from 1-100 kHz using an AC capacitance bridge. These measurements are repeated with a magnetic field imposed in the stretch direction of the PVDF film.

d_{31}	14-28 x 10^{-12} V/m
d_{32}	1.5-4 x 10^{-12} V/m
d_{33}	(-12) - (-35) x 10^{-12} V/m
g_{31}	170-216 x 10^{-3} Vm/N
g_{32}	19-30 x 10^{-3} Vm/N
g_{33}	(-300) - (-500) x 10^{-3} Vm/N
k_{31}	12% (@ 1 kHz)
k_{32}	1% (@ 1 kHz)
k_{33}	19% (@ 1 kHz)

Table 3-2. Piezoelectric constants of PVDF film. From *KYNAR PIEZO FILM TECHNICAL MANUAL* [22], Davis [24], and Kepler and Anderson [25].

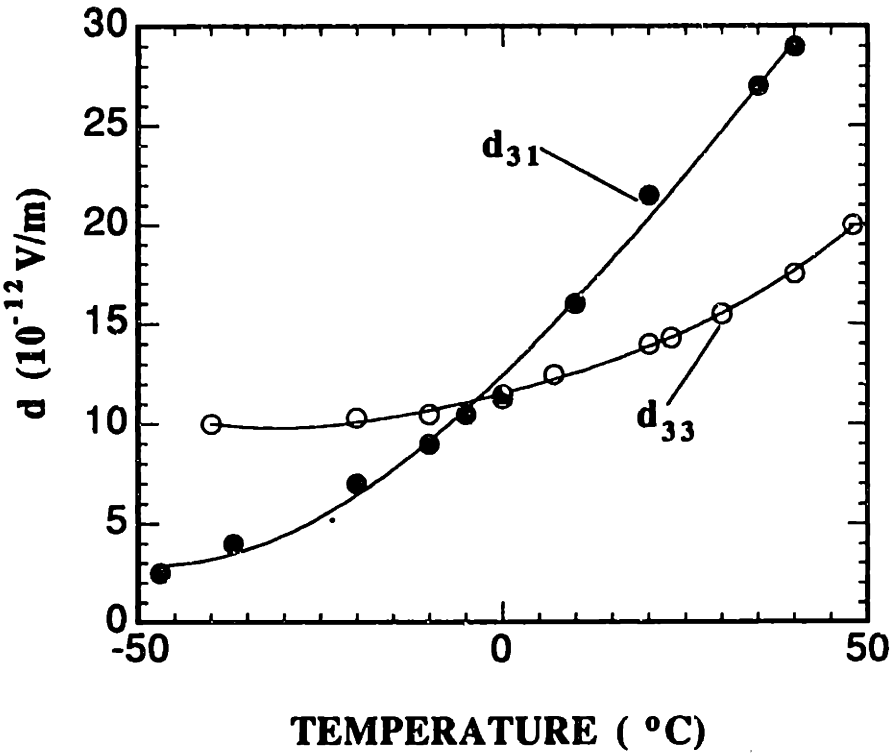

Figure 3-3. Temperature dependence of PVDF piezoelectric constants. Adapted from Ohigashi [31].

3.5.1 Experimental Procedure

A 1 cm x 4 cm sample of PVDF from Pennwalt Corp., 28 μm thick and electroded on both sides, is used. The metallization is removed (using a standard pencil eraser) from a portion of both sides to produce a 1 cm^2 capacitive area, with a small tab for electrical connection on each side. The accuracy of the capacitive area measurement is estimated to be ± 5%. A schematic diagram of the PVDF sample is shown in Figure 3-4.

A schematic of the experimental setup is shown in Figure 3-5. The PVDF sample is clamped on both ends with insulated jaws, and the clamp assembly is enclosed in a grounded aluminum box to shield the setup from external noise. Connections are made to the PVDF electrodes using copper shielded coaxial cable and silver loaded epoxy. The sample leads are connected to a General Radio model 1615-A capacitance bridge, which is used to measure the capacitance and dissipation factor of the sample. The bridge is balanced using an EG&G Princeton Applied Research model 128A lock-in amplifier. A Hewlett Packard model 202C low frequency oscillator is used to provide the drive signal, which is monitored using a Tektronix model 475 oscilloscope. All connections are made using shielded coaxial cable.

To provide a transverse megnetic field, a large General Electric ALNICO magnet is situated such that the sample and clamp assembly is located between the pole pieces of the magnet (see Figure 3-6). The magnetic field between the pole pieces is measured to be 1.17 x 10^3 gauss using a F.W. Bell model 4048 gauss meter.

Measurements of the sample capacitance and dissipation factor are performed over the frequency range from 1-100 kHz at voltages ranging from 1-40 V peak-to-peak. These measurements are performed with and without the magnetic field imposed in the transverse direction. The precision of the capacitance measurements is estimated to be ±0.1% and the precision of the dissipation factor measurements is estimated to be ±1%.

3.5.2 Results and Discussion

The relative dielectric constant, ε, is derived from the capacitance measurement using the formula:

$$\varepsilon = \frac{Cd}{\varepsilon_0 A} \tag{3-2}$$

where C is the measured capacitance, d is the film thickness, A is the capacitive area, and ε_0 is the permittivity of free space (ε_0 = 8.854 x 10^{-12} Farad/m). The accuracy of

the dielectric constant measurements is estimated to be ±5%, due mainly to uncertainty in the capacitive area A.

The measured dielectric constant and dissipation factor versus frequency at a drive voltage of 10 V peak-to-peak, with and without the imposed transverse magnetic field, are shown in Figures 3-7 and 3-8. Fairly good agreement with measurements performed by Andreev *et al.* [32] is observed. No effect of the transverse magnetic field on the dielectric constant or dissipation factor is observed. Also, no effect of drive voltage on the measured dielectric constant or dissipation factor is observed.

The dissipation factor of PVDF is highly temperature dependent. Figure 3-9 shows results obtained by Andreev *et al.* [32] relating the dissipation factor to temperature at 1 kHz and 1 MHz.

3.5.3 Conclusions

The dielectric constant and dissipation factor of PVDF are measured in the frequency range from 1-100 kHz. The measurements show fairly good agreement with previously published data. No dependence of the dielectric constant or dissipation factor on drive voltage or transverse magnetic field is observed.

3.6 The Role of PVDF in the Operation of the Strachan Prototype Devices

The pyroelectric and piezoelectric properties of PVDF relate thermal and mechanical action to electrical action. The temperature dependence of these properties, along with temperature dependence of the dielectric properties, is also involved in coupling thermal and mechanical action to electrical action. Some or all of these properties may be involved in a possible "thermo-mechano-electrical" energy conversion action of the PVDF stack in the Strachan prototype devices. However, the nature of such a mechanism is not well understood.

No effect of a transverse magnetic field on the dielectric properties of PVDF is observed. However, this does not dismiss the mechanisms described by Aspden as possible explanations for the prototype device operation. In the next chapter, an experiment designed to test for energy conversion effects in a single layer of PVDF will be described.

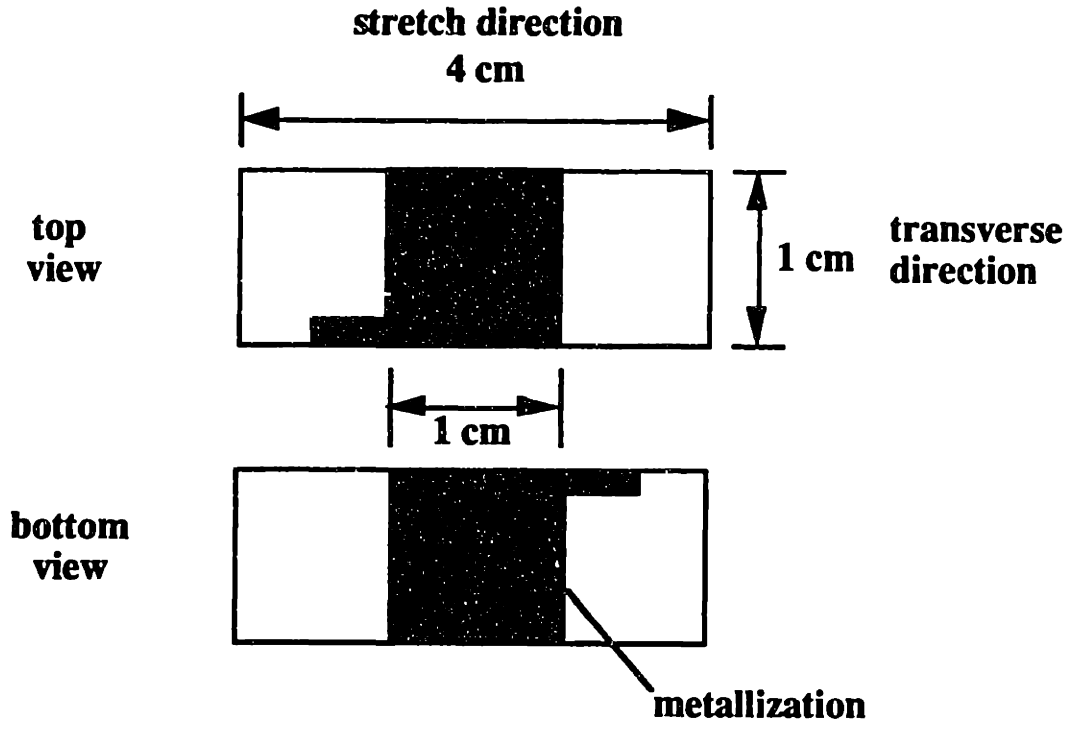

Figure 3-4. A schematic diagram of the PVDF sample.

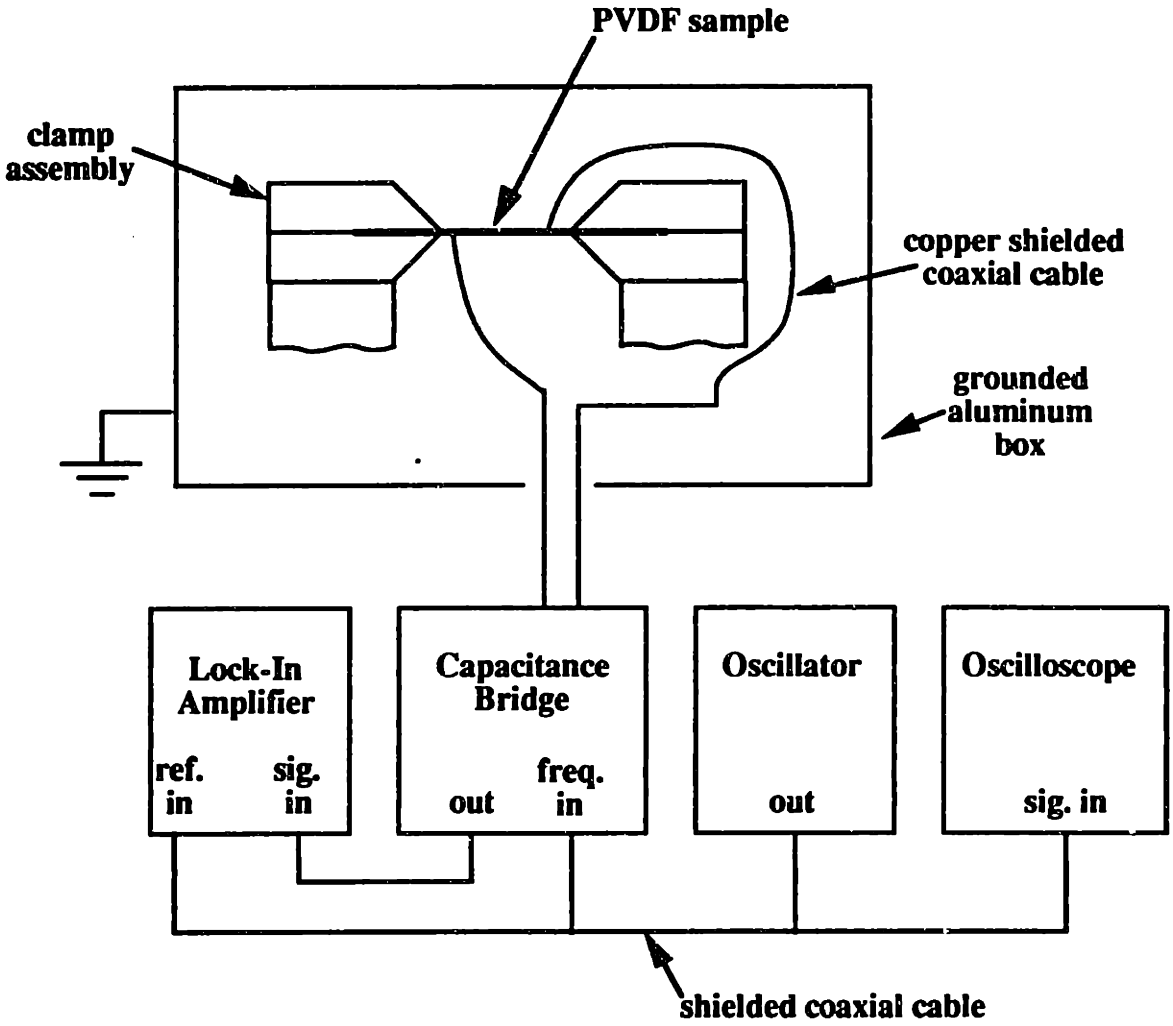

Figure 3-5. Schematic of the experimental setup for the PVDF dielectric properties measurements.

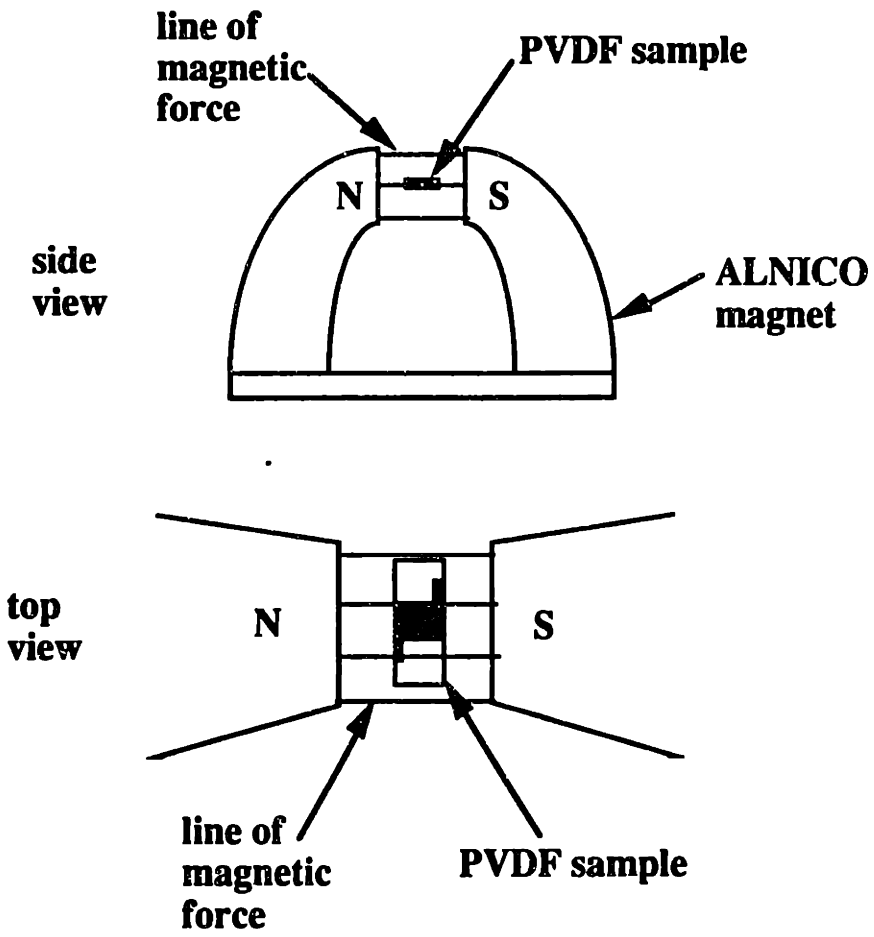

Figure 3-6. Schematic of the transverse magnetic field setup.

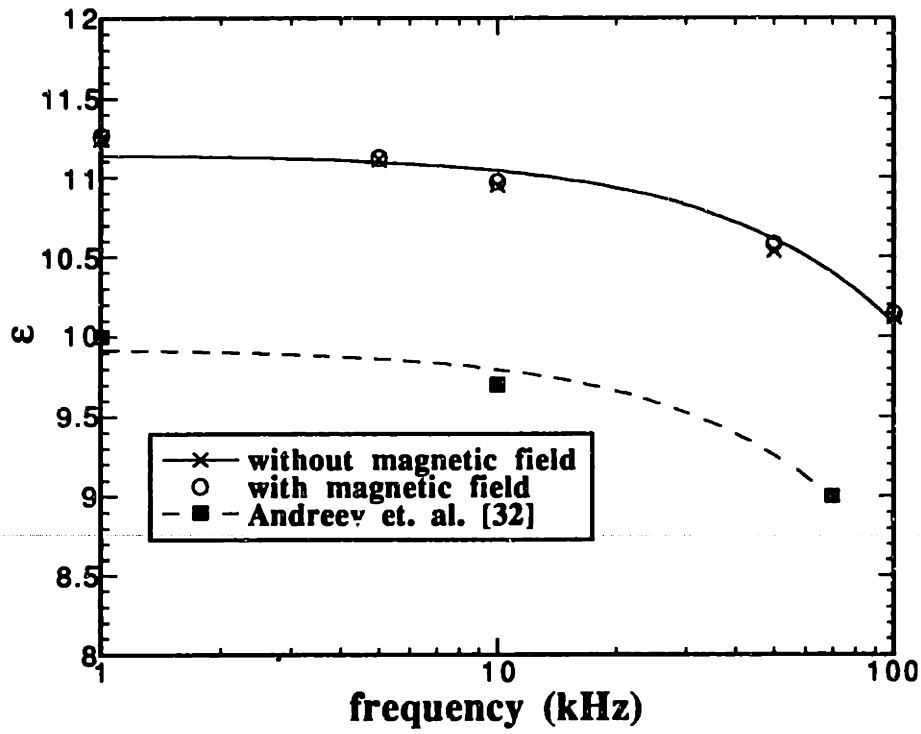

Figure 3-7. Dielectric constant of PVDF versus frequency.

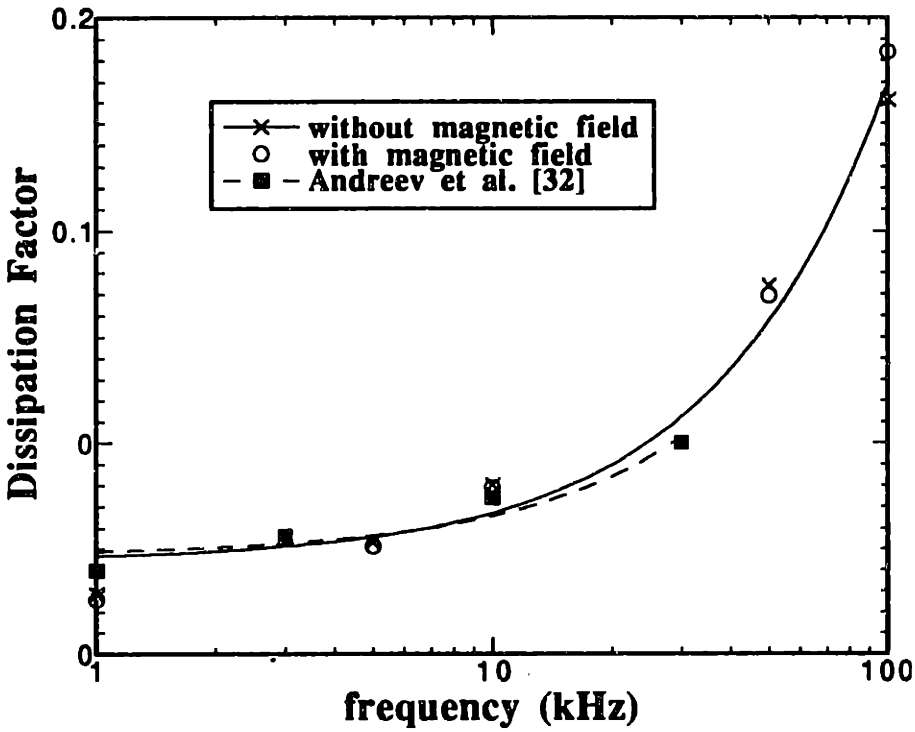

Figure 3-8. Dissipation factor of PVDF versus frequency.

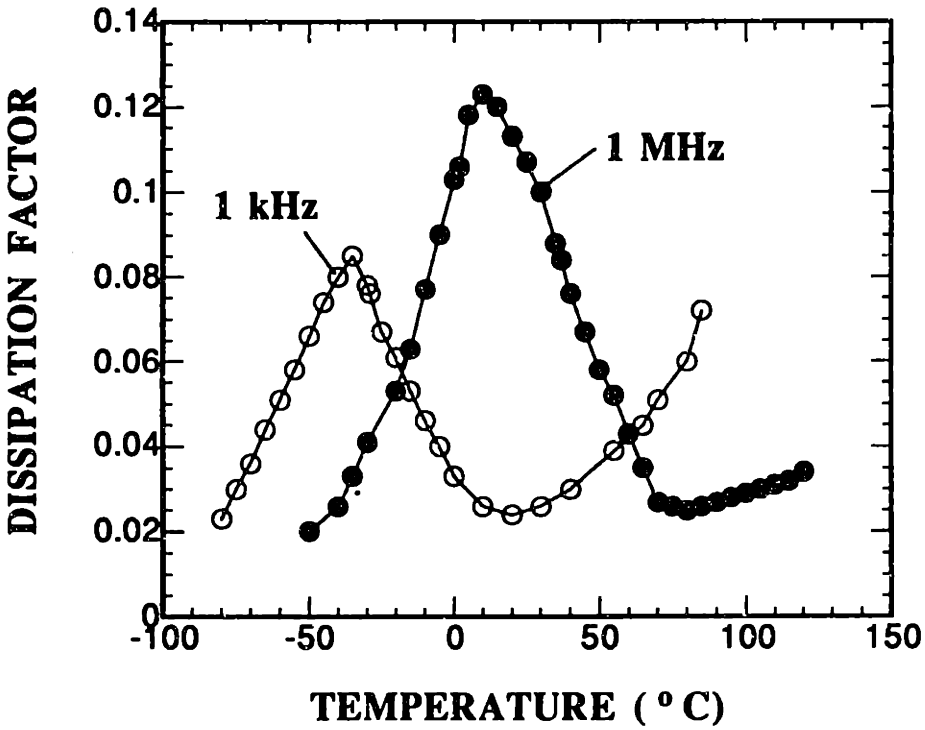

Figure 3-9. Dissipation factor of PVDF versus temperature at 1 kHz and 1 MHz. Adapted from Andreev *et al.* [32].

4. ENERGY CONVERSION IN A SINGLE PVDF LAYER

4.1 Introduction

Every thermal energy conversion device requires a working fluid whose entropy depends upon an independent property other than temperature.[33] In the Stirling cycle, the working fluid is an ideal gas, whose entropy is dependent upon pressure and temperature. In a conventional thermoelectric device, the working fluid is the electron gas, whose entropy is dependent upon temperature and the crystal lattice of the thermoelectric material - a change in entropy is associated with the passage of conduction electrons from one material to another.

A thermal energy conversion device also requires a means of bringing the working fluid into and out of contact with two heat reservoirs at different temperatures. This thermal "switching" is achieved in the Stirling cycle by displacing the ideal gas between the "hot" and "cold" pistons through the regenerator. In a conventional thermoelectric device, the electron gas can be moved between the "hot" and "cold" reservoirs by an electromotive force.

In the analysis of the Strachan-Aspden thermoelectric converter as a thermal energy conversion device, the first priority is to identify the mechanism for entropy transport. Aspden and Strachan claim that thermoelectric action in the bimetallic coatings of the PVDF layers acts as the entropy transport mechanism. Another possibility is that entropy is transported through the PVDF material itself because of the ferroelectric nature of PVDF. A surface effect between the PVDF and the metallic coating may also be responsible for entropy transport.

Entropy transport may be realized in the PVDF material because the entropy of the PVDF polymer chains is dependent upon temperature, applied stress, and applied electric field.[34] If so, then a "thermo-electro-mechanical" condition might be applied to the PVDF material where entropy transport (and therefore energy conversion) can be achieved. As with any cyclic thermal energy conversion device, though, the actions must be properly phased in to order to realize energy conversion. There is no apparent mechanism for thermal "switching" in the PVDF material, as the PVDF polymer chains are not mobile.

To test for a possible entropy transport effect in the PVDF material, an experiment is performed in which a single layer of PVDF is driven with an AC electrical voltage and an oscillating mechanical load, while a temperature gradient is applied along the layer. The frequencies of the electrical and mechanical drives are variable but equal, while their relative phase can be varied from 0° to 180°. The magnitude and relative phase of the PVDF layer voltage and current are measured with variation in drive conditions and applied temperature gradient to determine if an energy conversion mechanism is present. The product of the PVDF layer voltage and current gives a measure of the electrical power consumption of the PVDF layer. If an energy conversion mechanism is present, it might be detected as a variation in the magnitude and/or relative phase of the PVDF layer voltage and current with applied temperature gradient. The PVDF layer voltage output is also observed for any anomalous electrical spiking like that reported by Strachan for the first prototype device. These measurements are performed in the frequency range from 10-30 kHz, where Strachan and Aspden had reported operation of at least one of the prototype devices.[3-11]

4.2 Experimental Design

4.2.1 Stack Layout

A schematic of the stack setup is shown in Figure 4-1. A single layer 28 μm thick PVDF from AMP, Inc., coated on both sides with 2200 angstroms of Nickel and 800 angstroms Aluminum, is used. The layer is 12.7 mm x 38.1 mm, with a capacitive area of 12.7 mm x 12.7 mm. The remaining 12.7 mm portion on each side is metal-coated on one side only to provide for electrical connection to each side of the film. The Ni-Al metallization is removed using a rubber pencil eraser. A 12.7 mm x 12.7 mm x 1 mm thick PZT type 880 piezoelectric element, silver-electroded on both sides, from American Piezo Ceramics, Inc., is mounted beneath the PVDF layer. A 12.7 mm x 12.7 mm x 1.6 mm thick Pyrex spacer is mounted beneath the PZT element to provide electrical and

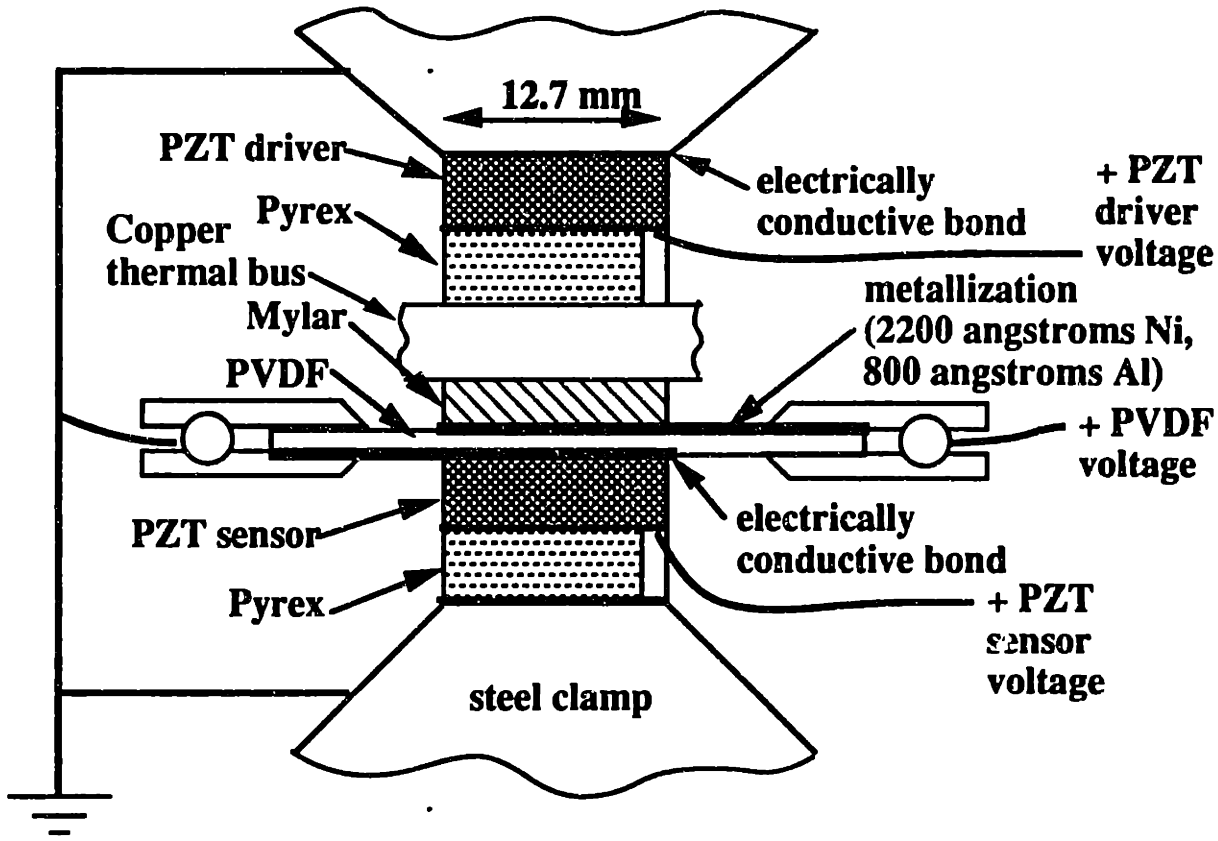

Figure 4-1. Schematic of the stack setup for the single PVDF layer energy conversion experiment.

thermal insulation between the PZT element and the steel clamp face. A 12.7 mm x 12.7 mm x 0.023 mm thick layer of Mylar is located above the PVDF layer to provide for electrical insulation between the PVDF layer and the copper thermal bus (see temperature gradient section, below). A 12.7 mm x 12.7 mm x 1.6 mm thick Pyrex spacer is mounted above the copper thermal bus. Another 12.7 mm x 12.7 mm x 1 mm PZT type 880 element is mounted between the Pyrex spacer and the upper steel clamp face.

The upper PZT element is used to mechanically drive the PVDF layer. The lower PZT element is used to measure the stress levels in the stack at the location of the PVDF layer.

4.2.2 Bonding and Electrical Connections

All surfaces are bonded with Loctite 312 acrylic adhesive to provide for acoustic coupling between each layer. Each surface is treated with Loctite Primer NF before bonding. To provide for electrical connection between the bottom electrode of the PVDF layer and the silver-electroded top surface of the lower PZT element, and between the silver-electroded top surface of the upper PZT element and the steel clamp surface, the PZT silver-electroded surfaces are coated with fine copper powder before bonding. The other electrical connections are shown in Figure 4-1. Both steel clamp halves and the copper thermal bus are electrically grounded. Small notches are machined in the square Pyrex spacers to allow for electrical connection to the positive electrode of the upper PZT element and the negative electrode of the lower PZT element.

4.2.3 Temperature Gradient Assembly

A schematic of the temperature gradient assembly is shown in Figure 4-2. A Minco model HK5255R31.6 thermofoil heater, 12.7 mm x 25.4 mm x 0.3 mm thick, is mounted on one side of the copper thermal bus. A cooling assembly, consisting of a 17.8 mm x 25.4 mm x 6.4 mm thick copper block, through which cooling water at 7 °C is passed, is mounted on the opposite side. Copper constantan (type T) thermocouples are epoxied to the copper bus on either side of the stack assembly to provide for temperature measurement.

The Minco thermofoil heater is powered by a DC power supply, and can provide up to 20 W of thermal power input. Assuming 1-D conduction primarily through the copper thermal bus, the temperature gradient along the stack, $\Delta T / L$, is given by:

$$\frac{\Delta T}{L} = \frac{Q}{kA} \tag{4-1}$$

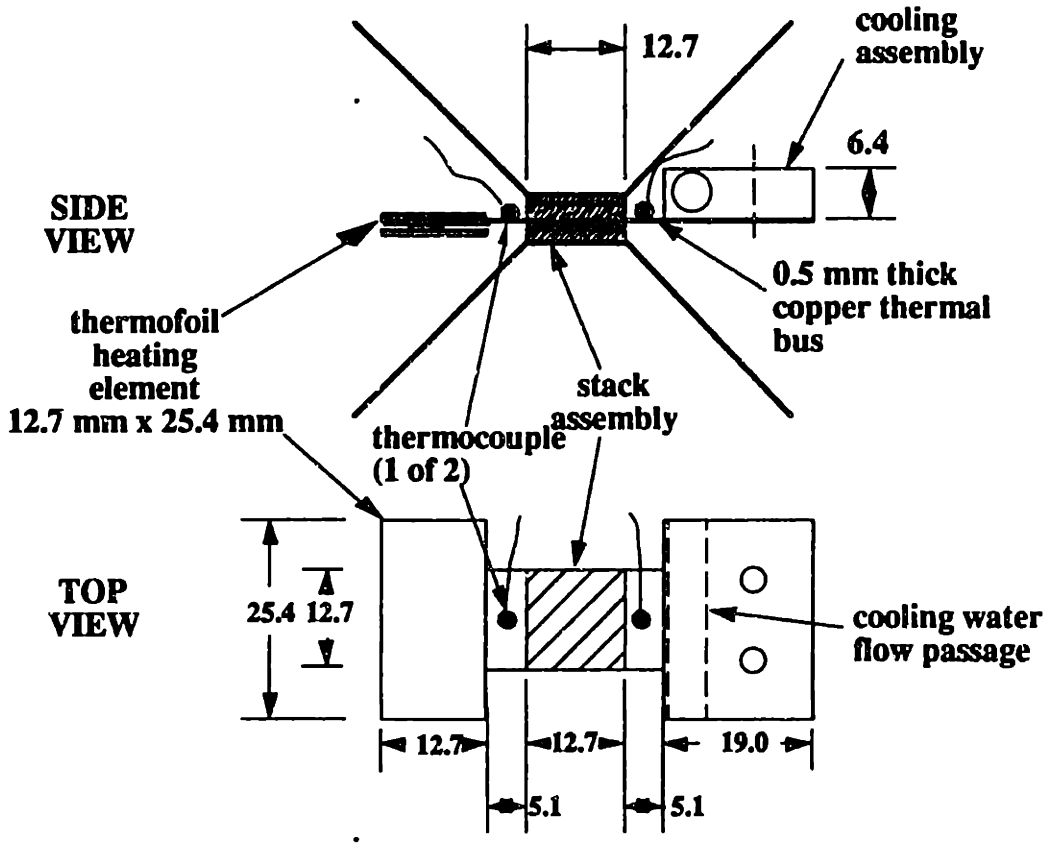

Figure 4-2. Temperature gradient assembly for the single PVDF layer energy conversion experiment. All dimensions are in mm.

where Q is the heat input to the hot side of the copper thermal bus, k is the thermal conductivity of copper (398 W/mK), and A is the cross-sectional area of the copper bus, it is calculated that a temperature gradient of up to 39 °C/cm can be established along the PVDF layer. Heating due to electrical dissipation in the PVDF layer and PZT element is calculated to be insignificant compared to Q.

4.2.4 Inertial Clamp Assembly

The stack is placed in a steel inertial clamp assembly, consisting of two 76.2 mm diameter type 303S stainless steel cylinders. Each cylinder is tapered to a 12.7 mm x 19.0 mm face on one side, to allow space for electrical connections and the temperature gradient assembly. Four type 303S stainless steel posts 6.4 mm in diameter are used to provide support for the upper clamp half. The inertial clamp assembly is shown in Figure 4-3.

The inertial clamp assembly is designed to avoid mechanical or acoustic resonances in the frequency range from 10-30 kHz. The steel clamp halves have a mass of 2.5 kg each. The natural spring-mass mechanical frequency, f_m, of the structure is given by

$$f_m = \frac{1}{2\pi}\sqrt{\frac{2K_{comp}}{M}} \tag{4-2}$$

where K_{comp} is the composite stiffness of the stack and steel conical sections and M is the mass of each clamp half (see Appendix A). The natural mechanical frequency is calculated to be 3200 Hz at 25 °C. Other neglected resonances in the clamp structure, temperature gradient assembly, and support structure are calculated to be much lower than the natural spring-mass frequency of the inertial clamp structure. The resonant mechanical frequency is experimentally found to be 3032 Hz at a stack temperature of 25 °C and 2886 Hz at an average PVDF layer temperature of 48 °C, which is due to the temperature dependent elastic constants of the stack materials (primarily the PVDF).[30,36] This shows good agreement with the predicted value.

The length of each clamp half is 79.4 mm. The first acoustic resonance, f_o, corresponds to the half-wave resonance of the steel clamp halves. Assuming the clamp half is a right circular cylinder, f_o is given by[13]

$$f_o = \frac{c}{2L} \tag{4-3}$$

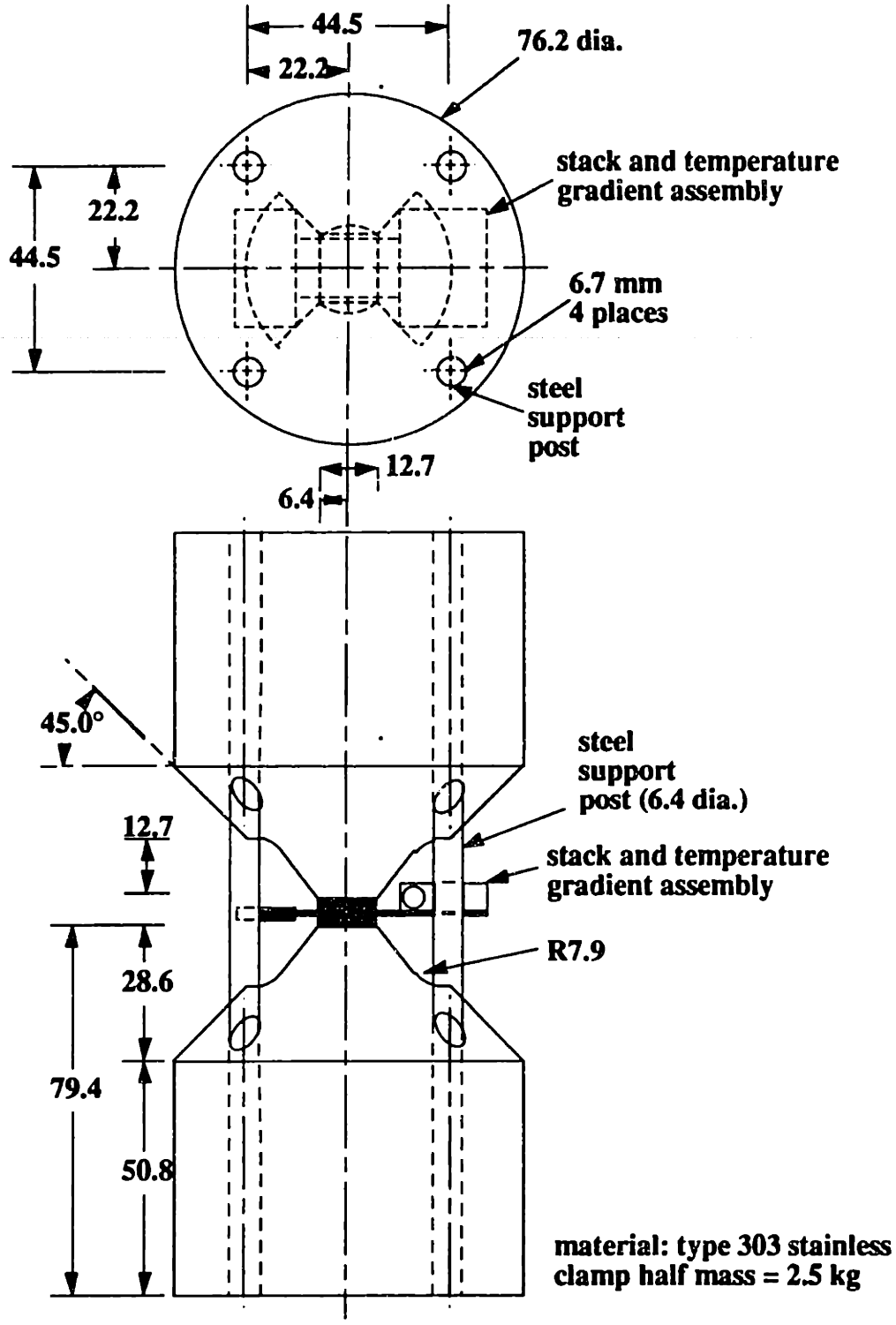

Figure 4-3. Inertial clamp assembly for the single PVDF layer energy conversion experiment (scale 2:3, all dimensions in mm).

where c is the velocity of sound in steel (~5000 m/s) and L is the length of the clamp half. The first acoustic resonance is calculated to be 31 kHz. Higher order resonances are therefore expected at integral multiples of this frequency (62 kHz, 93 kHz, etc.). Resonance experiments performed using PZT driver and sensor elements mounted between the clamp halves detect strong acoustic resonances at 34 kHz, 65 kHz, and 100 kHz, which shows good agreement with the predicted resonance frequencies. In addition, several weaker resonances are found between 34 and 100 kHz. No significant effect of the applied temperature gradient on the acoustic resonances is found. The first acoustic resonance of the stack assembly itself is calculated to be 400 kHz.

These calculations and experimental results show that the mechanical and acoustic resonances of the inertial clamp and composite stack structure should not interfere with measurements made between 10 and 30 kHz. Any resonant behavior could result in significant variation of the magnitude and relative phase of the PZT and PVDF voltages and currents, which could obscure any variation of these quantities due to energy conversion effects.

4.2.5 Mechanical Drive, Electrical Drive, and Measurement Setup

In order to provide an oscillating mechanical load to the PVDF layer, the PZT drive element can be driven at up to 250 V peak-to-peak. A schematic of the drive system is shown in Figure 4-4. The PZT element is driven by a Hewlett Packard 33120A function generator, whose output signal passes through an attenuator circuit to Channel 1 of a Crown DC300A two-channel audio amplifier. The amplifier output is passed through a circuit board containing a 1:5 transformer and circuitry for measuring the voltage and current input to the PZT element (see Figure 4-5), and then to the PZT driver leads.

The PVDF layer is electrically driven by a Hewlett Packard 3300A function generator with a Hewlett Packard 3302A trigger/phase lock module, triggered by the Hewlett Packard 33120A output. This produces a signal of the same frequency as the PZT drive circuit, with a controllable phase difference of 0-180°. The signal is then passed through Channel 2 of the Crown DC300A amplifier, a board containing circuitry for measuring the input voltage and current of the PVDF layer (see Figure 4-6), and then to the PVDF layer leads. The PVDF layer can be driven electrically at up to 50 V peak-to-peak using this drive setup. When the PZT is not in use, the PZT drive setup can be used to drive the PVDF layer at up to 250 V peak-to-peak.

A Tektronix TDS460A four-channel digitizing oscilloscope is used to monitor all input/outout signals. An IBM-compatible PC running Tektronix Docuwave software is

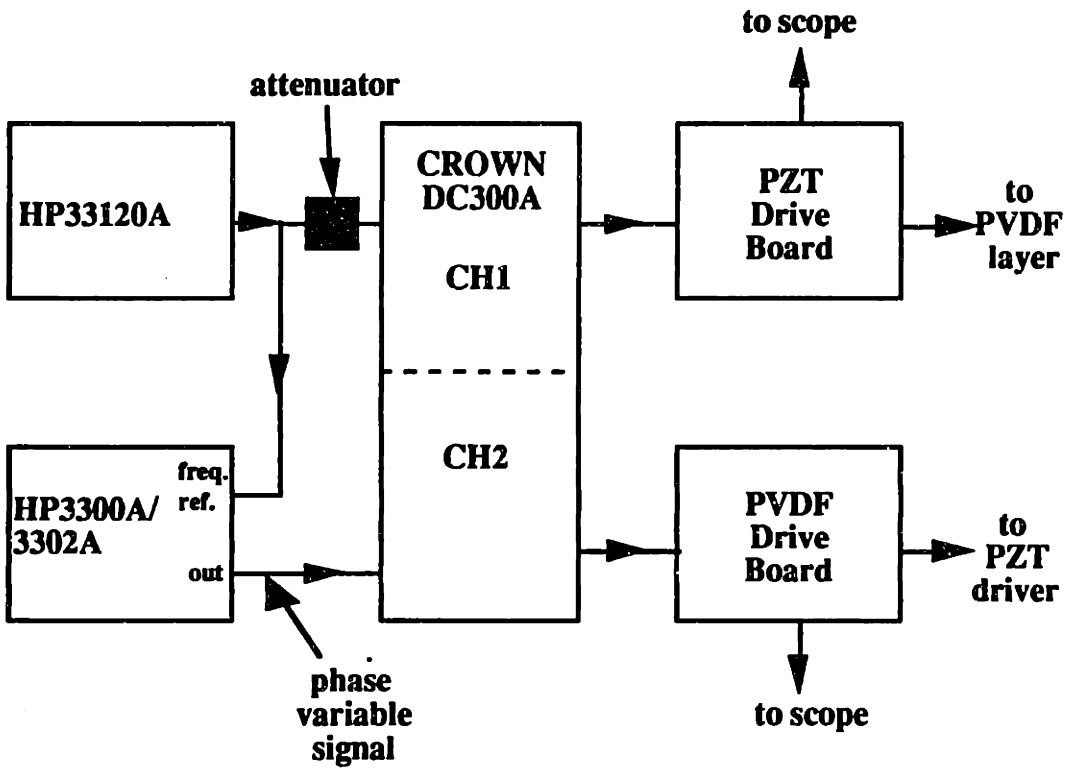

Figure 4-4. Schematic of the drive system layout for the PZT driver and PVDF layer.

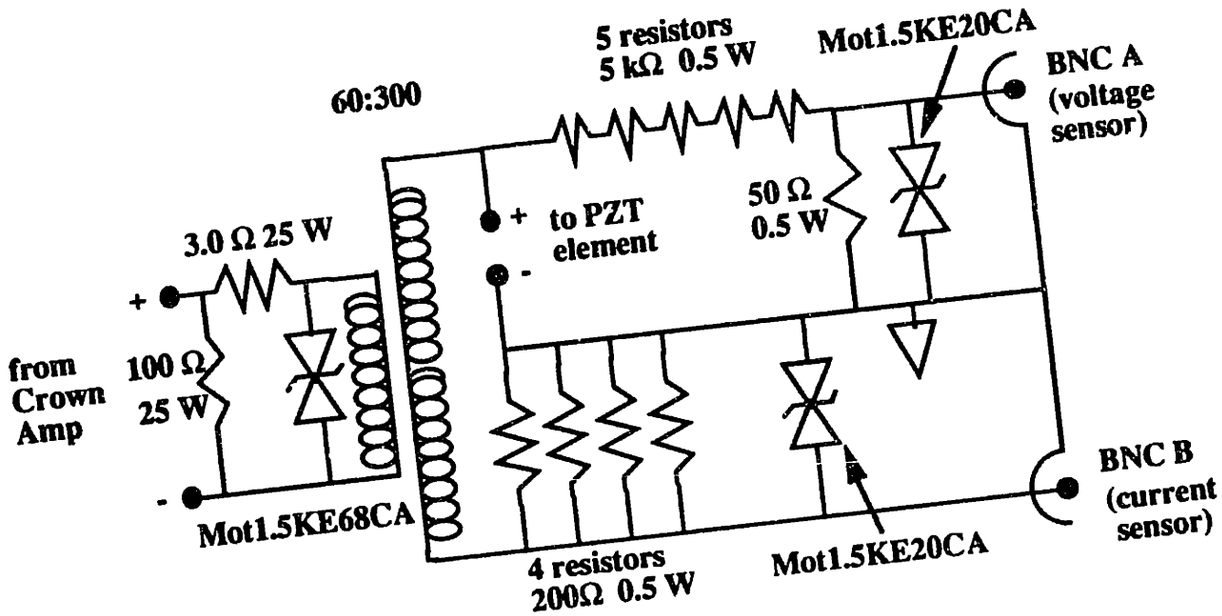

Figure 4-5. Drive circuit for the PZT driver element.

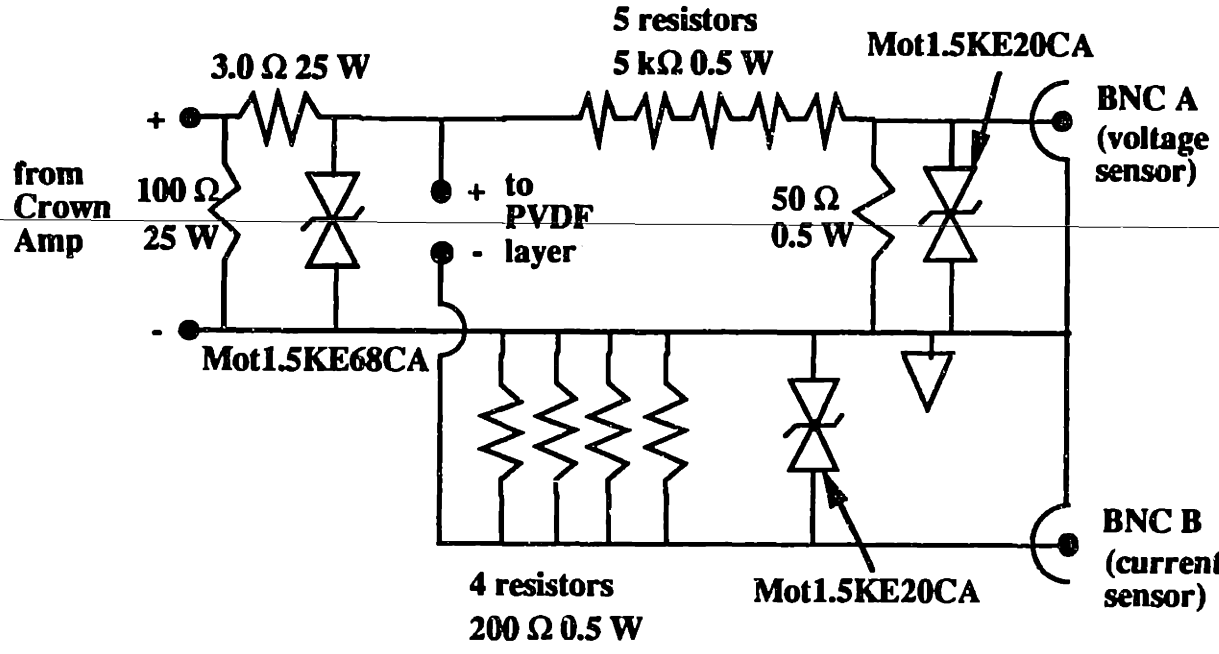

Figure 4-6. Drive circuit for the PVDF layer.

used to capture all waveforms of interest. Frequency and relative phase measurements are made using Mathsoft Mathcad software.

4.3 Mechanical Drive Experiments

The PZT driver element is driven at voltages up to 200 V peak-to-peak to provide an oscillating mechanical load to the PVDF layer. The effective force in the stack, F_{eff}, assuming all layers are unconstrained in the planar directions, is given by[34]

$$F_{eff} = K_{PZT}\Delta PZT\left(1-\frac{K_{PZT}}{K_{PZT}+K_{stack}}\right) \tag{4-4}$$

where K_{PZT} is the stiffness of the PZT element, K_{stack} is the combined stiffness of the other stack components and the conical sections of the steel clamp halves, and ΔPZT is the free deflection of the PZT element corresponding to the drive voltage, given by

$$\Delta PZT = d_{33}V_{drive} \tag{4-5}$$

where d_{33} is the piezoelectric strain constant of PZT and V_{drive} is the drive voltage.

The stiffness, K, of a given layer of constant cross-sectional area in the stack is given by

$$K = \frac{EA}{t} \tag{4-6}$$

where E is the Young's modulus of the layer material, A is the cross sectional area of the layer, and t is the thickness of the layer. The stiffness of the conical section of the steel clamp halves, K_{cone}, is given by

$$K_{cone} = \left(\int_{x=0}^{L}\frac{dx}{E_{steel}\pi(r_1-x)^2}\right)^{-1} \tag{4-7}$$

where L is the length of the conical section, r_1 is the larger radius of the cone, x is the distance along the length of the cone, and E_{steel} is the Young's modulus of steel (see Appendix A).

For a PZT drive voltage of 200 V peak-to-peak, F_{eff} is calculated to be 66 N peak-to-peak. The output voltage V_{out} of a piezoelectric sensor excited in the thickness mode, assuming it is unconstrained in the planar directions, is given by

$$V_{out} = \frac{F_{eff} g_{33} t}{A} \tag{4-8}$$

where g_{33} is the piezoelectric stress constant, t is the sensor thickness, and A is the cross-sectional area of the sensor. Using this relation, the output voltage of the PVDF and PZT layers corresponding to 66 N peak-to-peak oscillating force are calculated to be 1.7 V peak-to-peak and 4.6 V peak-to-peak, respectively. The presence of stray capacitance due to the Mylar layer and the scope input impedance and capacitance do not significantly decrease the output voltage of the PVDF layer between 10 and 30 kHz (see Appendix B).

The output voltages of the PVDF layer and PZT sensor element for 200 V peak-to-peak input to the PZT drive element at 10 kHz drive frequency are measured to be 0.81 V peak-to-peak and 1.58 V peak-to-peak, respectively. This is significantly lower than the expected voltages. This may be due to piezoelectric coupling of planar stresses and interfacial shear, imperfect bonding in the stack, and/or mechanical losses in the stack or inertial clamp assembly.

4.3.1 Experimental Procedure

Two experiments are performed by driving the PVDF layer with an oscillating mechanical load:

1) The PZT driver is driven at voltages ranging from 0-200 V peak-to-peak. The amplitudes of the PVDF output voltage and PZT sensor voltage are measured at room temperature (24 °C) and with a temperature gradient of 19 °C/cm along the PVDF layer. The accuracy of the voltage measurements is estimated to be ± 4 mV. These measurements are performed at drive frequencies of 10 kHz and 20 kHz.

2) The PVDF layer leads are connected across a 10 kΩ load resistor. The PZT driver is driven at 200 V peak-to-peak. The loaded PVDF output voltage amplitude and phase relationship with respect to the PZT driver voltage and current are measured at room temperature and with a temperature gradient of 19 °C/cm along the PVDF layer. The accuracy of the phase measurements is estimated to be ± 3°. These measurements are performed at drive frequencies of 10 kHz, 20 kHz, and 30 kHz.

4.3.2 Experimental Results

1) The peak-to-peak PVDF output voltage is plotted against the peak-to-peak PZT sensor voltage at 10 kHz and 20 kHz in Figure 4-7. Because the piezoelectric and elastic properties of PZT are not significantly affected by presence of the temperature gradient,[37] the PZT sensor voltage gives a temperature independent measure of the stress level in the stack. The observed stress levels and PVDF output voltages observed are slightly lower with the temperature gradient applied along the PVDF layer. However, this is consistent with the temperature dependence of the elastic and piezoelectric properties of PVDF.[30,36] The PZT sensor voltage is observed to be exactly in phase with the PVDF and PZT drive voltages.

2) Data from the measurements performed on the 10 kΩ resistor–loaded PVDF layer is given in Table 4-1. The measured PZT drive voltage and current, the load resistor voltage, the PZT sensor voltage, the phase difference between the PZT drive voltage and current ($\alpha_{V\text{-}I}$), and the phase difference between the PZT drive voltage and the load resistor voltage ($\alpha_{P\text{-}P}$) are given for measurements performed at room temperature and with a 19 °C/cm temperature gradient applied along the PVDF layer. The PZT sensor voltage is observed to be exactly in phase with the PZT drive voltage. No significant effect of the temperature gradient on any of the measured values is observed.

4.4 Electrical Drive Experiments

4.4.1 Experimental Procedure

The PVDF film is driven at 200 V peak-to-peak. The amplitude and phase relationships of the PVDF input voltage and current and the PZT sensor voltage are measured at room temperature and with a temperature gradient of 19 °C/cm applied along the PVDF layer. These measurements are performed at drive frequencies of 10 kHz, 20kHz, and 30kHz.

4.4.2 Experimental Results

Data from the electrical drive experiments performed on the PVDF layer is given in Table 4-2. The measured PVDF drive voltage and current, the load resistor voltage, the PZT sensor voltage, the phase difference between the PVDF drive voltage and current ($\alpha_{V\text{-}I}$), and the phase difference between the PVDF drive voltage and the PZT sensor voltage ($\alpha_{P\text{-}P}$) are given for measurements performed at room temperature and with a 19 °C/cm temperature gradient applied along the PVDF layer. No significant effect of the

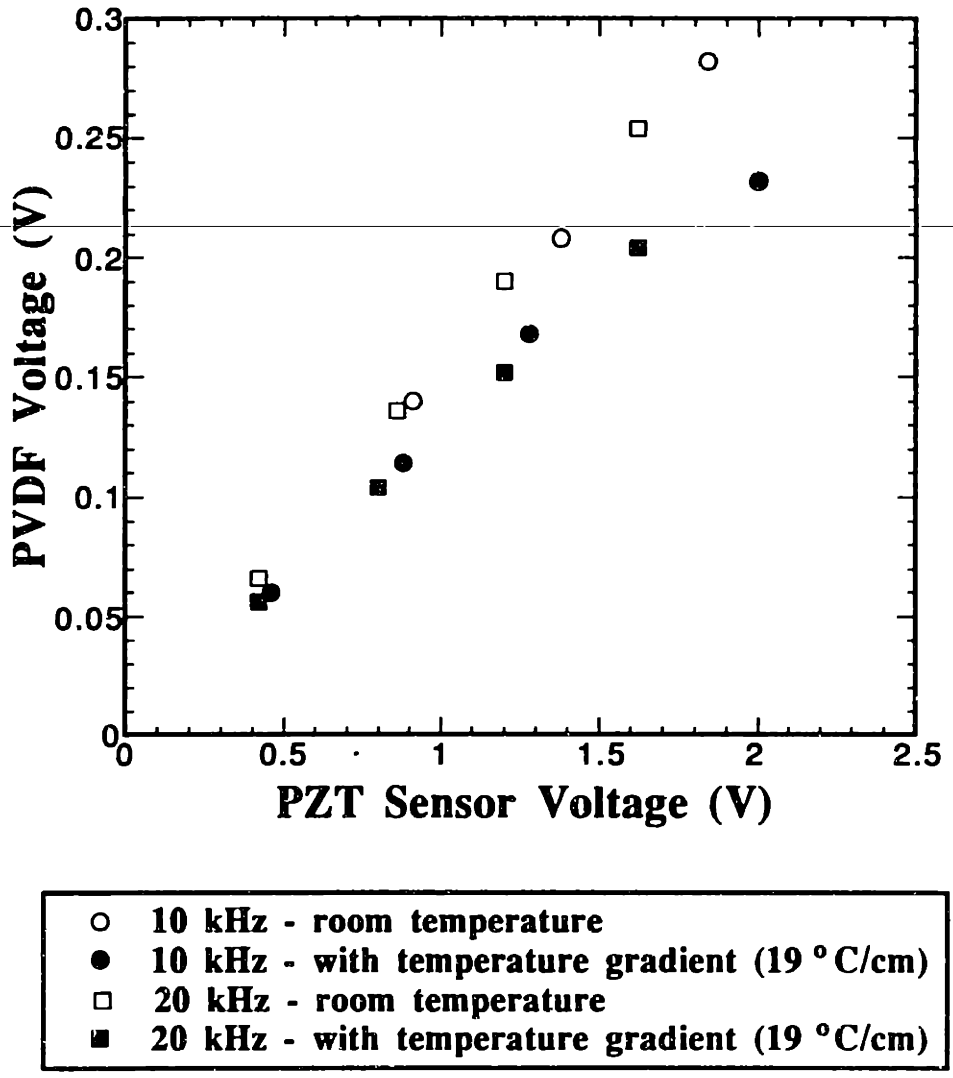

Figure 4-7. PVDF output voltage versus PZT sensor voltage for the mechanical drive experiments.

a) Operating frequency 10 kHz:

	room temperature	with temperature gradient (19 °C/cm)
PZT Drive Voltage	200 V p-p	200 V p-p
PZT Drive Current	20.0 mA	21.0 mA
PZT Sensor Voltage	1.80 V	1.78 V
Load Resistor Voltage	0.344 V	0.352 V
$\alpha_{V\text{-}I}$	115°	114°
$\alpha_{P\text{-}P}$	62°	62°

b) Operating frequency 20 kHz:

	room temperature	with temperature gradient (19 °C/cm)
PZT Drive Voltage	200 V p-p	200 V p-p
PZT Drive Current	40.0 mA	38.4 mA
PZT Sensor Voltage	1.58 V	1.60 V
Load Resistor Voltage	0.500 V	0.528 V
$\alpha_{V\text{-}I}$	103°	103°
$\alpha_{P\text{-}P}$	44°	45°

c) Operating frequency 30 kHz:

	room temperature	with temperature gradient (19 °C/cm)
PZT Drive Voltage	200 V p-p	200 V p-p
PZT Drive Current	57.6 mA	60.0 mA
PZT Sensor Voltage	1.20 V	1.26 V
Load Resistor Voltage	0.544 V	0.576 V
$\alpha_{V\text{-}I}$	99°	98°
$\alpha_{P\text{-}P}$	35°	36°

Table 4-1. Data for the 10 kΩ resistor–loaded single PVDF layer experiments.

a) Operating frequency 10 kHz:

	room temperature	with temperature gradient (19 °C/cm)
PVDF Drive Voltage	200 V p-p	200 V p-p
PVDF Drive Current	17.0 mA	18.0 mA
PZT Sensor Voltage	1.46 V	1.36 V
α_{V-I}	122°	120°
α_{P-P}	75°	74°

b) Operating frequency 20 kHz:

	room temperature	with temperature gradient (19 °C/cm)
PVDF Drive Voltage	200 V p-p	200 V p-p
PVDF Drive Current	31.2 mA	33.2 mA
PZT Sensor Voltage	2.80 V	2.72 V
α_{V-I}	109°	108°
α_{P-P}	80°	80°

c) Operating frequency 30 kHz:

	room temperature	with temperature gradient (19 °C/cm)
PVDF Drive Voltage	200 V p-p	200 V p-p
PVDF Drive Current	44.8 mA	48.8 mA
PZT Sensor Voltage	4.62 V	4.24 V
α_{V-I}	104°	105°
α_{P-P}	81°	81°

Table 4-2. Data for the single PVDF layer electrical drive experiments.

temperature gradient on any of the measured values is observed. The PZT sensor voltage is observed to be exactly in phase with the PZT drive voltage within the limits of experimental error (± 3 °).

4.5 Mechanical and Electrical Drive Experiments

4.5.1 Experimental Procedure

The PVDF layer is driven electrically at 50 V peak-to-peak while being driven mechanically by the PZT driver element, which is driven at 100 V peak-to-peak. The relative phase of the two drives (α_D) is varied from 0-180°. The PZT sensor voltage, PVDF drive current, the phase difference between the PZT sensor voltage and the PZT drive voltage, and the phase difference between the PVDF drive voltage and current are measured at room temperature and with a temperature gradient of 19 °C/cm applied along the PVDF layer. These measurements are performed at drive frequencies of 10 kHz and 20kHz.

4.5.2 Experimental Results

The power consumption in the PVDF layer P is given by

$$P = VI\cos\alpha_{V-I} \tag{4-9}$$

where V is the PVDF layer drive voltage, I is the PVDF layer drive current, and α_{V-I} is the phase difference between the drive voltage and current. P is plotted versus the relative drive phase in Figure 4-8. The results of measurements peformed at room temperature and with a 19 °C/cm temperature gradient applied along the PVDF layer at frequencies of 10 kHz and 20 kHz are shown. No significant effect of the temperature gradient on P is observed.

4.6 Conclusions

Various experiments are performed using a single layer of PVDF mounted in an inertial clamp assembly. The PVDF layer is driven mechanically and electrically, while a temperature gradient is applied across the PVDF layer. Various combinations of drive conditions are imposed upon the PVDF layer, while the amplitude and phase relationships of the input/output voltages and currents are observed for any energy conversion effects (or electrical spiking, as described by Strachan).

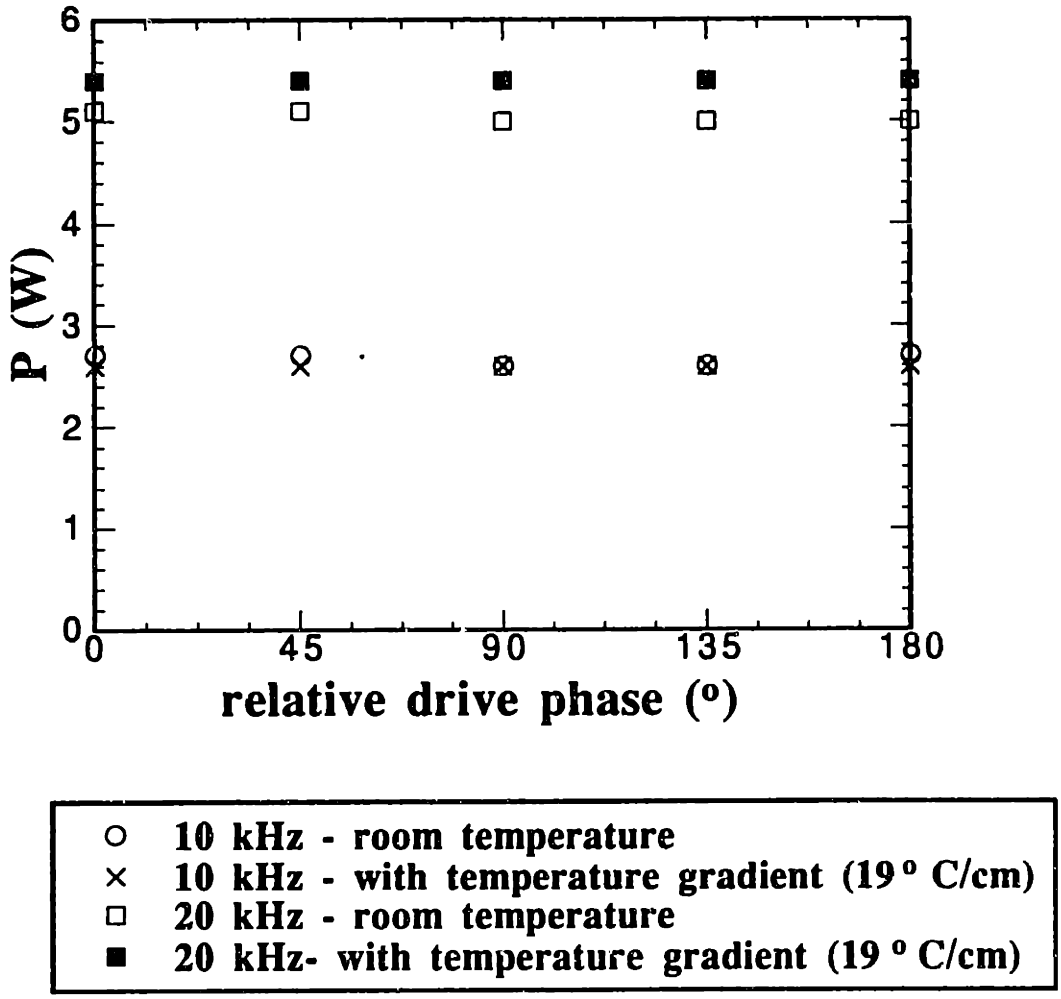

Figure 4-8: Power consumption P of the PVDF layer versus relative drive phase for the mechanical and electrical drive experiments.

No significant effect of the temperature gradient on energy conversion in the stack structure is observed. The temperature gradient does affect the elastic and piezoelectric properties of PVDF, but these relationships are fairly well understood and explain the experimental results well. No electrical spiking or other energy conversion effects similar to those described by Strachan are observed.

There are many possible explanations for the lack of any observed "Strachan"-type effects. The stresses developed in the stack may not be high enough to couple mechanical and electrical action with thermal action in the PVDF layer. Also, the drive frequencies used may not be in the proper range for observation of any energy conversion effects (It was learned after this experiment was performed that Strachan's first prototype device operated at 2 MHz, whereas it had originally been reported that the electrical "spiking" was observed in the kHz frequency range).

5. CONSTRUCTION OF THE "STRACHAN" PVDF STACKS

5.1 Introduction

In each of the prototype devices, Strachan used stacks of 28 μm thick PVDF that were constructed so as to be half-wave resonant at MHz-range frequencies (~0.55 mm thick). Strachan's construction technique, which is outlined in Chapter 2, consisted of a complex series of surface treatments and cure cycles involved with the use of a cyanoacrylate adhesive, which was required to provide for high-quality acoustic coupling between the PVDF layers and between the PVDF stack elements and the acrylic half-wave plates.

In order to accurately duplicate the construction of Strachan's prototype devices, it is necessary to duplicate the cyanoacrylate bonding technique he developed, or develop a bonding technique of equal or superior quality. Unless the cyanoacrylate adhesive or surface treatment used by Strachan is critical for observation of energy conversion effects, then any bonding technique that provides for very thin bond lines and high-quality acoustic coupling in the PVDF stack is adequate. Investigations of various PVDF bonding techniques (including Strachan's method) are described in this chapter. Microscopic observation methods are developed to observe bond line thicknesses. A piezoelectric resonance method is developed to test the resonant quality factor of the PVDF stacks constructed. A bonding technique using a low-viscosity strain gauge epoxy is determined to be the most effective of the bonding methods investigated and is used to

construct the MHz-resonant PVDF stacks that will be utilized in the replica of the Strachan-Aspden prototype devices.

5.2 Cyanoacrylate Bonding Experiments

An attempt is made to duplicate Strachan's cyanoacrylate bonding technique. The method used is very similar to that used by Strachan, which is described in section 2-2. Test stacks of PVDF are constructed using cyanoacrylate adhesive and the resultant bonds are inspected for strength and quality.

28 μm thick uniaxially stretched PVDF film from AMP Inc., coated with 2200 angstroms Ni and 800 angstroms Al on one side, is used. The film is supplied with metallization on both sides. A pencil eraser is used to remove the metallization from one side. The film is cut into twenty 25.4 mm x 38.1 mm pieces. Both sides of each are treated with a 2% solution of tetrabutyltitanate in petroleum ether in a dry atmosphere. After this treatment, the metallized surfaces appear iridescent. Each surface is then exposed to a 100% humidity atmosphere at 40 °C for 30 seconds. A white, powdery substance is observed on each surface after this treatment. The purpose of this surface treatment is to produce an alkaline surface condition for better cyanoacrylate bonding.

The PVDF stack is built up one layer at a time to a thickness of 0.55 mm (2 MHz half-wave resonant). Loctite 406 ethyl cyanoacrylate adhesive is used. After each layer is added, the stack is placed in a press with teflon platen surfaces. The press setup is shown in Figure 5-1. Each bond is cured for 2 minutes at a cure pressure of approximately 7 x 10^5 Pa. The 25.4 mm x 38.1 mm x 20 layer thick stack is then trimmed using sheet metal shears into 10 stack elements, each 25.4 mm x 3.8 mm x 20 layers thick.

Using this method, a bond line thickness of 64 μm is achieved, which only allows 6 layers of 28 μm thick PVDF film to be used in each 0.55 mm thick stack. The bond line thicknesses were measured using a Bausch & Lomb stereo microscope. The bonds produced by this technique are very weak. The individual layers can be easily peeled apart. Inspection of the bonded surfaces reveals that the cyanoacrylate adhesive forms small islands on the surface, which leaves many large voids between the bonded layers. This bonding cannot provide the desired acoustic coupling and structural strength for the PVDF stacks. Therefore, the cyanoacrylate bonding method is abandoned. It is unclear why Strachan's cyanoacrylate bonding technique could not be duplicated in this experiment. The cure pressures used in this experiement (~7 x 10^5 Pa) were much lower than those used by Strachan (~10^8 Pa). Also, Strachan used ammonia to speed the

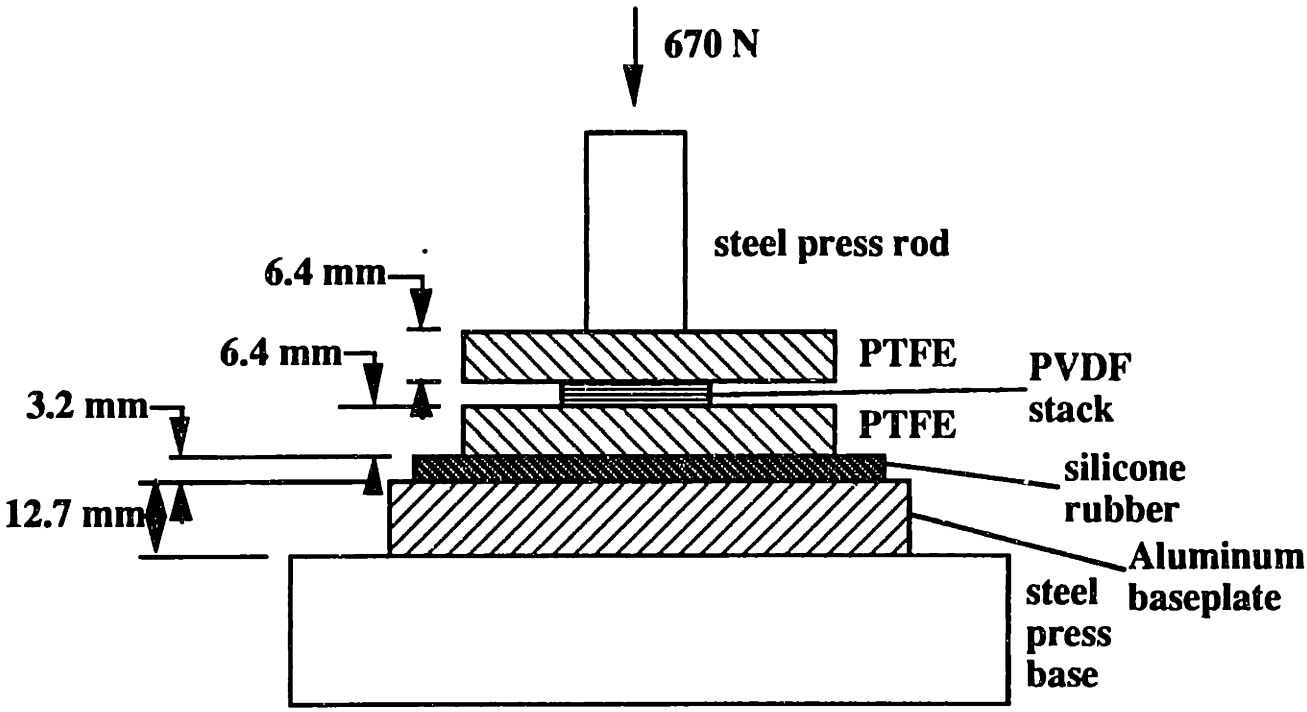

Figure 5-1. Schematic of the cyanoacrylate bonding press setup.

cyanoacrylate adhesive curing process. It is possible that these differences may account for the lack of success in duplicating Strachan's technique.

Loctite type 312, 411, and 325 adhesives are also used in the construction of several PVDF stacks. The bonds produced are found to be unsatisfactory for the desired application.

5.3 Strain Gauge Epoxy Bonding

The use of a cyanoacrylate adhesive for bonding PVDF is abandoned in favor of the use of a high-temperature setting, low viscosity strain gauge epoxy. Good adhesive layers of submicron thickness have been realized using this type of epoxy for bonding PVDF.[38,39] Measurements Group, Inc. type AE-15 epoxy is used. Experiments are performed to test the quality of the PVDF stacks constructed using this epoxy in order to optimize the bonding procedure.

5.3.1 Strain Gauge Epoxy Press Setup

In order to cure the PVDF stacks bonded using strain gauge epoxy at elevated temperatures and high pressures, a heated press setup is used. A schematic of the press setup is shown in Figure 5-2. A hand-cranked hydraulic press (constructed by Advanced Mechanical Technologies, Watertown, MA) is used. A Wagezelle 1 x 10^5 N load cell, 2 V full-scale, is mounted on the press in order to measure the applied loads. Two face ground hardened steel platens measuring 102 mm x 38.1 mm x 25.4 mm thick are used. A cartridge heater is mounted in each platen to provide for elevated-temperature operation. A NANMAC temperature controller is used to provide thermostat control, using a type K (Chromel-Alumel) thermocouple mounted in the upper platen. A type K thermocouple is mounted in the lower platen and is monitored using a Keithley model 871 digital thermometer. The stack bonding procedure is as follows:

1) The PVDF film is cut to size.

2) The epoxy is mixed. The PVDF stack is built up one layer at a time. A thin film of epoxy is applied between successive layers. Two stacks are made.

3) The stacks are mounted between the steel platens using wax paper as a mold release. The stacks are aligned to be equidistant from the press centerline.

4) The desired pressure is applied using the press hand crank, while observing the load cell voltage output.

5) The cure pressure is applied for 5-10 minutes before applying heat to the stack. This is done to allow additional time for the epoxy to be squeezed out from between the PVDF layers before the cure temperature is applied.

6) The temperature control is adjusted and heat is applied to the stack. It takes approximately 4-5 minutes for the cure temperature (70 °C) to be reached.

7) The epoxy takes approximately 1.5 hours to cure. The press loading and cure temperature are maintained at the desired levels during this time.

5.3.2 Bond Line Thickness

An attempt is made to measure the bond line thickness of the strain gauge epoxy bonds. A Bausch & Lomb stereo microscope is used to observe sectioned PVDF stacks. A precision micrometer (±0.005 mm resolution) is used to measure the thickness of the PVDF stacks.

Using these measurement methods, the bond line thickness is determined to be 7 ±1 μm for PVDF stacks assembled with strain gauge epoxy and cured at low pressures (1.4 - 3.4 x 10^5 Pa). Measurements performed on stacks cured at higher pressures (1.4 - 5.5 x 10^7 Pa) could not resolve any bond line thickness. Therefore, the bond line is estimated to be less than 1 μm for the stacks cured using higher cure pressures.

Thinner bond lines result in better acoustic coupling, as epoxy is a highly acoustically dissipative material (~1-3 dB/cm attenuation coefficient).[40] The relative dielectric costant ε of the epoxy resin is approximately 2-3,[41] as opposed to ε≈10 for PVDF. Therefore, because the epoxy in the PVDF stacks is situated between the capacitor plates of the successive PVDF layers, the voltage applied across each PVDF layer will be diminished due to the effective capacitive divider circuit if the bond line thickness is significant compared to the PVDF layer thickness.

5.3.3 Etching Procedure for the PVDF Film Metallization

The 28 μm thick uniaxially stretched PVDF film is supplied by AMP, Inc. with a metallized coating of 2200 angstroms Ni and 800 angstroms Al on both sides. The metallization can be removed using a standard pencil eraser. However, this technique is

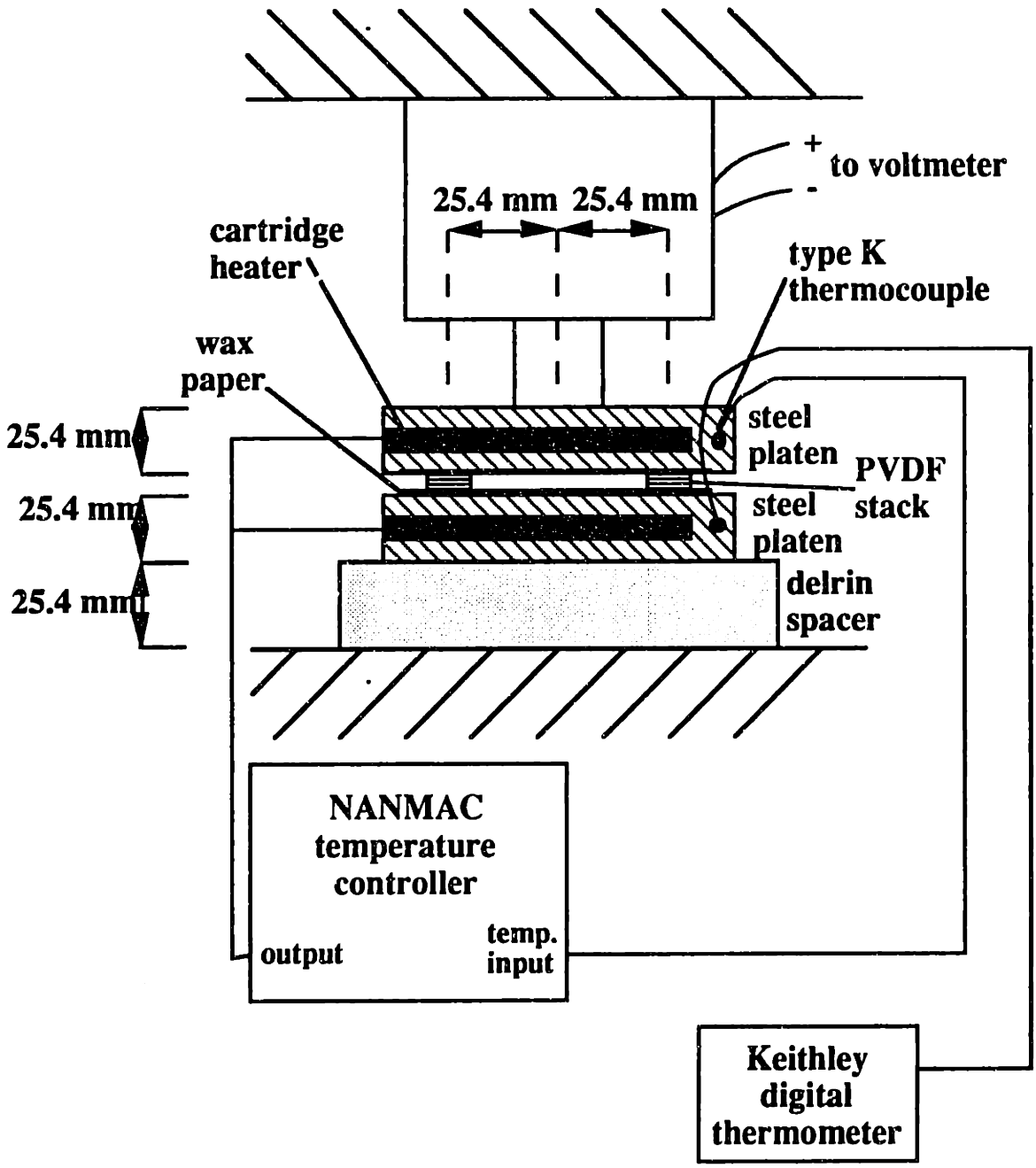

Figure 5-2. Schematic of the heated press assembly.

time consuming, may result in the presence of wrinkles in the PVDF film, and leaves a rubber "eraser dust" that must be washed from the PVDF film surface.

In order to remove the metallization from the 28 μm thick PVDf film, an etching technique using Hydrochloric acid (HCl) is developed. The PVDF sheet, measuring 21.6 cm x 28 mm, is placed in a Pyrex tray. Butyl rubber sealant is placed around the outside edge of the film in order to prevent any HCl from reaching the bottom side of the PVDF. A 92% HCl solution is poured over the top surface of the PVDF and allowed to etch the surface for approximately 1 minute. The entire tray is then rinsed thoroughly using distilled water and dried with lint-free tissues. The etched PVDF is then cut from inside the butyl rubber sealant using a razor blade.

5.3.4 Resonance Experiments

Various PVDF stack configurations are constructed using a cure pressure of 1.7 x 10^7 Pa, and are tested for bond quality by resonating the stacks in the "free-free" condition (unconstrained ends) and measuring the resonant quality factor, Q. The resonant frequency and resonant Q are measured for each stack. Measurements are performed at room temperature (~24 °C) and at liquid nitrogen temperatures (~77 K).

The PVDF stacks are constructed from 28 and 119 μm thick PVDF film from AMP, Inc. and Pennwalt Corp., respectively. The metallization is removed from one side using a pencil eraser for the 119 μm thick film and the HCl etching technique described above for the 28 μm thick film. Electrical connection is made by copper brush leads touching either side of the stack. The stacks constructed from 119 μm PVDF film have a face area of 12.7 mm x 12.7 mm, whereas those constructed from 28 μm film have a face area of 5.1 mm x 25.4 mm.

The measurement setup is shown in Figure 5-3. A HP 33120A signal generator is used to provide the drive signal, which is passed through an Electronic Navigation Industries, Inc. model 310L 10 watt RF amplifier. This produces a drive voltage of approximately 30-40 V peak-to-peak. A resistor sized to the approximate value of the PVDF stack impedance at the estimated resonance frequency is connected in series with the PVDF stack. A Tektronix TDS360A digitizing oscilloscope is used to measure the drive voltage, the PVDF stack voltage, and the phase difference between the two waveforms. This allows measurement of the PVDF stack impedance with varying drive frequency.

The equivalent circuit for a piezoelectric resonator developed by Ohigashi [31] is shown in Figure 5-4. The circuit element values C_0, C, L, and R are given by[31]

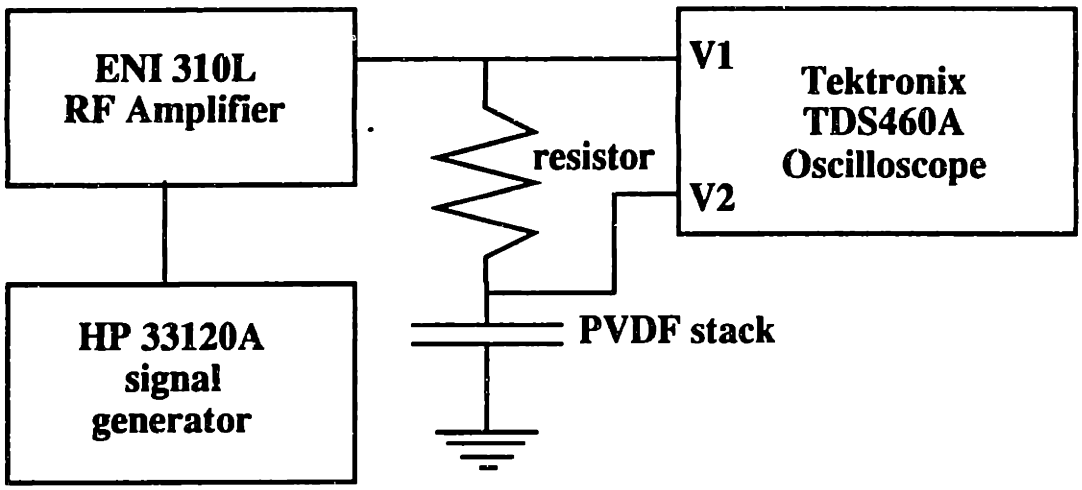

Figure 5-3. Setup for the PVDF stack resonant Q measurements.

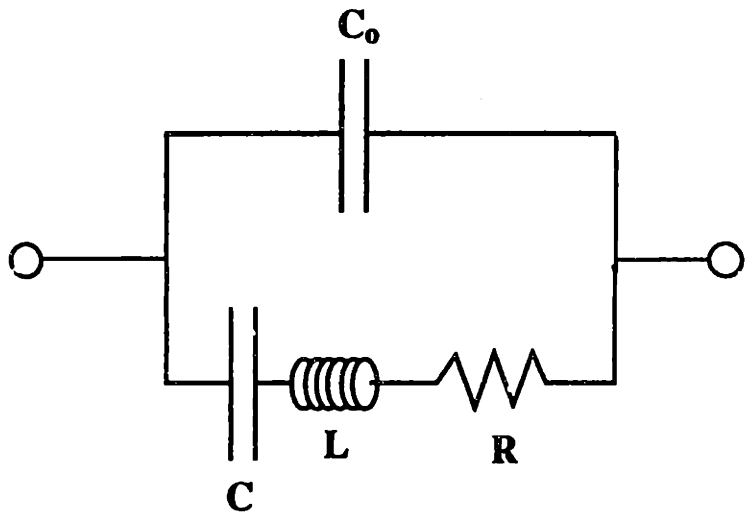

Figure 5-4. Equivalent circuit for a piezoelectric free resonator (from Ohigashi [31]).

$$C_0 = \frac{A\varepsilon\varepsilon_0}{d} \tag{5-1}$$

$$C = \frac{8C_0}{\pi^2} k_{33PVDF}^2 \tag{5-2}$$

$$L = \frac{1}{(2\pi f_0)^2 C} \tag{5-3}$$

$$R = \frac{\tan\delta}{2\pi f_0 C} \tag{5-4}$$

where A is the stack face area, ε is the relative dielectric constant of PVDF, ε_0 is the permittivity of free space (ε_0 = 8.854 x 10^{-12} Farad/m), d is the thickness of the PVDF stack, k_{33PVDF} is the electromechanical coupling constant of PVDF, $\tan\delta$ is the mechanical loss tangent of PVDF ($\tan\delta = 1/Q$), and f_0 is the half-wave resonant frequency of the PVDF stack, which is given by[31]

$$f_0 = (2d)^{-1}\left(\frac{c_{33}}{\rho}\right)^{0.5}\left(1 - \frac{4k_{33PVDF}^2}{\pi^2}\right) \tag{5-5}$$

where c_{33} is the thickness elastic constant of PVDF and ρ is the density of PVDF. Properties of PVDF film at 24 °C and 77 K are adapted from Ohigashi [31].

The impedance of the PVDF stack, Z, is then given by

$$Z = \frac{\left(j\omega L + \frac{1}{j\omega C} + R\right)\cdot\frac{1}{j\omega C_0}}{j\omega L + \frac{1}{j\omega C} + R + \frac{1}{j\omega C_0}} \tag{5-6}$$

where ω is the angular drive frequency.

Using this model, predictive curves for the magnitude of the stack impedance ($|Z|$) versus frequency are developed. By varying the value of $\tan\delta$ to fit the predicted and experimental impedance versus frequency curves (see Figures 5-5 and 5-6), the resonant Q of the PVDF stack can be determined. The measured resonant Q values at 24 °C and 77 K are given in Table 5-1.

The bulk PVDF resonant Q at 9.17 MHz and 24 °C is measured to be 10, using a single layer of 119 μm thick film (see Figure 5-5). This shows good agreement with the results of Ohigashi [31], who reports a mechanical loss tangent of 0.1 for PVDF in the MHz range, which corresponds to a Q of 10. The resonant Q for a 20 layer stack of 28 μm stack of PVDF is measured to be 5.6, which indicates that the acoustic dissipation is nearly doubled by the presence of several epoxy bonds. The 77 K data show that acoustic dissipation of PVDF is greatly decreased at lower temperatures. The drop-off in Q with increasing number of PVDF layers is much more severe at 77 K than at 24 °C because the additional acoustic dissipation due to the presence of the epoxy bonds is much greater than the bulk dissipation of the PVDF material at 77 K, whereas the acoustic dissipation due to the epoxy bonds and the bulk PVDF acoustic dissipation are of comparable magnitude at 24 °C.

Stacks cured at pressures up to 5.5×10^7 Pa are tested, but no increase in resonant Q with increasing cure pressure is observed at cure pressures over 1.7×10^7 Pa. Therefore, it is determined that a cure pressure of 1.7×10^7 Pa is adequate.

5.4 Conclusions

In this chapter, an attempt to duplicate Strachan's cyanoacrylate bonding technique is reported to result in unsatisfactory bond thickness and quality, and is therefore abandoned. An alternative PVDF bonding method using a low viscosity strain gauge epoxy is developed. Thickness measurements and piezoelectric resonance experiments are used to determine the effect of the number of bonds on the resonant Q of a PVDF stack, and to optimize the bonding procedure. Using Measurements Group, Inc. type AE-15 epoxy, and curing at pressures over 1.7×10^7 Pa for 1.5 hours at 70 °C, high-quality bonds can be achieved. A resonant Q of 5.6 is reported for a 20 layer stack of 28 μm thick PVDF at 24 °C.

The bonding procedure developed will be used to construct the MHz-resonant stacks for the Strachan-Aspden replica device, which will be described in the following chapter.

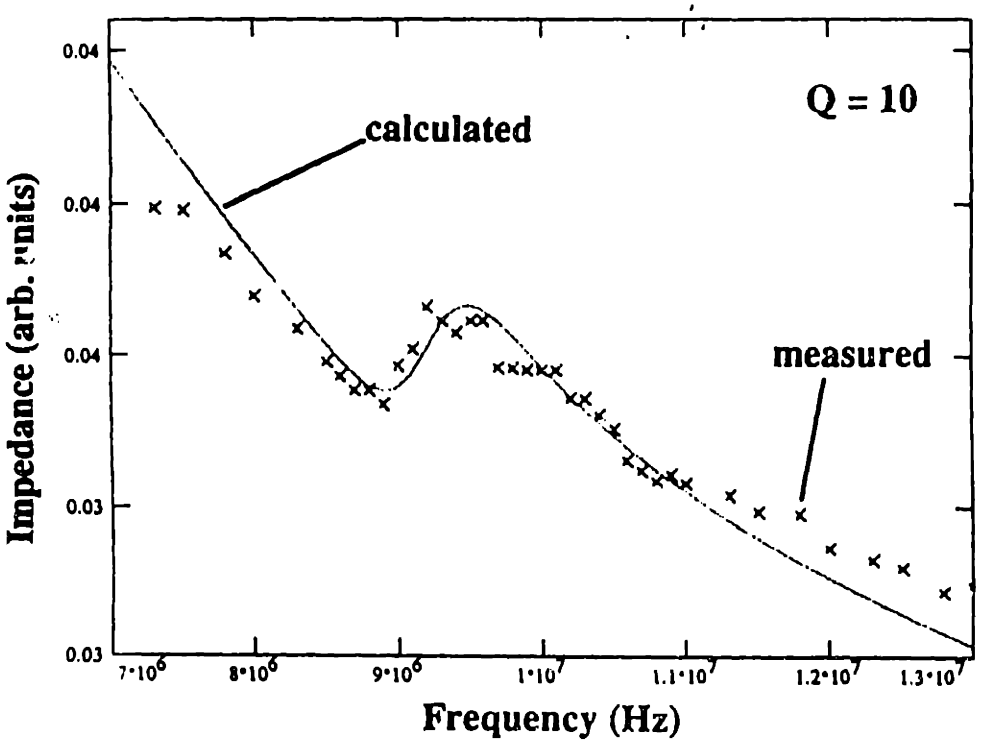

Figure 5-5. Impedance versus frequency plot for the single layer of 119 μm PVDF at 24 °C.

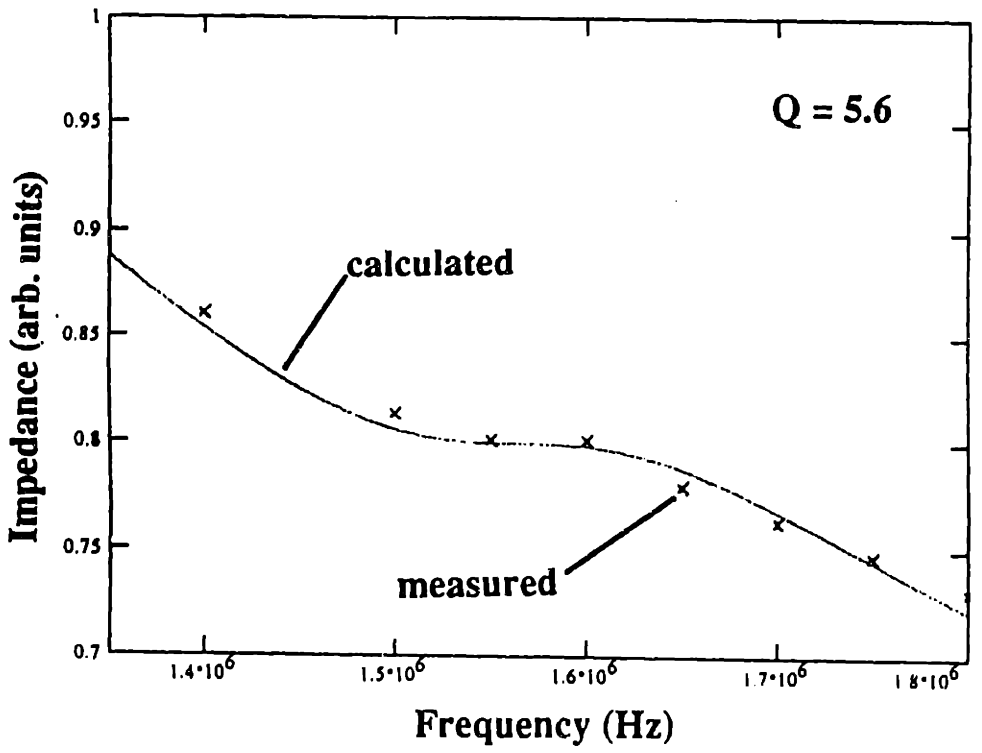

Figure 5-6. Impedance versus frequency plot for the 20 layer stack of 28 μm PVDF at 24 °C.

stack configuration (# layers x thickness of each layer)	stack thickness	resonant frequency @ 24 °C	resonant Q @ 24 °C	resonant frequency @ 77 K	resonant Q @ 77 K
1 x 119 μm	119 μm	9.17 MHz	10	12.0 MHz	300
2 x 119 μm	242 μm	4.50	7.0	6.10	167
5 x 28 μm	165 μm	7.04	5.9	8.92	33
20 x 28 μm	650 μm	1.56	5.6	2.07	7.1

Table 5-1. Measured resonant frequency and Q for the PVDF stack samples.

6. CONSTRUCTION AND TESTING OF THE STRACHAN-ASPDEN REPLICA DEVICE

6.1 Introduction

In order to reproduce the results obtained by Strachan and Aspden, a replica of the first prototype device is constructed. This experiment attempts to duplicate Strachan's first experiments involving thermoelectric energy conversion in PVDF, where he observed electrical spiking associated with the application of a temperature gradient across the first prototype device (see section 2.2).

Several PVDF stack elements are constructed using the epoxy bonding technique described in chapter 5. The elements are tested for electrical integrity. These elements, along with several acrylic half-wave plates, are used in the construction of a composite stack similar to Strachan and Aspden's first prototype device. The device consists of 10 PVDF "driver" elements and one PVDF "listener" element. Unlike Strachan's first prototype device, no magnetic recording tape or PZT is incorporated into the stack structure (the PVDF "driver" elements are used to provide the acoustic drive). A high-voltage drive system is developed to drive the PVDF "driver" elements at frequencies from 10 kHz-2 MHz and voltage levels from 0-400 V peak-to-peak. A temperature gradient assembly is developed to apply a transverse temperature gradient to the replica device. It is hoped that the conditions of Strachan's first experiment can be achieved using this device and that his observation of voltage spiking in a PVDF element not

connected to the drive circuit (the "listener" element) can be confirmed. A series of tests is used to characterize the performance of the device replica with varying drive frequency and temperature (and temperature gradient), while searching for any anomalous effects related to energy conversion.

6.2 PVDF Stacks

The strain-gauge epoxy bonding method described in section 5-3 is used to construct the Strachan-Aspden replica device. PVDF stacks are constructed using 21 layers of 28 μm thick PVDF film from AMP, Inc., coated on one side with 2200 angstroms Ni and 800 angstroms Al. This PVDF film is similar to that used by Strachan in the construction of the prototype devices. The HCl etching technique described in section 5.3.3 is used to remove the metallization from one side of the PVDF film.

A schematic of the stack assembly is shown in Figure 6-1. The face dimension of the PVDF stack is 5.1 mm x 25.4 mm. The stretch direction of the PVDF film is oriented in the 5.1 mm dimension. A single layer tab of PVDF 12.7 mm long extends from the top and bottom of the stack for electrical connection. All PVDF layers are metallized on the top side only. The stacks are cured at 70 °C and 5.5 x 10^7 Pa for 1.5 hours. 15 stacks are constructed. The average stack thickness is 0.64 mm.

The capacitance and resistance between the leads of each PVDF stack are measured using a BK Precision 875A LCR meter. The stack capacitance is calculated using equation (5-1) to be approximately 20 pF. The resistance between the leads of a properly made stack is assumed to be >>10 MΩ. Those stacks that deviate significantly from these expected values are discarded. After this testing procedure, 11 "good" stacks remain. Using equation (4-3), the half-wave resonant frequency of the PVDF stacks is calculated to be approximately 1.55 MHz at 24 °C.

6.3 Stack Assembly

6.3.1 Acrylic Half-Wave Plates.

The speed of sound in the acrylic material used in the construction of the Strachan-Aspden replica device is measured to be 2613 m/s at 24 °C using PZT "driver" and "listener" elements mounted on either side of a sample of the acrylic material. This shows good agreement with the measurement of 2717 m/s for acrylic reported by Folds [42]. Using equation (4-3), the thickness of acrylic required to be half-wave resonant at 1.55 MHz is 0.84 mm. Several 5.1 mm x 25.4 mm x 0.84 mm thick acrylic plates are constructed.

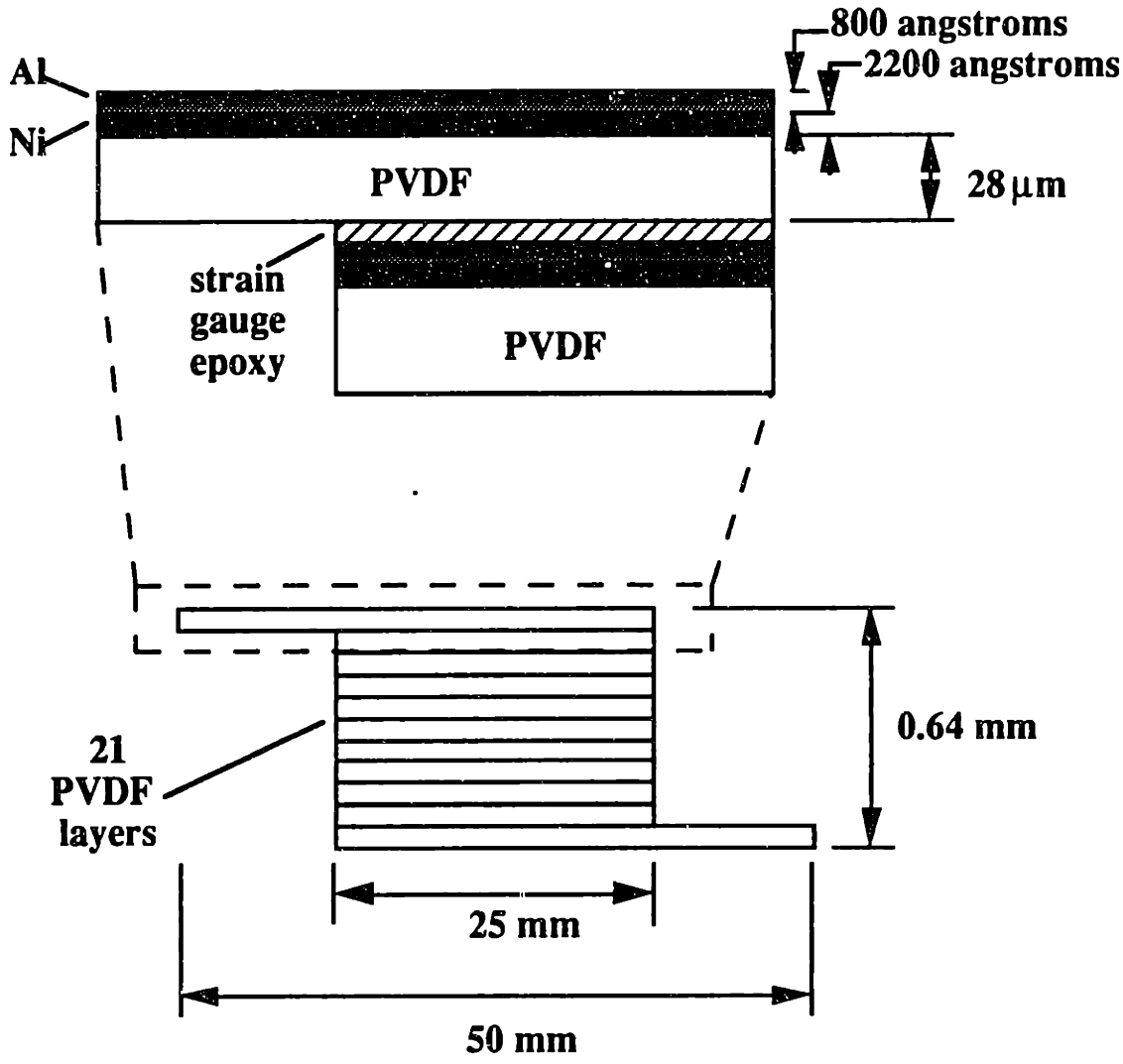

Figure 6-1. Strachan-Aspden replica device PVDF stack schematic.

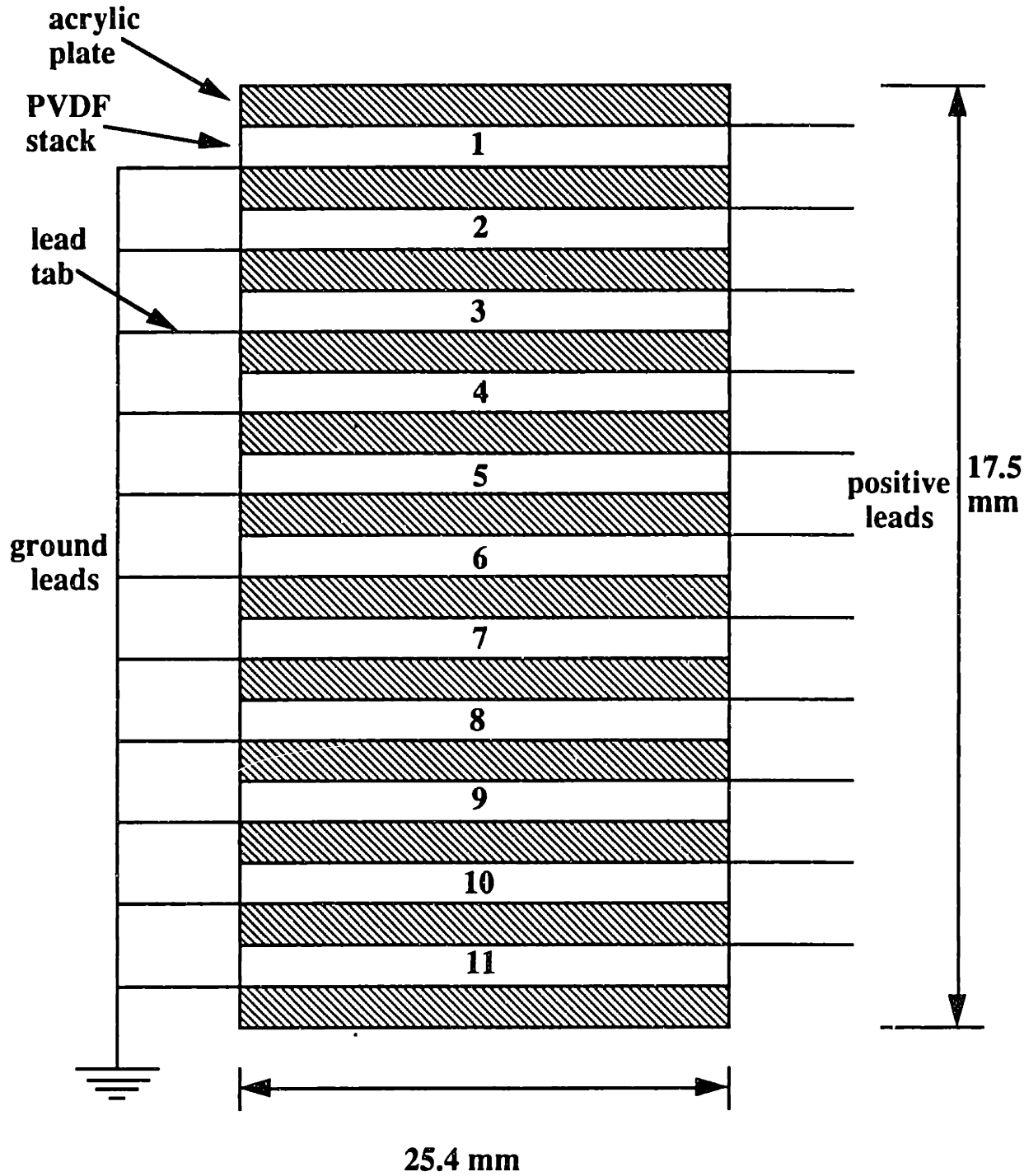

Figure 6-2. Schematic of the Strachan-Aspden replica device.

Stack #	Measured Capacitance (pF)
1	17.86
2	18.98
3	18.32
4	19.02
5	18.19
6	21.26
7	20.30
8	22.64
9	19.55
10	20.97
11	18.69

Table 6-1. PVDF stack capacitance measurement results.

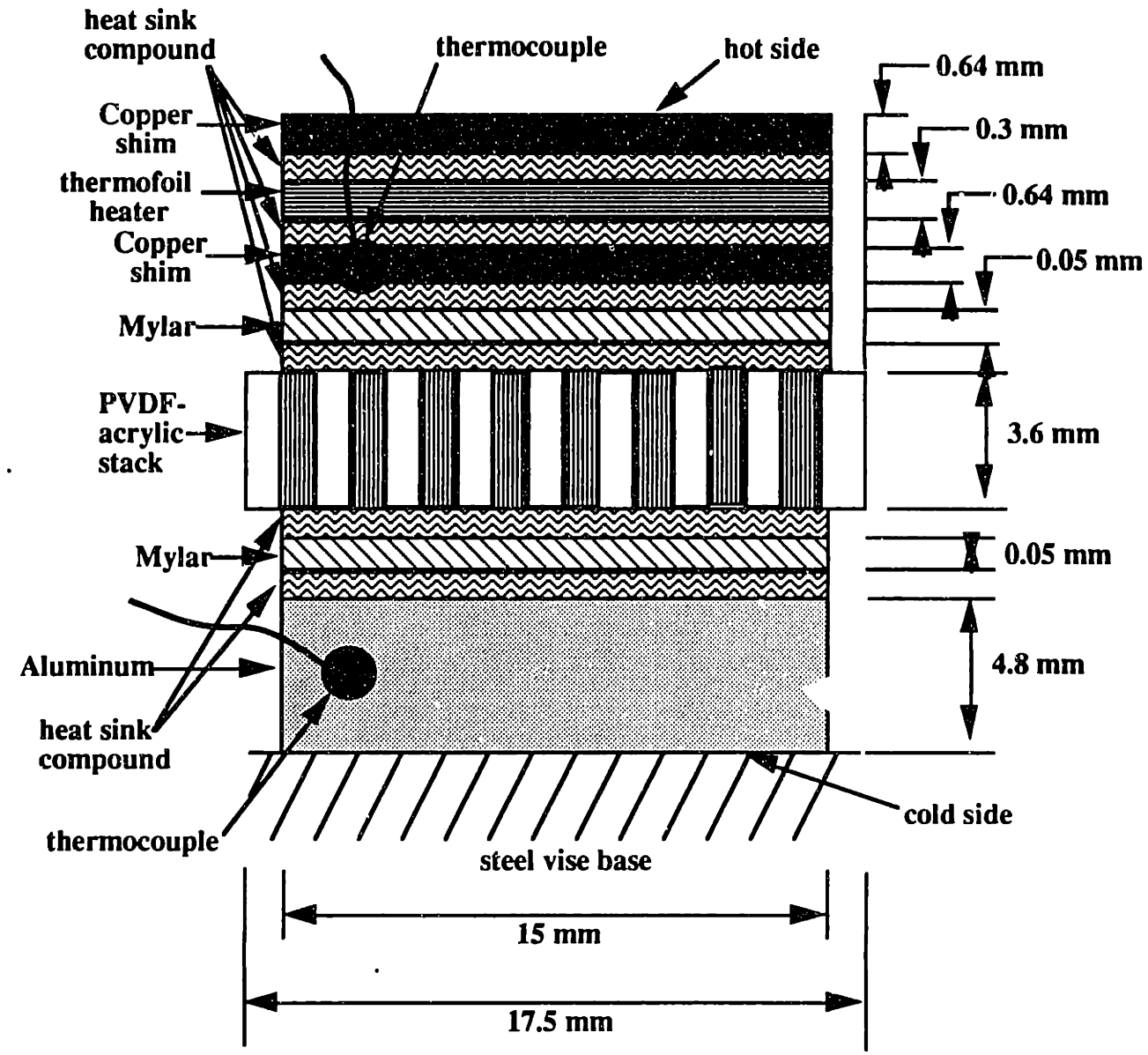

Figure 6-3. Schematic of the temperature gradient assembly.

of the stack. 0.023 mm thick mylar sheets on either side of the stack are used to provide for electrical insulation. A thin layer of heat sink compound is used between each layer to provide for better thermal contact and electrical insulation. Type K thermocouples are mounted in the aluminum block and the copper shim piece under the thermofoil heater to provide for temperature measurement. An additional Minco thermofoil heater can be mounted under the aluminum block in order to provide for isothermal device operation at temperatures above 24 °C. A 1 kg steel weight and delrin spacer are used to apply a vertical clamping force on the temperature gradient assembly to provide for better thermal contact between the individual layers and to prevent buckling of the PVDF-acrylic composite stack.

6.4.2 Clamping

A schematic of the device setup is shown in Figure 6-4. The PVDF-acrylic composite stack is clamped in a precision machinist's vise. Belleville disc springs are mounted on the clamping bolt and are used to apply a clamping force of 400-450 N. This produces a compressive stress of ~4-5 MPa in the PVDF-acrylic composite stack. This assures that the composite stack is always in a compressive condition during operation.

6.4.3 Electrical Grounding

The vise and the copper shim pieces are both connected to electrical ground. The whole assembly is epoxied to a delrin baseplate. A copper ground sheet is placed under the delrin baseplate and connected to electrical ground. The PVDF "driver" and "listener" stack leads pass through electrically grounded copper tubing. This grounding helps to reduce capacitive coupling between the PVDF "driver" and "listener" stack leads.

6.4.4 Electrical Drive and Measurement Setup

A schematic of the drive and measurement setup is shown in Figure 6-5. An Hewlett Packard 33120A function generator is used to provide the drive signal for the replica device experiments. The HP function generator can operate at voltages up to 20 V peak-to-peak. The Crown DC300A audio amplifier and 5:1 transformer board (see Figure 4-5) used for the single PVDF layer energy conversion experiment (described in chapter 4) is used to provide drive voltages up to 320 V peak-to-peak at frequencies ranging from 10-160 kHz. An Electronic Navigation Industries, Inc. model 310L 10 watt RF amplifier and 42:1 ferrite core transformer board (see Figure 6-6) is used to provide drive voltages up to 400 V peak-to-peak at frequencies ranging from 70 kHz-2 MHz.

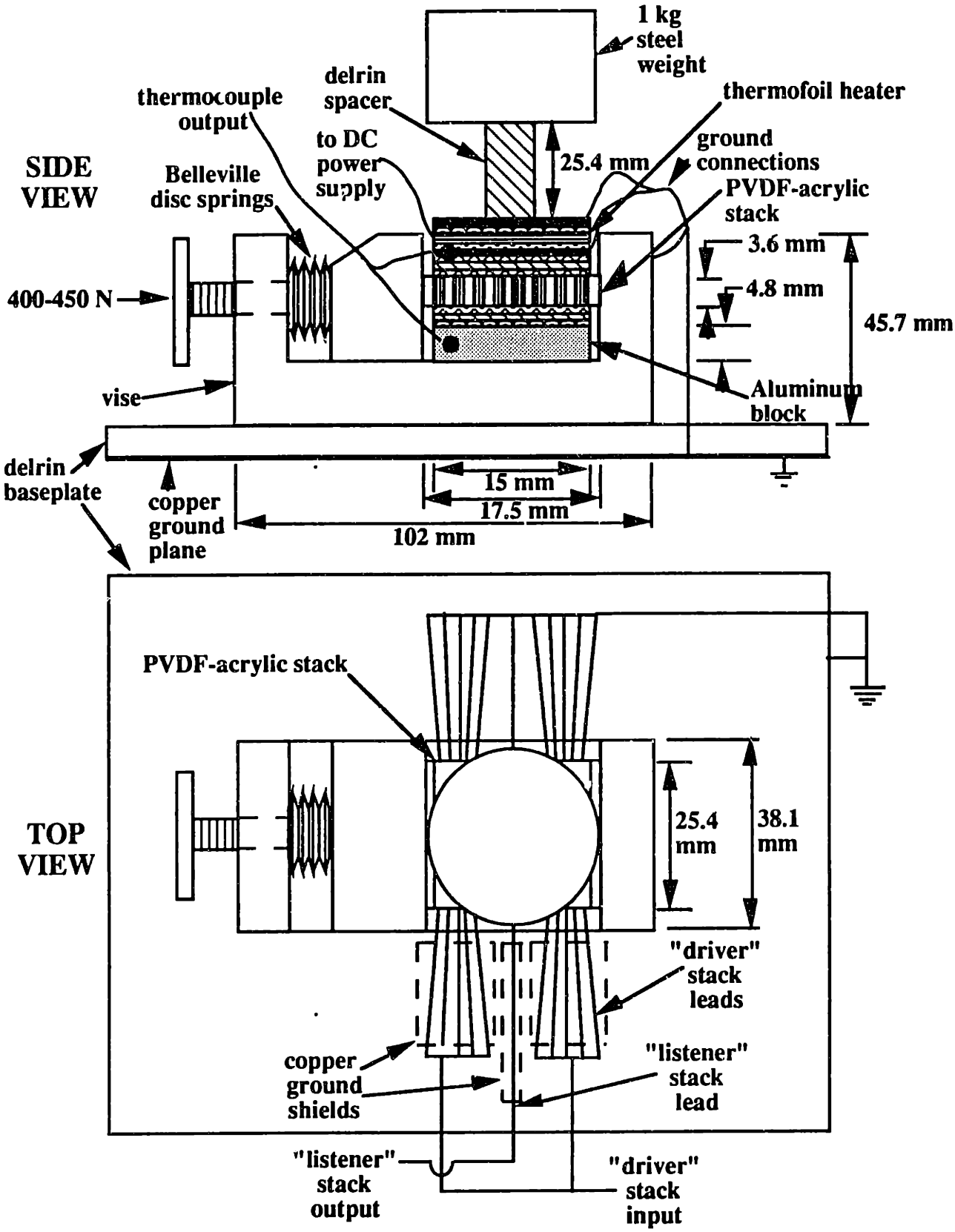

Figure 6-4. Schematic of the Strachan-Aspden replica device clamp assembly.

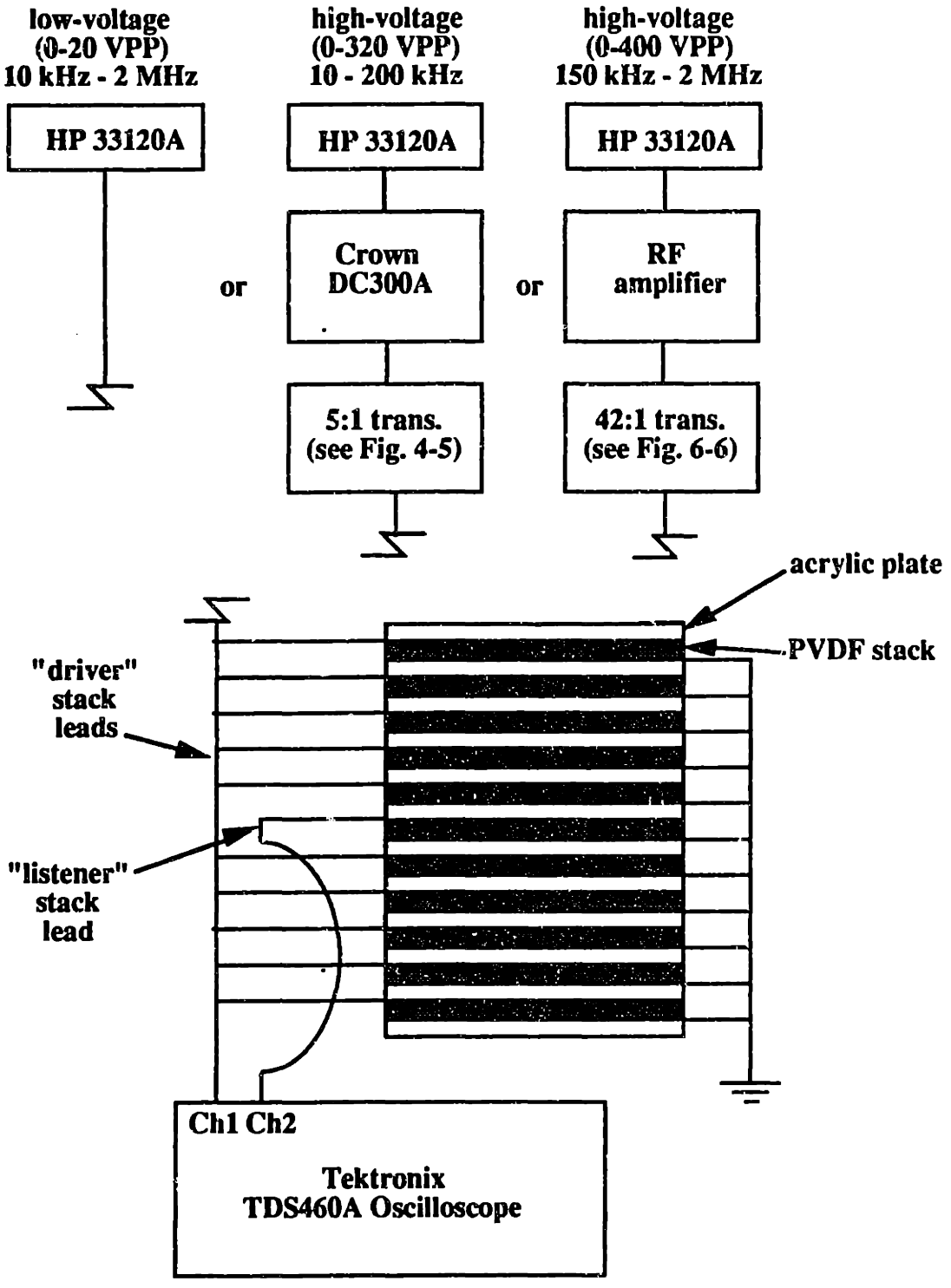

Figure 6-5. Schematic of the Strachan-Aspden replica device drive and measurement setup.

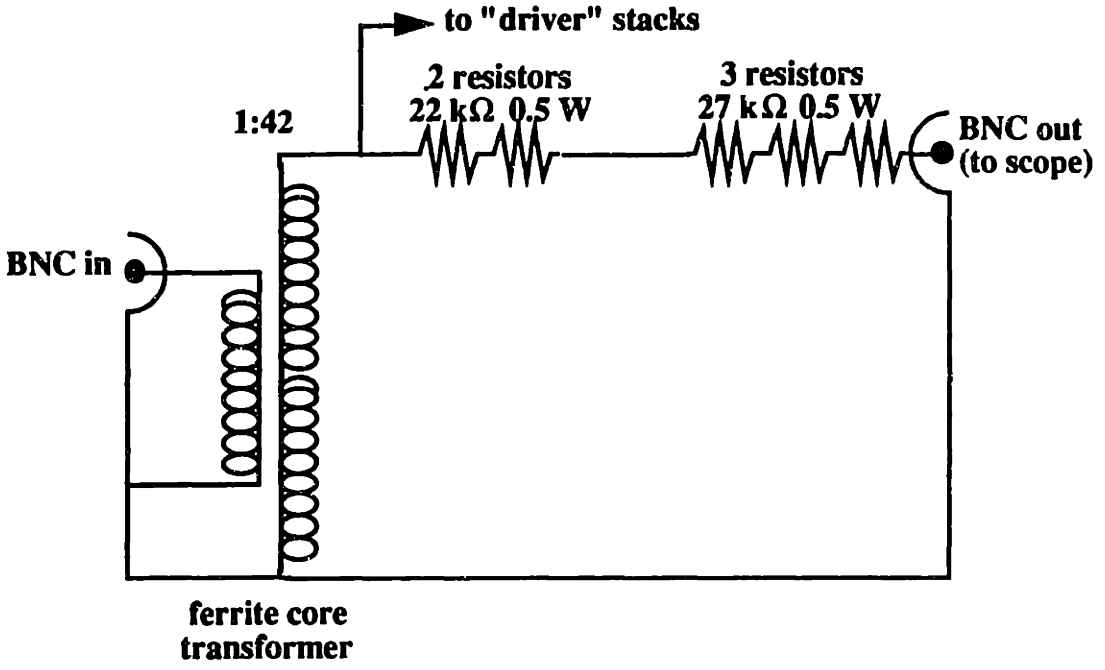

Figure 6-6. Schematic of the RF drive setup transformer board circuit.

A Tektronix TDS460A digitizing oscilloscope is used to display the PVDF "driver" and "listener" stack output voltages and perform amplitude and phase measurements. The accuracy of the amplitude and phase measurements is estimated to be ± 1 mV and ± 2°, respectively.

6.5 Experimental Procedure

The 10 PVDF "driver" stacks are driven at voltages ranging from 0-400 V peak-to-peak at frequencies ranging from 10 kHz-2 MHz. The PVDF "listener" stack output voltage amplitude and phase relationship to the drive signal is observed at various stack temperatures and with various applied temperature gradients. The "listener" stack output is observed for the presence of any electrical "spiking" as described by Strachan.

6.6 Results and Discussion

6.6.1 Frequency Sweeps

The device performance is characterized by performing frequency sweeps at a drive voltage of 20 V peak-to-peak using the HP33120A function generator. Figures 6-7 and 6-8 show the ratio of the PVDF "listener" stack output voltage to the drive voltage (V_{out} / V_{in}) and the phase difference between the PVDF "listener" stack output voltage and the drive voltage (α) versus frequency at stack temperatures (isothermal condition) of 26.8 °C, 34.6 °C, and 45.6 °C. Figures 6-9 and 6-10 show the same quantities for frequency sweeps performed with temperature gradients of 17.7 °C/cm and 39.4 °C/cm applied across the stack assembly.

Acoustic resonances are found at frequencies of approximately 80 kHz, 340 kHz, 600 kHz, 900 kHz, and 1.5 MHz. V_{out} / V_{in} ranges from 0.5 - 15 x 10^{-3}. α ranges from 0-500°. No siginificant differences are observed between the measured V_{out} / V_{in} and α values versus frequency for the frequency sweeps performed with an isothermal stack condition at elevated temperatures and with a temperature gradient applied across the stack. No "Strachan-type" spiking is observed during these experiments.

6.6.2 Output Voltage Model

The ratio of the PVDF "listener" stack output voltage V_{out} to the PVDF "driver" stack input voltage V_{in}, derived from equations (4-4) and (4-8), is given by

$$\frac{V_{out}}{V_{in}} = \frac{g_{33} l d_{33} K_d}{A} \left(1 - \frac{K_d}{K_d + K_l} \right) \tag{6-1}$$

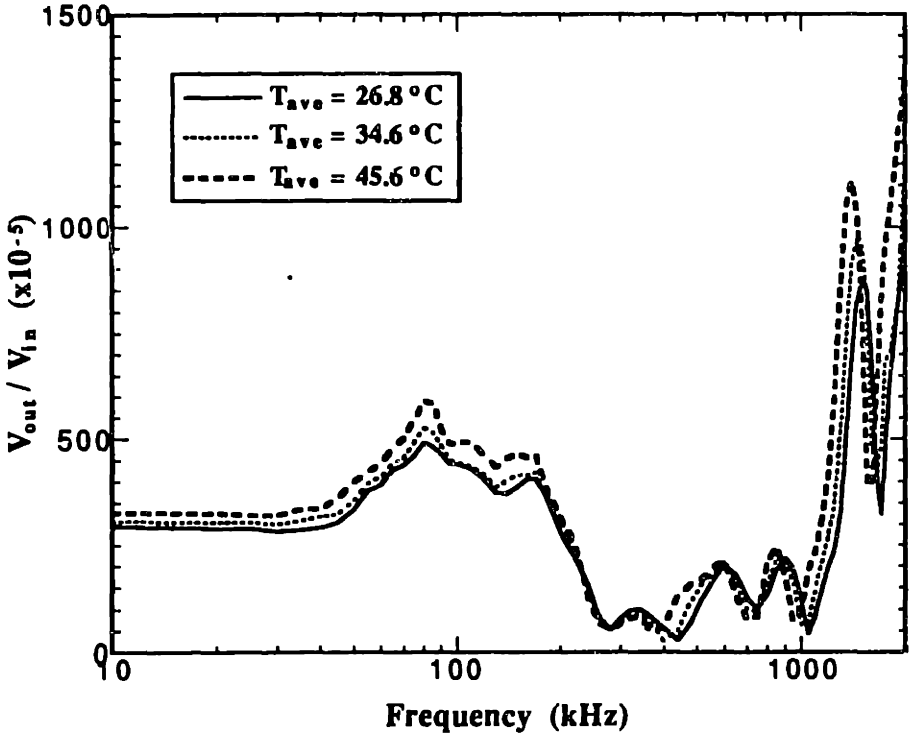

Figure 6-7. Measured V_{out} / V_{in} versus frequency at (isothermal) stack temperatures of 26.8 °C, 34.6 °C, and 45.6 °C.

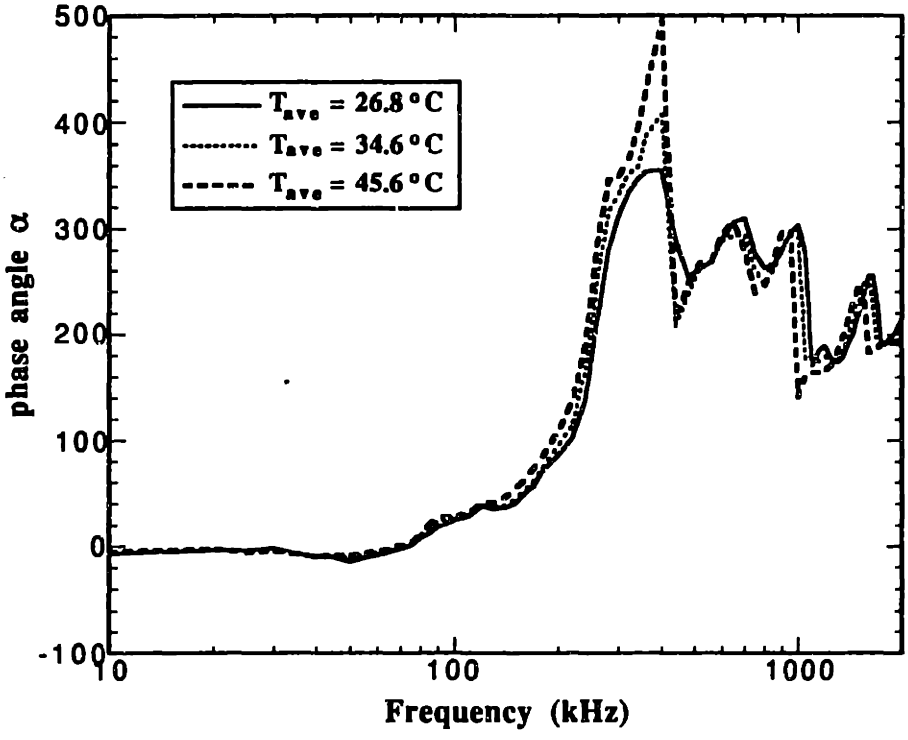

Figure 6-8. Measured phase angle α versus frequency at (isothermal) stack temperatures of 26.8 °C, 34.6 °C, and 45.6 °C.

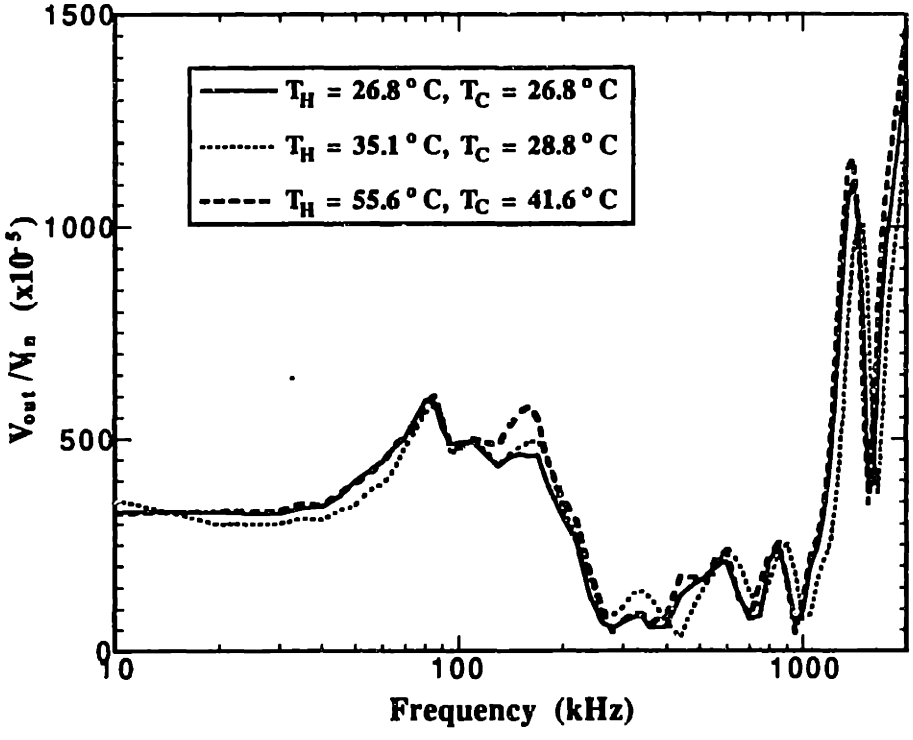

Figure 6-9. Measured V_{out} / V_{in} versus frequency at 26.8 °C and with temperature gradients of 17.7 °C/cm and 39.4 °C/cm applied across the stack assembly.

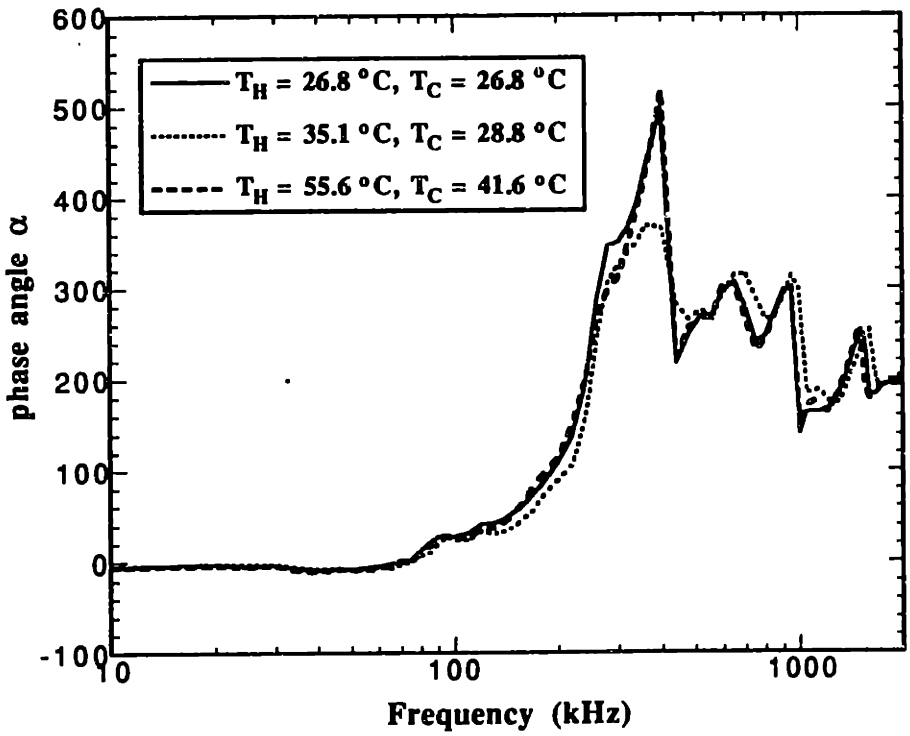

Figure 6-10. Measured phase angle α versus frequency at 26.8 °C and with temperature gradients of 17.7 °C/cm and 39.4 °C/cm applied across the stack assembly.

where g_{33} and d_{33} are the piezoelectric stress and strain constants of PVDF, l is the thickness of the PVDF "listener" stack, A is the cross-sectional area of the stack, K_d is the combined stiffness of the PVDF "driver" stacks, and K_l is the combined stiffness of the PVDF "listener" stack and acrylic half-wave plates. K_d and K_l are calculated using equation (4-6). The vise clamp faces are assumed to be infinitely stiff.

Using equation (6-1), and the temperature dependence of the properties of PVDF and acrylic,[31,43] V_{out} / V_{in} can be calculated versus temperature. The predicted and experimental values of V_{out} / V_{in} versus temperature are shown in Figure 6-11. The experimental values are all derived from measurements at 10 kHz, to avoid the effects of resonant behavior (see section 6.6.3, below). Good agreement is observed between the predicted and experimental values of V_{out} / V_{in}.

6.6.3 Acoustic Resonances

In addition to loading effects of stray capacitances on the measured output voltage of the PVDF "listener" stack (see Appendix B), acoustic resonances should also account for variation of V_{out} / V_{in} with frequency. Because the acoustic impedances of PVDF and acrylic are similar (Z_{PVDF} = 3.9 x 10^6 kg/m^{2}s and $Z_{acrylic}$ = 3.3 x 10^6 kg/m^{2}s), the half-wave resonance of the PVDF-acrylic stack assembly, f_{stack}, is approximated by

$$f_{stack} = \left(\frac{2n_a l_a}{c_a} + \frac{2n_p l_p}{c_p} \right)^{-1} \tag{6-2}$$

where n_a and n_p are the number of acrylic half-wave plates (12) and PVDF stacks (11) in the stack assembly, respectively, l_a and l_p are the thickness of the acrylic half-wave plates and PVDF stacks, respectively, and c_a and c_p are the speeds of sound in acrylic and PVDF, respectively. Using material properties from Folds [42] and Ohigashi [31], f_{stack} is calculated to be 75 kHz at 25 °C. Harmonic resonances are expected at approximately 150 kHz, 300 kHz, etc. This shows good agreement with the observed stack resonance values in the 20 V peak-to-peak frequency sweep experiments. f_{stack} is plotted versus temperature in Figure 6-12. Good agreement is observed between the predicted and experimental values.

The half-wave resonant frequency of the PVDF "listener" stack, f_{PVDF}, is given by

$$f_{PVDF} = \frac{c_p}{2l_p} \tag{6-3}$$

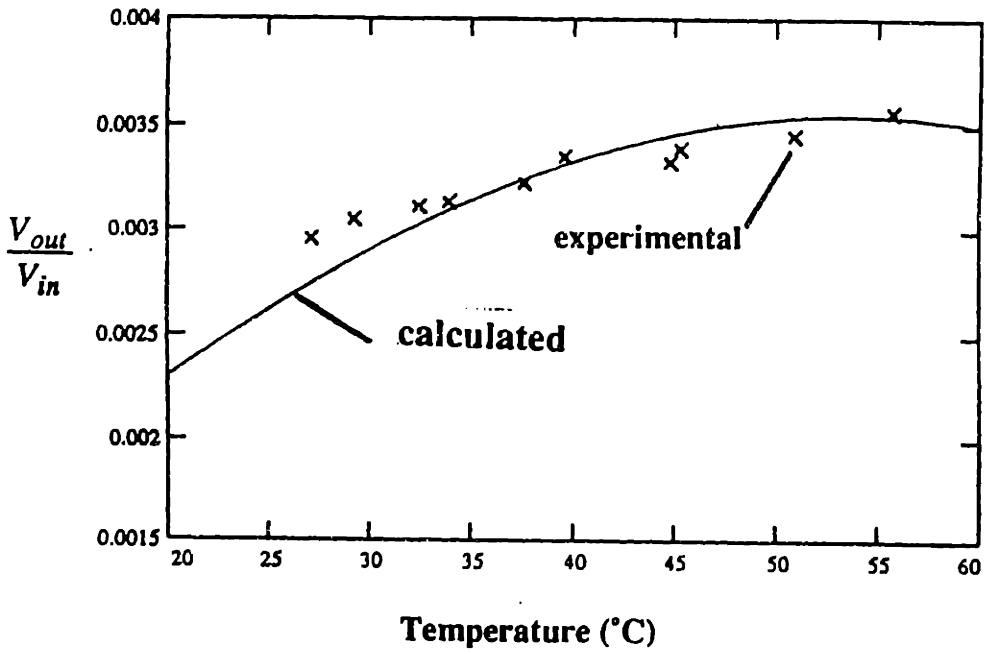

Figure 6-11. Calculated and experimental V_{out} / V_{in} versus temperature (isothermal condition).

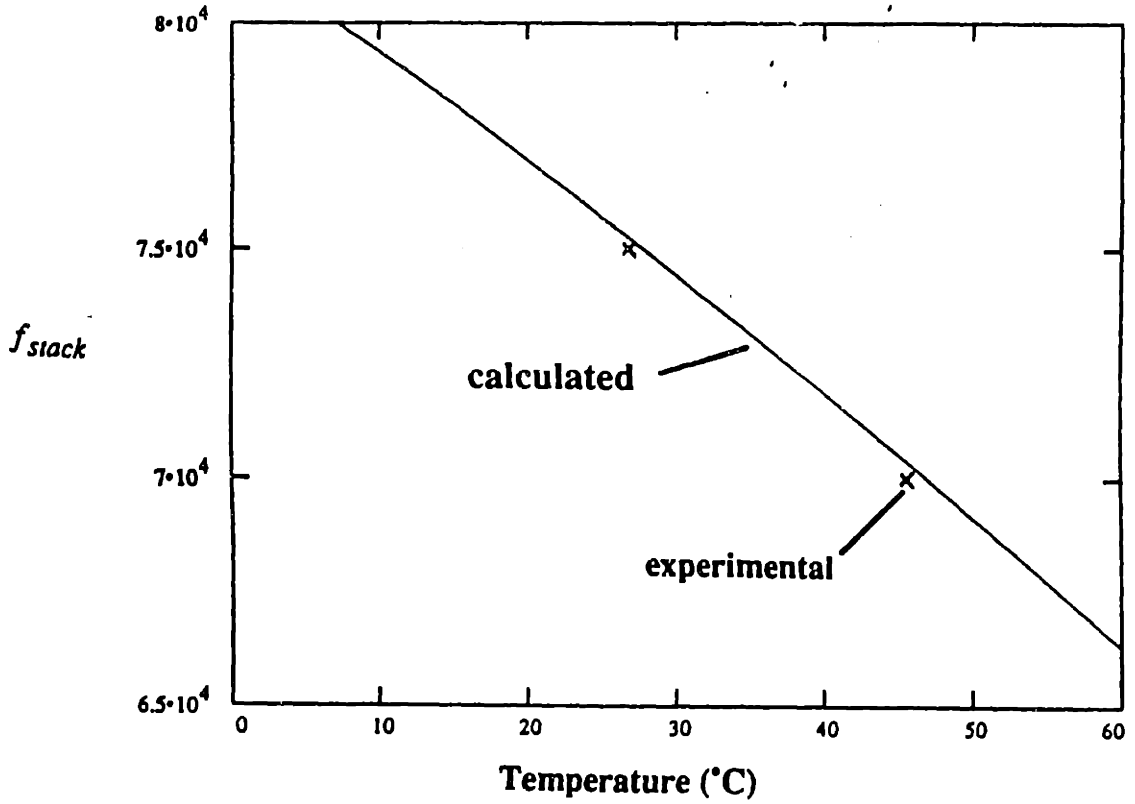

Figure 6-12. Calculated and experimental PVDF-acrylic composite stack half-wave resonant frequency f_{stack} versus temperature (isothermal condition).

Using material properties from Folds [42] and Ohigashi [31], f_{PVDF} is calculated to be 1.55 MHz at 25 °C. f_{PVDF} is plotted versus temperature in Figure 6-13. Good agreement is observed between the predicted and experimental values.

6.6.4 High Voltage Drive Experiments

The audio-range and RF-range high-voltage drive setups described in section 6.4.4 are used to drive the PVDF "driver" stacks in order to achieve higher stress and voltage amplitudes in the PVDF "listener" stack. The maximum applied drive voltage versus frequency is shown in Figure 6-14. The highest applied voltage is approximately 400 V peak-to-peak between 70 and 140 kHz, which is achieved using the RF amplifier and ferrite core transformer board. Higher voltages between 70 and 140 kHz could have been achieved, but a voltage of 400 V peak-to-peak is determined to safely avoid any arcing or dielectric breakdown in the PVDF stacks. At other frequencies, the maximum voltage used is limited by the output power of the drive setups.

Frequency sweeps are performed from 10 kHz-2 MHz using the high-voltage drive setups at 24.7 °C and with a 43.8 °C/cm temperature gradient applied across the stack assembly (T_H = 50.5 °C, T_C = 34.9 °C). The observed values of V_{out} / V_{in} and α during the high-voltage drive experiments are very similar to those measured in the low-voltage (20 V peak-to-peak) frequency sweeps. Also, no electrical spiking is observed in the PVDF "listener" stack output voltage profile.

6.7 Conclusions

A replica of Strachan and Aspden's first prototype device is constructed, consisting of ten 1.55 MHz-resonant PVDF "driver" stacks, one 1.55 MHz-resonant PVDF "listener" stacks, and 12 acrylic half-wave plates. A high voltage drive system is developed to provide drive voltages up to 400 V peak-to-peak at frequencies ranging from 10 kHz-2 MHz. A series of frequency sweeps are performed to characterize the performance of the device with varying temperature (and temperature gradient). The observed variation of stack voltage output and resonant frequencies with temperature is consistent with the temperature dependent properties of the stack materials. No significant differences are observed between frequency sweeps performed with an isothermal stack condition at elevated temperatures and with a temperature gradient applied across the stack. No electrical spiking like that reported by Strachan is observed. No other anomalies that could be related to energy conversion effects are observed.

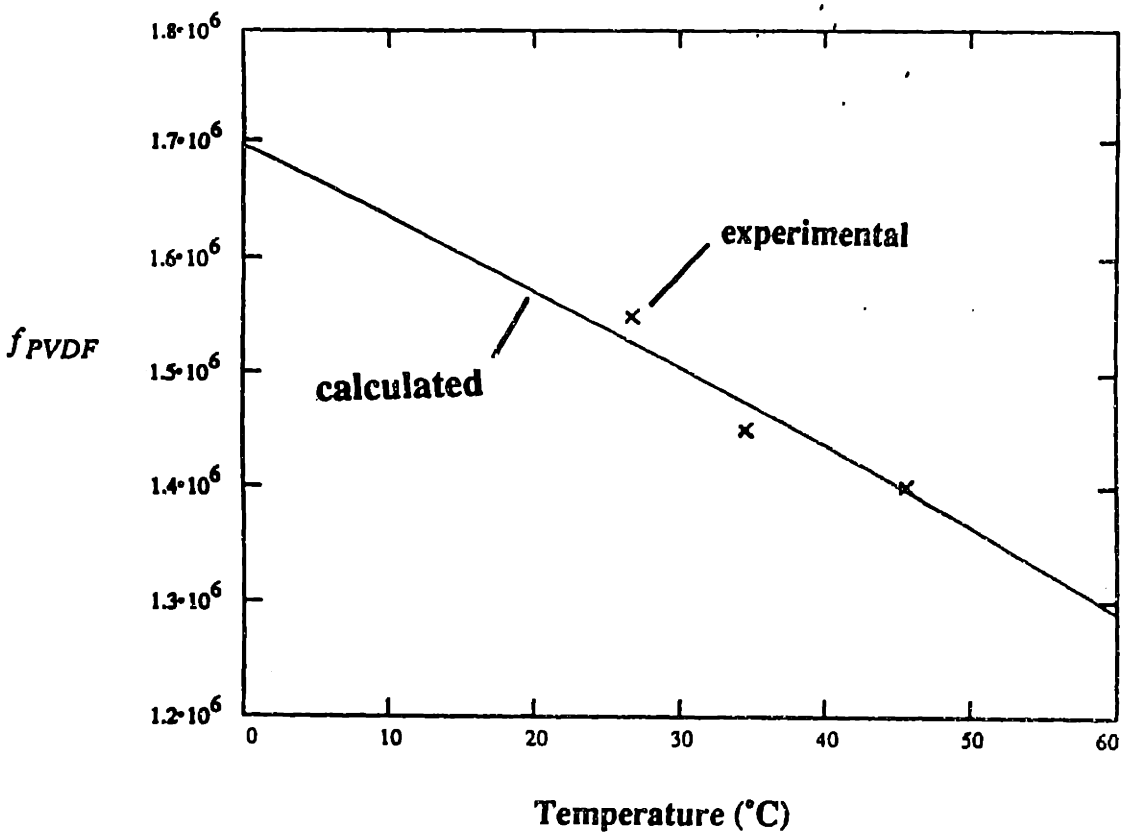

Figure 6-13. Calculated and experimental PVDF "listener" stack half-wave resonant frequency f_{PVDF} versus temperature (isothermal condition).

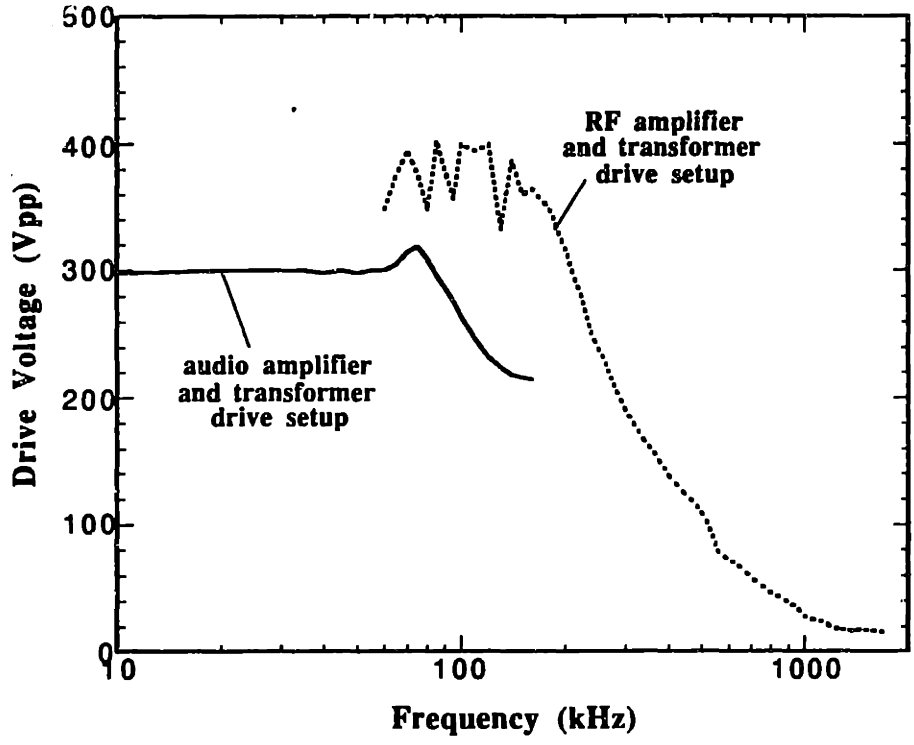

Figure 6-14. Maximum drive voltage used versus frequency for the high-voltage drive experiments.

7. Conclusions and Recommendations

In this study, Strachan and Aspden's claims of a high-efficiency AC thermoelectric generator design are investigated. An overview of Strachan's experiments with the prototype PVDF stack devices is given. Aspden's explanation for the operation of the devices involving AC effects on circulating DC thermoelectric currents and the experiments performed by Strachan to test this hypothesis are described. An analysis of DC thermoelectric effects in the Ni-Al bimetallic coatings is performed, showing that a circulating DC thermoelectric current on the order of 18 mA and a transverse magnetic field on the order of 2.6 gauss can be developed by Seebeck action in the bimetallic coating of the PVDF film when a transverse temperature gradient of 70 °C is applied. No connection is established between this Seebeck action and any possible energy conversion mechanism. DC thermoelectricity in the bimetallic coating of the PVDF film is shown not to be able to account for the efficiencies and temperature gradients observed by Strachan in the prototype devices.

The dielectric, piezoelectric and pyroelectric aspects of PVDF are reviewed, as any or all of these properties may be involved in the energy conversion mechanism observed by Strachan. The relative dielectric constant and dissipation factor of PVDF are measured with a transverse magnetic field imposed across the PVDF film sample, to determine if Aspden's hypothesis of the presence of a magnetic field due to circulating

DC thermoelectric currents could somehow affect the dielectric properties of PVDF. No effect of the transverse magnetic field on the dielectric properties of PVDF is observed.

To test for energy conversion effects in PVDF, a single layer of PVDF is mounted in an inertial clamp assembly with a PZT piezoelectric driver element. The PVDF layer can be driven electrically and/or acoustically (with the PZT), using a high-voltage (0-300 V peak-to-peak) audio-range drive system at frequencies ranging from 10-30 kHz. The relative phase of the electrical and acoustic drives can be varied from 0-180°. Various experiments are performed in which the relative phase and amplitude of the electrical and acoustic drives is varied with and without a transverse temperature gradient of 19 °C/cm applied across the PVDF layer. Experiments are performed with the PVDF layer output leads open-circuited and connected across a 10 kΩ resistor. No anomalous effects that could be related to energy conversion (such as electrical spiking) are observed.

An attempt to duplicate Strachan's cyanoacrylate bonding method for the construction of multilayer PVDF stacks is reported to result in unsatisfactory bond thickness and quality, and is therefore abandoned. An alternative PVDF bonding method using a low-viscosity strain gauge epoxy bonding method is developed. Thickness measurements and piezoelectric resonance experiments are used to optimize the bonding procedure. A cure cycle for Measurements Group, Inc. type AE-15 epoxy at 1.7×10^7 Pa and 70 °C for 1.5 hours is found to produce high quality bonds. A resonant Q of 5.6 is reported for a 20 layer stack of 28 μm thick PVDF at 1.56 MHz and 24 °C.

The strain gauge epoxy bonding method is used to construct 21 layer stacks of 28 μm thick PVDF for use in a replica of Strachan's first prototype device. It is hoped to duplicate the conditions of Strachan's experiments with the first prototype device, where he observed electrical spiking in a PVDF stack not connected to the drive circuit.[10] The replica consists of ten PVDF "driver" stacks and one PVDF "listener" stack mounted in a clamp assembly. High-voltage audio-range and RF-range drive systems are used to drive the PVDF "driver" stacks at voltages up to 400 V peak-to-peak at frequencies ranging from 10 kHz-2 MHz. The listener stack output voltage and phase relationship to the drive voltage is monitored during frequency sweeps performed at several stack temperatures (isothermal condition) and with temperature gradients of up to 43.8 °C/cm applied across the stack. No siginificant differences are observed between frequency sweeps performed with an isothermal stack condition at elevated temperatures and with a temperature gradient applied across the stack. The PVDF "listener" stack output voltage and resonance frequency peaks agree well with static and acoustic models developed for the replica device. No anomalous effects are observed due to the presence of the transverse temperature gradient.

If a "Strachan"-type energy conversion mechanism exists, then there are several possible reasons why it is not observed during the course of this study. First, the stress and/or voltage levels achieved in the PVDF layers/stacks is this study might not be high enough to couple the energy conversion mechanism. Strachan reports voltage levels of approximately 2000 V peak-to-peak in a 20-layer PVDF stack not connected to the drive circuit in the first prototype device,[10] which corresponds to a stress amplitude of approximately 10-11 MPa peak-to-peak. In this study, the maximum stress amplitude achieved is approximately 0.04 MPa peak-to-peak (in the single PVDF layer energy conversion experiment described in chapter 4). Second, since Strachan's bonding method using ethyl cyanoacrylate adhesive with a tetrabutyltitanate/petroleum ether/water vapor surface treatment is not used in either the single PVDF layer or replica device experiments, any mechanism related to chemical reactions involved with either the surface treatment or adhesive could not be observed. Third, the manner of PVDF excitation might not be the same used by Strachan in the operation of his prototype devices. It is unclear whether the output voltage reported by Strachan for the first prototype device was from a PVDF stack that was only driven acoustically. It may be necessary to provide an electrical drive to the PVDF stack while also driving it acoustically. Although various drive conditions are attempted during the single PVDF layer energy conversion experiments and Strachan-Aspden replica device experiments, no anomalous effects are observed.

There are various possible explanations for the energy conversion mechanism related to the operation of Strachan's prototype devices. Aspden's hypothesis regarding AC effects on circulating DC thermoelectric currents in the bimetallic coating of the PVDF film is described in section 2.5 and in several publications.[3-6] The piezoelectric and pyroelectric nature of PVDF may be involved in a possible energy conversion mechanism. A chemical reaction involving PVDF, Ni, Al, and/or any of the chemicals used by Strachan for surface preparation and bonding in the construction of his PVDF stacks could possibly be involved in a chemical reaction energy conversion mechanism. This could explain the limited operational lifetime of the prototype devices.[10] Strachan now feels that magnetic recording tape and tetrabutyltitanate are required in the construction of the PVDF stacks for the energy conversion effect to be observed, even though the second prototype device was constructed without using magnetic recording tape.[9,11,44] As of yet, no satisfactory explanation for the operation of Strachan's prototype devices has come to light.

The high voltage levels necessary for observation of the energy conversion effect in Strachan's prototype devices may couple a polarization switching mechanism in the

PVDF film. Extremely high electric potentials can be developed if polarization switching occurs in a stack of PVDF layers where the polarizations of the layers are all parallel and vertical.[25] Spiking can be observed in the poling current of PVDF films, which may or may not be related to Barkhausen pulses observed in other ferroelectrics.[25] This may explain the electrical spiking observed by Strachan in his experiments with the first prototype device. It is not known how this mechanism could be related to an energy conversion effect.

In order to provide for higher stress and voltage levels to be achieved in the PVDF material to more accurately duplicate the conditions of Strachan's prototype devices, a simple experiment is proposed. A schematic of the experimental design is shown in Figure 7-1. The device consists of ten PZT "driver" elements, 25.4 mm x 2.5 mm x 1 mm thick, two acrylic insulator plates, 25.4 mm x 2.5 mm x 0.84 mm thick, and one PVDF "listener" layer, 25.4 mm x 2.5 mm x 28 μm thick. The stack is assembled using the strain gauge epoxy bonding technique described in section 5.3. The stack assembly is mounted in a clamp assembly, and provision is made for a temperature gradient of up to 70 °C to be applied across the PVDF layer in the 2.5 mm dimension. A high-voltage drive system can be used to drive the PZT "driver" elements, which are electrically connected in parallel. The PVDF "listener" layer output voltage can be observed using an oscilloscope for anomalous electrical effects. The half wave resonant frequency of this assembly is calculated using equation (6-3) to be 220 kHz at 24 °C. The ratio of V_{out}/V_{in} for this device is calculated using the model described in section 6.6.2 to be 0.007 at 24 °C. For a drive voltage of 100 V peak-to-peak, this corresponds to a PVDF "listener" layer voltage of 0.7 V peak-to-peak, and an oscillating stress of 0.074 MPa peak-to-peak. This is significantly higher than the voltage and stress levels realized in the Strachan-Aspden replica device described in chapter 6. Also, a resonant Q much higher than the Strachan-Aspden replica device is expected for this experimental setup, as the mechanical loss tangent of PZT is much lower than that of PVDF.

Since there are so many possible explanations for energy conversion effects in the prototype devices, the first priority of any future research in this area is to duplicate Strachan's result (i.e. to observe an anomalous electrical effect in a PVDF stack driven acoustically and/or electrically in the presence of a transverse temperature gradient). If an anomalous effect is discovered, a series of experiments can be designed to determine the conditions necessary for observation of the effect and to investigate possible mechanisms. Only after Strachan's result has been duplicated and the energy conversion mechanism has been well understood can working energy conversion devices be constructed using the Strachan design.

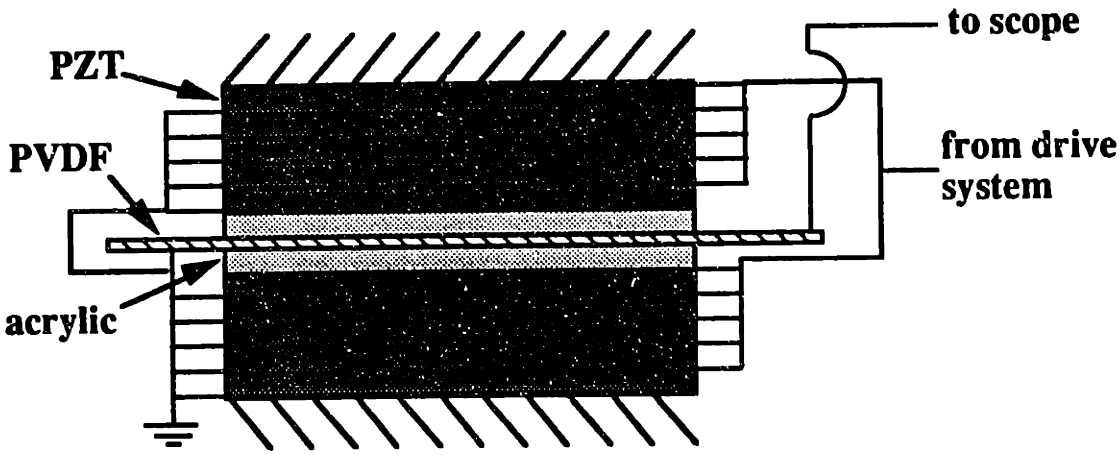

Figure 7-1. Schematic of the proposed experimental setup to provide for higher voltage and stress amplitudes in the PVDF material.

Appendix A: Composite Stack Stiffness and Inertial Clamp Mechanical Resonance for the Single PVDF Layer Energy Conversion Experiment

Stack Stiffness

A schematic of the series spring model used for determination of the stack stiffness in the single PVDF layer energy conversion experiment (see chapter 4) is shown in Figure A-1.

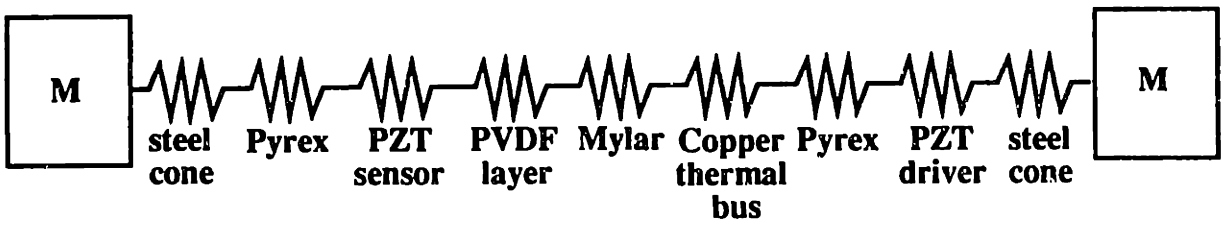

Figure A-1. Series spring model for resonant frequency calculation.

The composite stiffness for this series spring arrangement, K_{comp}, is given by

$$K_{comp} = \left(\frac{2}{K_{cone}} + \frac{2}{K_{Pyrex}} + \frac{2}{K_{PZT}} + \frac{1}{K_{Mylar}} + \frac{1}{K_{Cu}} + \frac{1}{K_{PVDF}} \right)^{-1} \quad \text{(A-1)}$$

where the stiffness K for each element (except the steel conical sections) is given by

$$K = \frac{EA}{t} \quad \text{(A-2)}$$

where E is the Young's modulus of the layer material, A is the cross sectional area of the layer, and t is the thickness of the layer.

The model of the steel conical section used for this analysis is shown in Figure A-2. The stiffness of the conical section, K_{cone}, is obtained from

$$dK_{cone} = \frac{EA(x)}{dx} \quad \text{(A-3)}$$

where x is the distance along the conical section and $A(x)$ is the cross-sectional area of conical section. $A(x)$ is given by

$$A(x) = \pi(r_1 - x)^2 \tag{A-4}$$

where r_1 is the larger radius (at x=0), since the included angle of the conical section is 45°. Then

$$dK_{cone} = \left(\frac{dx}{EA(x)}\right)^{-1} \tag{A-5}$$

and

$$K_{cone} = \left(\int_{x=0}^{L} \frac{dx}{E\pi(r_1 - x)^2}\right)^{-1} \tag{A-6}$$

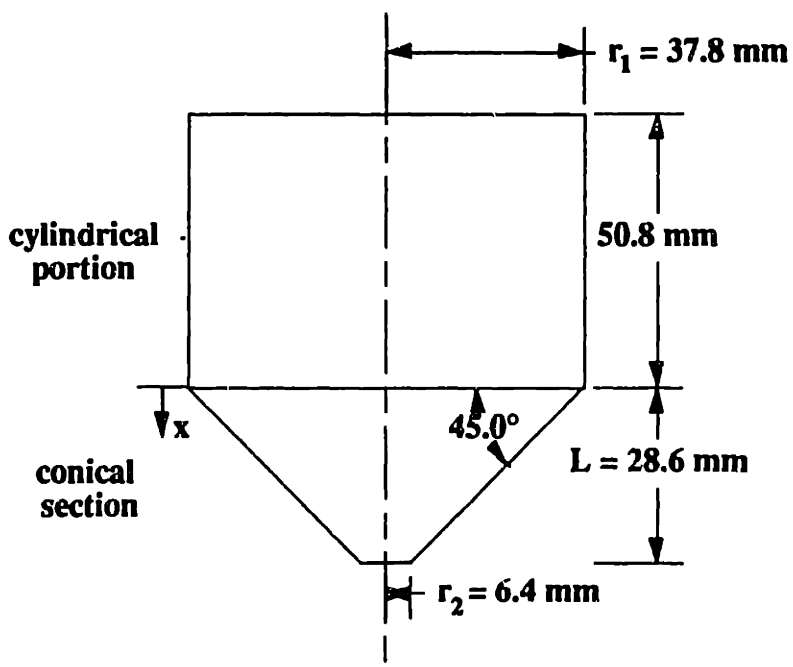

Figure A-2. Model of steel clamp half, showing cylindrical portion and conical section.

Using Mathsoft Mathcad numerical integration software, K_{cone} is determined to be 9.79 x 10^9 N/m. The stiffness of the 76.2 mm diameter cylindrical portion of the steel clamp half is calculated to be 7.13 x 10^{10} N/m, and is considered to be infinitely stiff for

this analysis. The steel conical-section stiffness calculation is only an approximation, as some of the steel material is removed to allow space for the temperature gradient assembly (see Figure 4-3). The calculated stiffness for each stack component and K_{comp} using material properties at 24 °C is given in Table A-1. Material properties are obtained from Ohigashi [31], APC technical sheets for type 880 PZT [37], and Crandall, Dahl, and Lardner [45].

Stack Component	Calculated Stiffness, K
Steel Conical Sections (2)	9.79×10^9 N/m
Pyrex Spacers (2)	7.11×10^9 N/m
PZT elements (2)	1.32×10^{10} N/m
PVDF layer	1.15×10^{10} N/m
Copper thermal bus	3.94×10^{10} N/m
Composite Stiffness, K_{comp}	5.02×10^8 N/m

Table A-1. Calculated stiffness values for the stack components at 24 °C.

Mechanical Resonant Frequency

The inertial clamp can be represented as two masses M and a spring K_{comp} with unconstrained ends (see Figure A-3).

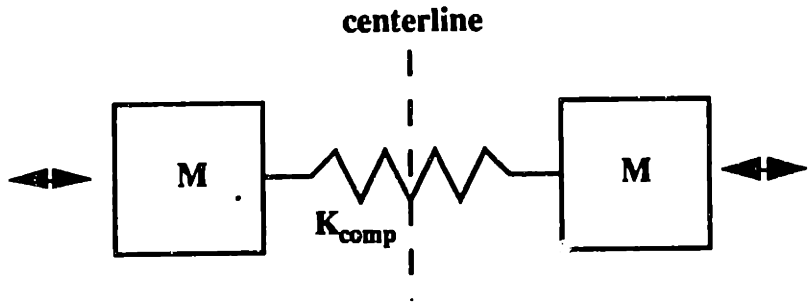

Figure A-3. Inertial clamp mechanical resonance model.

It is assumed that the length scale of the composite stack that forms the spring is small compared to the length scale of the inertial clamp halves. Therefore, any motion of the system is symmetric around the centerline of the system (regardless of any asymmetry in the stack itself) and can be represented as a single spring of stiffness $2K_{comp}$ and a single mass M (see Figure A-4).

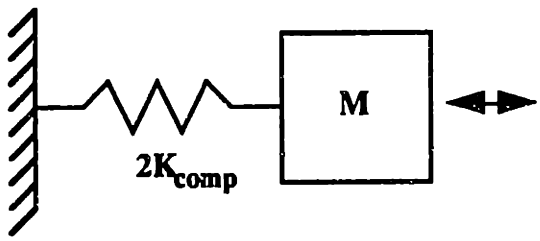

Figure A-4. Spring-mass model for inertial clamp.

Note that the spring constant is now $2K_{comp}$, as the spring is now 1/2 as long, and therefore twice as stiff. The spring-mass resonant frequency f_m is then given by

$$f_m = \frac{1}{2\pi}\sqrt{\frac{2K_{comp}}{M}} \tag{A-7}$$

where K_{comp} is the composite stiffness of the stack and steel conical sections and M is the mass of each clamp half. Using a K_{comp} of 5.02 x 10^8 N/m and a clamp half mass of 2.5 kg, f_m is calculated to be 3200 Hz.

Appendix B: Measurement of PVDF Capacitor Voltages

In this study, the output voltage of PVDF capacitive elements is measured in both the single layer energy conversion experiment and in the Strachan-Aspden replica device experiments. The effect of loading due to stray capacitances and the oscilloscope input impedance on the measured voltage in these experiments is analyzed in this appendix.

Loading of PVDF Layer Due to Scope and Mylar Capacitive Divider

In the single PVDF layer energy conversion experiment described in chapter 4, the stack arrangement is such that the PVDF and Mylar layers form a capacitive divider (see Figure B-1). The Tektronix TDS460A oscilloscope also possesses an input capacitance of 13 pF and an input impedance of 1 MΩ. The equivalent circuit is shown in Figure B-2, with the PVDF layer represented as an oscillating current source. The capacitances of the PVDF and Mylar layers are measured to be 790 pF and 186 pF respectively using a BK Precision 875A LCR meter.

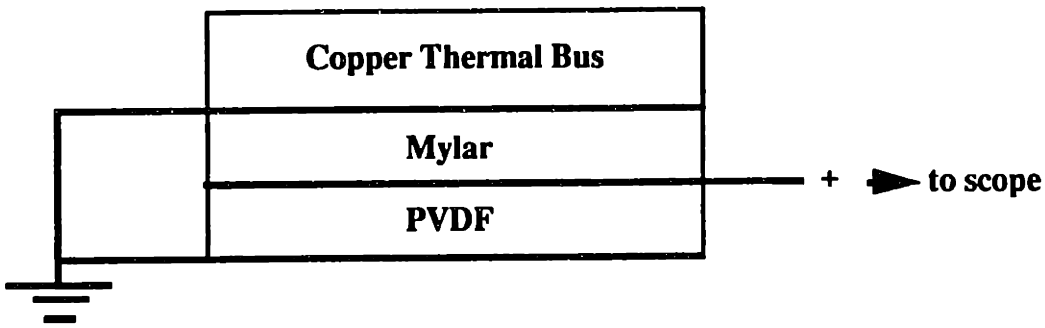

Figure B-1. Schematic of the PVDF-Mylar capacitive divider.

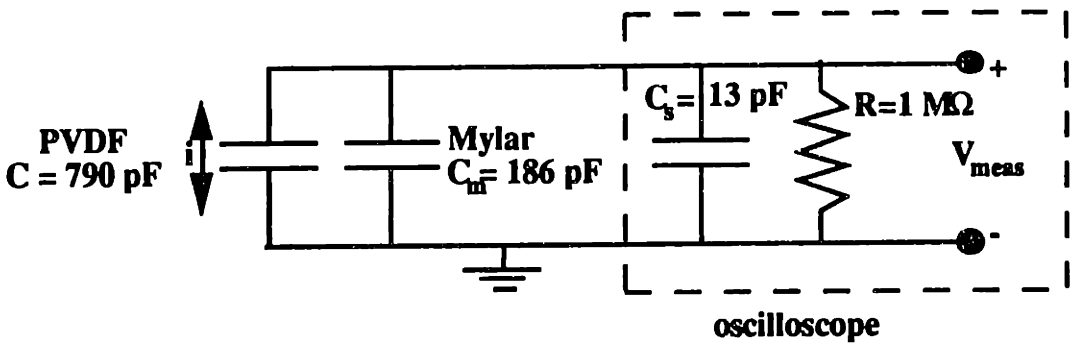

Figure B-2. Equivalent circuit for the open circuit single PVDF layer voltage measurements.

For a capacitor with dielectric

$$\frac{q}{A} = \varepsilon_0 E + P \tag{B-1}$$

where q is the free charge, A is the capacitive area, ε_0 is the permittivity of free space, (ε_0 = 8.854 x 10^{-12} F/m), E is the electric field, and P is the electric polarization.[19] If we assume q is an oscillating function of time, $q(t)$, then

$$q(t) = q_0 e^{j\omega t} \tag{B-2}$$

where q_0 is the oscillating charge amplitude and ω is the angular frequency. Since the current i is equal to $\frac{dq}{dt}$,

$$i = i_0 e^{j\omega t} = \frac{d}{dt}\left(q_0 e^{j\omega t}\right) = j\omega q_0 e^{j\omega t} \tag{B-3}$$

and

$$q = \frac{i}{j\omega} \tag{B-4}$$

Therefore,

$$\frac{i}{j\omega A} = \varepsilon_0 E + P \tag{B-5}$$

The measured voltage V_{meas} is given by

$$V_{meas} = iZ \tag{B-6}$$

where Z is the circuit impedance, given by

$$Z = R + \frac{1}{j\omega(C_m + C_s)} \tag{B-7}$$

where R is the oscilloscope input resistance, C_m is the Mylar layer capacitance, and C_s is the oscilloscope input capacitance. Therefore,

$$V_{meas} = El = i\left(R + \frac{1}{j\omega(C_m + C_s)}\right) \tag{B-8}$$

where l is the thickness of the PVDF layer. Substituting equation (B-8) into equation (B-5), and rearranging,

$$V_{meas} = El = \frac{-Pl}{\varepsilon_0}\left(1 - \frac{1}{(j\omega R\varepsilon_0 A/l) + (\varepsilon_0 A/(C_m + C_s)l)}\right)^{-1} \qquad \text{(B-9)}$$

where the quantity $-Pl/\varepsilon_0$ is the open circuit voltage (i=0) of the PVDF layer, V_{open}. V_{meas}/V_{open} is plotted versus frequency in Figure B-3. The voltage attenuation is less than 2% for frequencies over 10 kHz, and is therefore considered insignificant for the single PVDF layer energy conversion measurements.

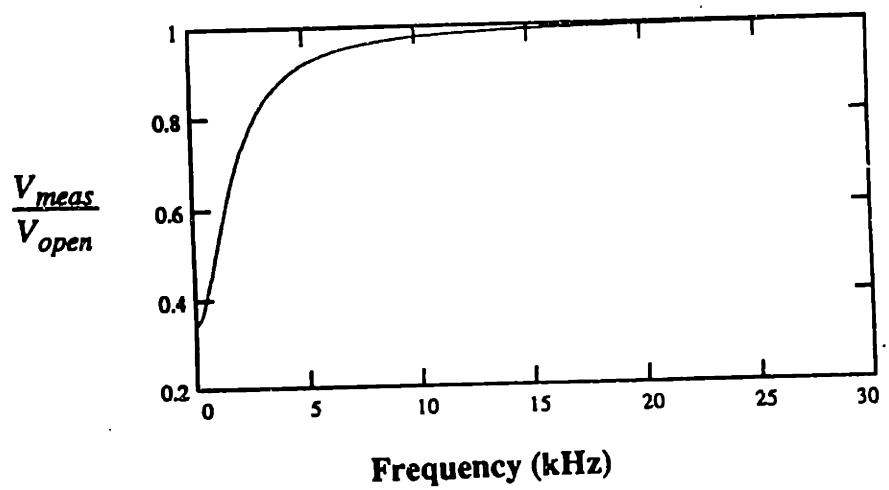

Figure B-3. Calculated V_{meas}/V_{open} versus frequency for the single PVDF layer energy conversion experiments.

Loaded Single Layer Experiments

In the loaded single PVDF layer energy conversion experiment (see section 4.3), a 10 kΩ resistor is placed in parallel with the PVDF layer. The circuit layout is shown in Figure B-4.

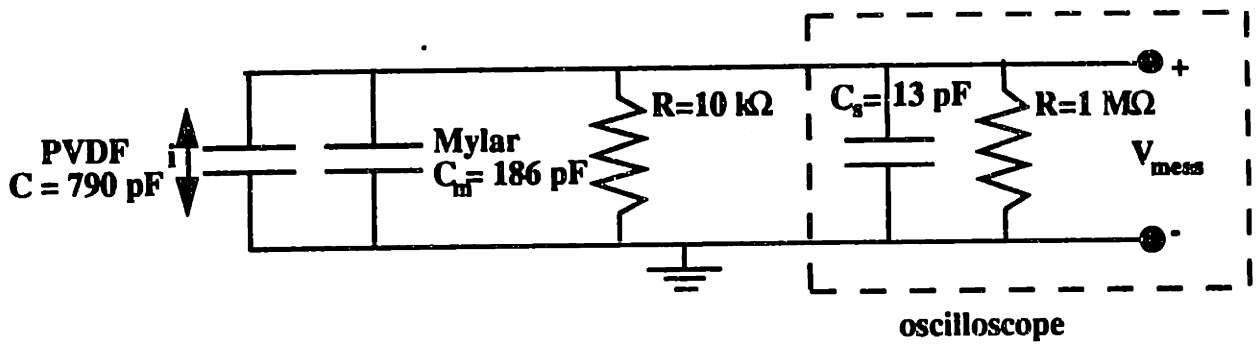

Figure B-4. Circuit for the 10 kΩ resistor-loaded single PVDF layer energy conversion experiments.

An analysis similar to that for the open circuit measurements, above, shows that

$$\frac{V_{meas}}{V_{open}} = \left(1 - \frac{1}{(j\omega R_p \varepsilon_0 A / l) + (\varepsilon_0 A / (C_m + C_s) l)}\right)^{-1} \qquad \text{(B-10)}$$

where R_p is the parallel combination of the oscilloscope 1 MΩ input impedance and the 10 kΩ load resistance, given by

$$R_p = \frac{1M\Omega \times 10k\Omega}{1M\Omega + 10k\Omega} = 9.9k\Omega \qquad \text{(B-11)}$$

V_{meas} / V_{open} is plotted versus frequency in Figure B-5. V_{meas} is only approximately 35% of V_{open} between 10 and 30 kHz, indicating that the PVDF layer is significantly loaded by the 10 kΩ resistor as the experiment intended. Actual measurements show that V_{meas} / V_{open} is approximately 0.61, which shows poor agreement with this prediction.

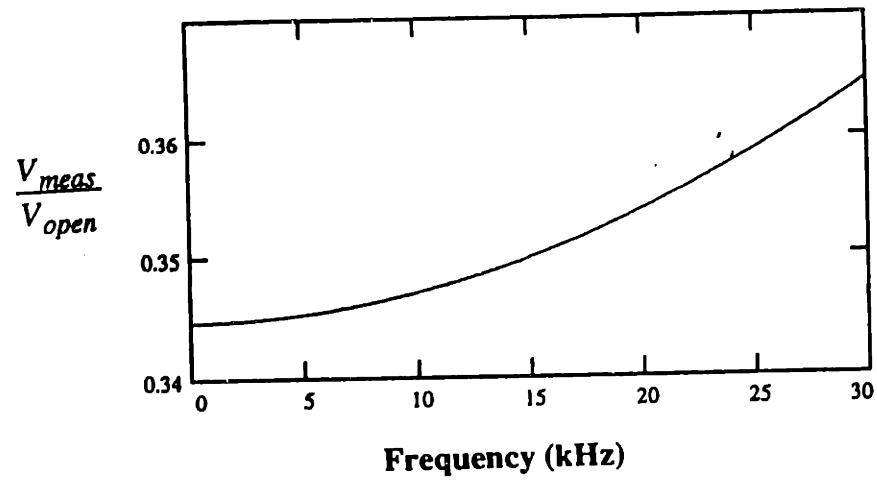

Figure B-5. Calculated V_{meas} / V_{open} versus frequency for the 10 kΩ resistor-loaded single PVDF layer energy conversion experiments.

Strachan-Aspden Replica Device Experiment

In the experiments performed with the Strachan-Aspden replica device, the output voltage of a 0.64 mm thick PVDF capacitor "listener" stack is measured using the Tektronix TDS460A oscilloscope (see chapter 6). The capacitive divider arrangement is shown in Figure B-6 and the equivalent circuit is shown in Figure B-7. The capacitance of the acrylic half-wave plate is estimated to be approximately 3.5 pF. An analysis similar to that for the single PVDF layer experiments, above, shows that

$$\frac{V_{meas}}{V_{open}} = \left(1 - \frac{1}{(j\omega R\varepsilon_0 A / l) + (\varepsilon_0 A / (C_a + C_s)l)}\right)^{-1} \quad \text{(B-12)}$$

where C_a is the acrylic capacitance value. V_{meas} / V_{open} is plotted versus frequency in Figure B-8. V_{meas} is more 2% greater than V_{open} for frequencies less than 36 kHz, and therefore will significantly affect measurements performed below 36 kHz.

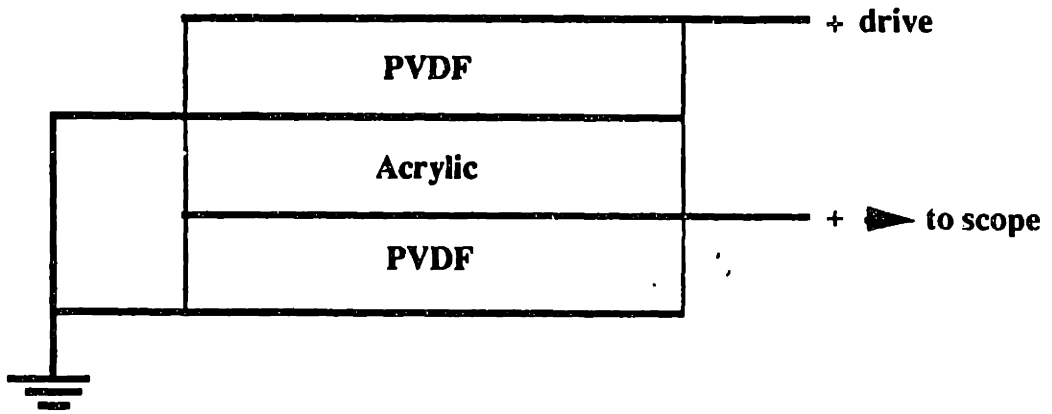

Figure B-6. PVDF-Acrylic capacitive divider arrangement for the Strachan-Aspden replica device experiment.

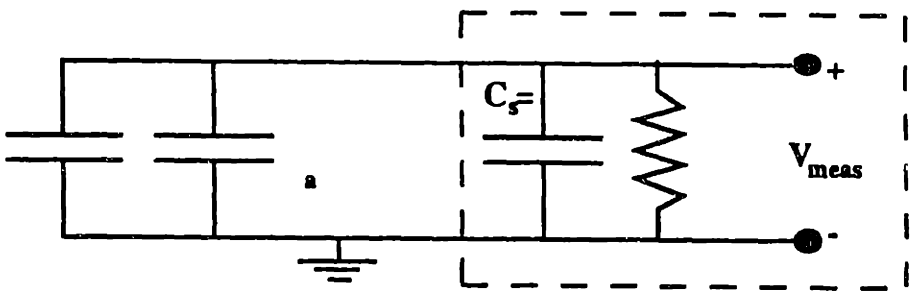

Figure B-7. PVDF-Acrylic capacitive divider equivalent circuit for the Strachan-Aspden replica device experiment.

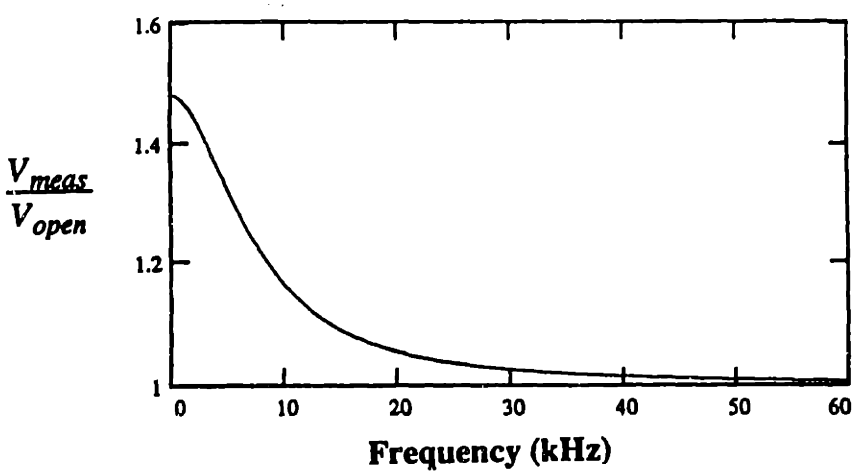

Figure B-8. Calculated V_{meas} / V_{open} versus frequency for the Strachan-Aspden replica device PVDF "listener" stack.

REFERENCES

1. Heikes, R.R., and Ure, R.W., 1961, *Thermoelectricity, Science and Engineering*, Interscience Publishers, New York, p. 547.

2. Rowe, D.M., ed., 1995, *CRC Handbook of Thermoelectrics*, CRC Press, Boca Raton, Florida, pp. 7-17, 390, 479-501.

3. Aspden, H., 1992, "The Electronic Heat Engine," *Proceedings of the 27th Intersociety Energy Conversion Engineering Conference*, August 3-7, San Diego, CA, pp. 357-363.

4. Aspden, H., and Strachan, J.S., 1992, "Electricity Without Magnetism," *Electronics World*, July 1992, pp. 540-542.

5. Strachan, J.S., "A New Perspective on Thermoelectric Power Generation," *Speculations in Science and Technology*, Vol. 13, pp. 289-293.

6. Aspden, H., and Strachan, J.S., 1993, "Solid-State Thermoelectric Refrigeration," *Proceedings of the 28th Intersociety Energy Conversion Engineering Conference*, August 8-13, Atlanta, GA, pp. 891-896.

7. Aspden, H., and Strachan, J.S., 1991, "Thermoelectric Energy Conversion," U.S. Patent 5,065,085.

8. Strachan, J.S., and Aspden, H., 1994, "Thermoelectric Energy Conversion," U.S. Patent 5,288,336.

9. Aspden, H., additional remarks supplementary to U.S. Patent Application Serial No. 07/429,608, 18 March 1991.

10. Strachan, J.S., private communication to Charles Bullock, Carrier Corporation, 10 February 1994.

11. Aspden, H., and Strachan, J.S., private communication to Joseph L. Smith, MIT, 7 March 1994.

12. Goldman, R., 1962, *Ultrasonic Technology*, Reinhold Publishing Corporation, New York, pp. 67-68.

13. Ensminger, D., 1988, *Ultrasonics: Fundamentals, Technology, Applications*, Marcel Dekker, Inc., New York, p. 512.

14. Cravalho, E.G., and Smith, J.L., 1981, *Engineering Thermodynamics*, reprinted by authors, Cambridge, MA, pp. 156-158.

15. Aspden, H., and Strachan, J.S., 1993, "Strachan-Aspden Thermoelectric Device," video recording.

16. MacDonald, D.K.C., 1962, *Thermoelectricity: An Introduction to the Principles*, John Wiley & Sons, Inc., New York, pp. 4-7.

17. Goldsmid, H.J., 1960, *Applications of Thermoelectricity*, John Wiley & Sons, New York, pp.1-15.

18. Lienhard, J.H., 1987, *A Heat Transfer Textbook*, Prentice-Hall, Inc., Englewood Cliffs, NJ, pp.591-592.

19. Halliday, D., and Resnick, R., 1978, *Physics, Part 2*, John Wiley & Sons, New York, pp. 665-668, 679, 751-752.

20. Bozorth, R.M., 1993, *Ferromagnetism*, IEEE Press, New York, pp. 267-276.

21. Kucherov, Y., private communication to Professor John G. Brisson, MIT, 24 October 1995.

22. *KYNAR Piezo Film Technical Manual*, Pennwalt Corporation, King of Prussia, PA, 1983.

23. Inderherbergh, J., 1991, "Polyvinylidene Fluoride (PVDF) - Appearance, General Properties and Processing," *Ferroelectrics*, Vol. 115, pp. 295-302.

24. Davis, G.T., 1993, "Piezoelectric and Pyroelectric Polymers," in *Polymers for Electronic and Photonic Applications*, C.P. Wong, Ed., Academic Press, New York, pp. 435-465.

25. Kepler, R.G., and Anderson, R.A., 1992, "Ferroelectric Polymers," *Advances in Physics*, Vol. 41, No. 1, pp. 1-57.

26. Furukawa, T., 1989, "Piezoelectricity and Pyroelectricity in Polymers," *IEEE Transactions on Electrical Insulation*, Vol. 24, pp. 375-394.

27. Park, D.H. and Yoshino, K., 1989, "Dependence of Dielectric Breakdown of Thin Poly (Vinylidene Fluoride) Film on Temperature and Thickness," *Electrical Engineering in Japan*, Vol. 109, No. 4, pp. 1-6.

28. Das-Gupta, D.K., 1991, "Pyroelectricity in Polymers," *Ferroelectrics*, Vol. 118, pp. 165-189.

29. Burkard, H., and Pfister, G., 1974, "Reversible Pyroelectricity and Inverse Piezoelectricity in Polyvinylidene Fluoride," *Journal of Applied Physics*, Vol. 45, pp. 3360-3364.

30. Schewe, H., 1982, "Piezoelectricity in Uniaxially Oriented Polyvinylidene Fluoride," *IEEE Ultrasonics Symposium Proceedings*, B.R. McAvoy, Ed., October 27-29, San Diego, CA, pp. 519-524.

31. Ohigashi, H., 1976, "Electromechanical Properties of Polarized Polyvinylidene Fluoride Films as Studied by the Piezoelectric Resonance Method," *Journal of Applied Physics*, Vol. 47, pp. 949-955.

32. Andreev, A.M., Donskaya, O.K., Kostenko, E.M., Mezenin, O.L., and Sazhin, B.I., 1992, "Increasing the Energy Density of Capacitors by Introducing Polyvinylidene Fluoride in the Dielectric Structure," *Elektrotekhnika*, Vol. 63, No. 1, pp. 52-54.

33. Smith, J.L., 1993, "Entropy Flow and Generation in Energy Conversion Systems," in *Thermodynamics and the Design, Analysis, and Improvement of Energy Systems*, AES-Vol. 30, HTD-Vol. 266, ASME Winter Annual Meeting, November 28 - December 3, New Orleans, LA, pp. 181-187.

34. Physik Instrumente catalog, Polytec PI, Inc., 23 Midstate Dr., Suite 104, Auburn, MA, 01501, pp. 5.5-5.19.

35. Ikeda, T., 1990, *Fundamentals of Piezoelectricity*, Oxford University Press, New York, pp. 11-14.

36. Xu, Q.C., Ramachandran, A.R., Newnham, R.E., and Tancrell, R.H., 1987, "Measurement of Complex Coefficients for Thick PVDF Polymer," *IEEE Ultrasonics Symposium Proceedings*, B.R. McAvoy, Ed., October 14-17, Denver, CO, pp. 663-666.

37. APC technical data sheets for type 880 PZT, American Piezo Ceramics, Inc., Duck Run Rd., P.O. Box 18, Mackeyville, PA, 17750.

38. Brown, L., South Dakota State University, private communication, 29 March 1996.

39. Omote, K., and Ohigashi, H., 1996, "Properties of Transverse Ultrasonic Transducers of Ferroelectric Polymers Working in Thickness Shear Modes," *IEEE Transactions on Ultrasonics, Ferroelectrics, and Frequency Control*, Vol. 43, No. 2, pp. 312-317.

40. Prassianakis, J.N., 1990, "Correlation of Mechanical and Acoustical Properties of Plasticized Epoxy Polymers," *Journal of Applied Polymer Science*, Vol. 39, No. 10, pp. 2031-2041.

41. Technical data sheets for STYCAST epoxy resins, Emerson & Cumming, Inc., 77 Dragon Court, Woburn, MA, 01888.

42. Folds, D. L., 1972, "Experimental Determination of Ultrasonic Wave Velocities in Plastics, Elastomers and Syntatic Foam as a Function of Temperature, *JASA*, Vol. 22, No. 1, p. 161.

43. Baer, E., Ed., 1964, *Engineering Design for Plastics*, Reinhold Publishing Corp., New York, p. 407.

44. Strachan, J.S., private communication to John G. Brisson, MIT, 26 August 1996.

45. Crandall, S.H., Dahl, N.C., and Lardner, T.J., *An Introduction to the Mechanics of Solids*, McGraw-Hill, Inc., New York, p. 286.